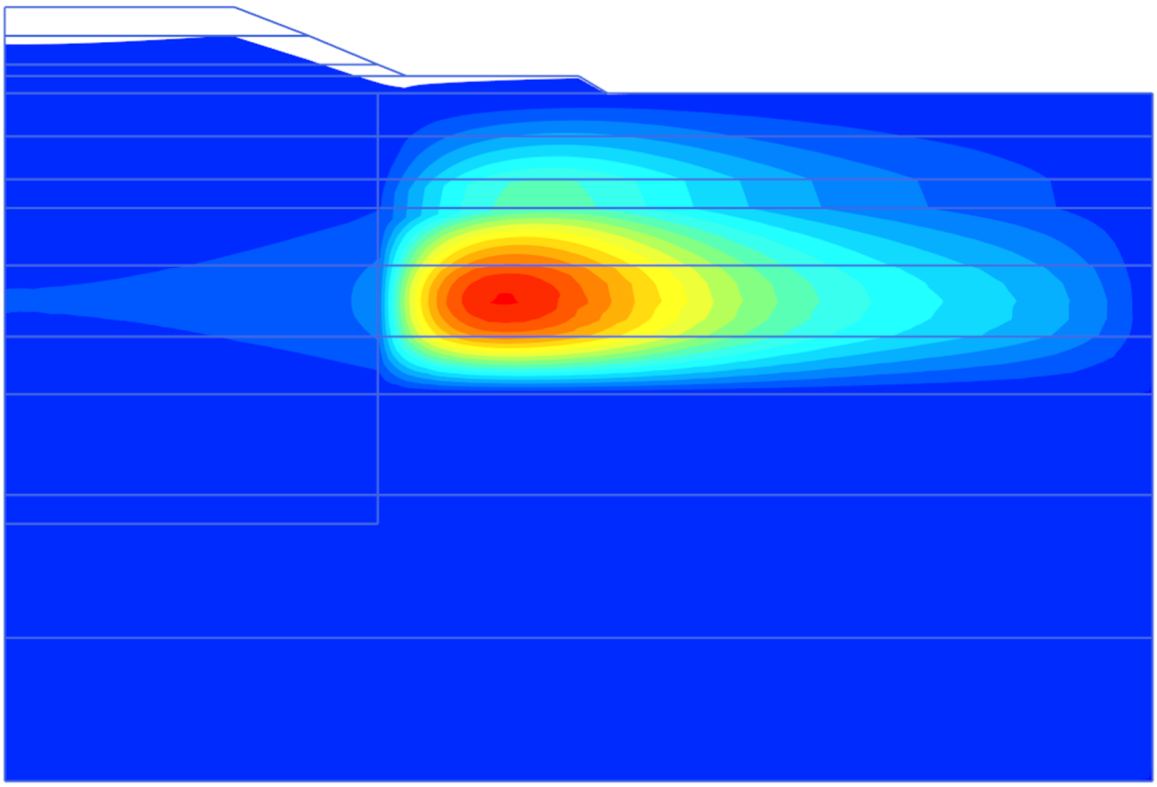

Numerical Analysis of a PVD-improved Embankment on soft clay

Class A and class C prediction of the Ballina test embankments

Master's Thesis in Master Programme Infrastructure and Environmental Engineering

SALOMON SUNDSTRÖM

DEPARTMENT OF ARCHITECTURE AND CIVIL ENGINEERING

DIVISION OF GEOLOGY AND GEOTECHNICS

CHALMERS UNIVERSITY OF TECHNOLOGY

Gothenburg, Sweden 2023

REPORT NO. xxxx/xxxx

Numerical Analysis of a PVD-improved Embankment on soft clay

Class A and class C prediction of the Ballina test embankments

SALOMON SUNDSTRÖM

Department of Architecture and Civil Engineering

CHALMERS UNIVERSITY OF TECHNOLOGY

Gothenburg, Sweden 2023

Numerical Analysis of a PVD-improved Embankment on soft soil
Class A and class C prediction of the Ballina test embankments
SALOMON SUNDSTRÖM

Technical report no xxxx:xx
Department of Architecture and Civil Engineering
Chalmers University of Technology
SE-412 96 Göteborg
Sweden
Telephone + 46 (0)31-772 1000

Cover: excess pore pressures beneath the embankment when simulating for 1100 days.

Gothenburg, Sweden 2023

Numerical Analysis of a PVD-improved Embankment on soft clay

Class A and class C prediction of the Ballina test embankments

SALOMON SUNDSTRÖM

Department of Architecture and Civil Engineering

Chalmers University of Technology

Abstract

The construction of embankments on soft soil is challenging to engineers due to difficulties associated with their short and long-term stability. This thesis aims to utilize numerical modelling to analyse the behaviour of embankments on soft clay, with special focus on the Ballina test embankments. Two distinct predictions are made: one considering the presence of prefabricated vertical drains (PVDs) installed in the soil and another completely without PVDs. The constitutive model used is the Creep-SCLAY1S model in PLAXIS 2D. The obtained results are compared with on-site measurements to evaluate the effectiveness and reliability of the modelling approach.

The thesis involves analysing available soil data and creating a representative soil profile, deriving input parameters for the constitutive model. Furthermore, a simple homogenisation technique is implemented to model the global effect of the PVDs, through changing the vertical hydraulic conductivity in the soil. A comprehensive sensitivity analysis is conducted to identify factors with a significant influence on the simulation results. The results for the PVD-improved embankment demonstrate satisfactory predictions with vertical and horizontal deformations aligning reasonably well when compared with measurement data over a 3-year period. Moreover, the implemented averaging technique effectively captures the enhanced consolidation settlements introduced by the PVDs over the time period. Comparisons with the unimproved embankment indicate little actual improvements in stability for the improved case in the first 3 years. However, spanning over a 40-year period, the vertical settlements approach the same order of magnitude for the two cases, and the horizontal displacements are significantly less for the improved embankment. Indicating a time-dependent nature of stability improvement using PVDs.

Ultimately, the parameter derivation process and high-quality laboratory data are vital for accurate simulations. As revealed by the sensitivity analysis, there is significant variations in the results depending on which laboratory test is used to derive the pre-consolidation pressure. The discrepancy can likely be attributed to the unusually high strain-rates used for the CRS laboratory tests, in combination with the unusually low strain rates adopted for the IL-tests – emphasizing the experience and skill required of the engineer in order to arrive at accurate predictions.

Keywords: Numerical modelling, creep, soft clay, test embankment, Creep-SCLAY1S, Vertical Drains, Prefabricated Vertical Drains, PVD

Acknowledgements

I would like to thank my supervisor/examiner Minna Karstunen for introducing me to the subject, for excellent guidance and for many interesting thoughts and discussions throughout. I would also like to thank Sinem Bozkurt for invaluable assistance with the numerical modelling process.

Salomon Sundström

Gothenburg, June 2023

Table of contents

List of Figures

1. Introduction

Soft soils, commonly found in coastal regions, often including densely populated urban areas, present notable challenges to the construction industry due to their unique hydro-mechanical properties. The stability and safety of buildings and infrastructure in these areas are often compromised, and the costs of construction must be balanced against high maintenance costs (Graham, 2006). Thus, accurately predicting the behaviour of soft soils over both the long term and short term is crucial for engineers when designing effective foundations and support systems in these complex conditions.

In addition to engineering considerations, it is important to acknowledge the significant potential environmental impact of accurate predictions of soil behaviour during design projects. Allowing engineers to make well informed decisions of the optimal foundations design, thus preventing overdesign, and reducing unnecessary material usage, and will reduce the carbon footprint of the project and its environmental impact. Furthermore, by proactively addressing concerns regarding settlements, long-term stability of the structures is ensured, and unnecessary repairs, reconstructions, and replacements can be avoided with obvious environmental implications.

Especially accurate predictions of vertical displacement at multiple depths below the structure, the dissipation of pore pressures and the horizontal displacements at the toe of the structure remain significant challenges (Amavasai et al., 2017). In present times, numerical modelling has emerged as a widely recognized tool for predicting soil behaviour under varying boundary conditions and loading circumstances. Furthermore, to ensure the effectiveness and accuracy of constitutive models developed for numerical modelling, the use of trial embankments to calibrate the models against real-world measurements is crucial.

1.1. Aim and Objectives

The aim of this master's thesis is to utilize numerical analysis as a tool to model the behaviour of embankments constructed on soft soil, with special focus on the Ballina trial embankment located in New South Wales, Australia. The prediction will be carried out using the Creep-SCLAY1S constitutive model within PLAXIS 2D. The analysis aims to make two distinct predictions: one considering the installation of prefabricated drains (PVDs) at the site, and one without PVDs. The obtained results are compared with on-site measurement data, enabling conclusions to be drawn regarding the effectiveness and reliability of the modelling process.

The following objectives are set:

- Analyse available soil data and create a soil profile representative of on-site conditions.
- Derive necessary input parameters for the Creep-SCLAY1S constitutive model.
- Perform a comprehensive numerical analysis of the Ballina trial embankment using the Creep-SCLAY1S model in PLAXIS 2D.
- Model Prefabricated Vertical Drains (PVDs) using a simple homogenisation method for modifying the vertical hydraulic properties of the soil.
- Conduct a class A prediction on vertical and horizontal settlements and their time-dependency, as well as pore pressure developments for the embankment without PVDs.
- Conduct a class C prediction on vertical and horizontal settlements and their time-dependency, as well as pore pressure developments for the embankment with PVDs.
- Conduct a sensitivity analysis on sensitive parameters and factors with high relevance on the prediction and draw conclusions from the results.

1.2. Limitations

Naturally, attempting to model the real-life behaviour of soft soil is a difficult task and many factors can influence the results. For this thesis, the main limitations that were identified are:

- Embankment may not be sufficiently long for plane strain assumption.
- Installation effects on the hydraulic conductivity in the soil are largely unknown.
- Modelling PVDs in plain strain may not fully represent real-world behaviour.
- Available laboratory tests may not be conducted at high enough stress levels to represent the intrinsic behaviour of the soil.
- Measurement results for the embankment without PVDs installed were not available.
- Limitations connected to the constitutive model used:
    - The elastic behaviour in the elastic region is assumed to be isotropic.
    - No small strain stiffness is included.
    - Non-linear variation of OCR is not included in the Creep-SCLAY1S model.

2. Background

The following chapter includes the theoretical background part of the conducted literature study. Here, the behaviour of soft soil and its key characteristic is described, followed by an outline of construction of embankments on soft soil, and using prefabricated vertical drains (PVDs) as a ground improvement method. Finally, numerical modelling of soft soil in general, followed by a detailed description of the Creep-SCLAY1S model and its input parameters is found.

2.1. Behaviour of Soft Soil

Deposits of soft clay have often been formed and then aged for hundreds to thousands of years. These deposits have been subjected to various complicated naturogenic effects, such as chemical bonding, surface erosion, creep, desiccation, and leaching (Bjerrum, 1967). The process of a clay forming in-situ is referred to as "geological stress history" which has a significant impact on the behaviour of soil under stress (Hanzawa, 1989). Moreover, the magnitude of deformations depends on other factors as water content, density, grain-size distribution, and organic content (Larsson, 2008).

In soil that are coarse grained the intrinsic particles are generally bound by contact with each other to form a skeletal cellular framework. This means a significant portion of the soil's mass is occupied by pore fluids, usually water and air (Larsson, 2008). When subjected to deformation, soil experiences substantial and often irreversible changes in volume as particles rearrange. Thus, any attempt to describe soil response to loading must incorporate the potential for significant changes in volume (Muir Wood, 1990). This is especially true for deposits of soft clays where particles are sedimented slowly and in an undisturbed environment. Such deposits possess an open structure with large voids bound together by inter-particle forces rather than direct contact (fabric and bonding). As a result, these soils exhibit high compressibility and are prone to significant deformations under lading (Larsson, 2008). However, when subjected to large enough stress levels, the structure of soil obtained during sedimentation is erased, resulting in a shift in its response. Burland (1990) introduced a new concept, i.e. intrinsic properties of natural sedimentary clays. The intrinsic properties are inherent to the soil, meaning they are independent on the natural state of the soil, influenced by the soil structure and provide a reference when assessing the in-situ state of the soil.

When observing soil behaviour under loading in 1D conditions it is also apparent that an increase in effective stress makes the soil compress (Muir Wood, 1990). A soil subjected to lading is experiencing compression and has the volume of its particle structure changed, and the pore fluids must flow throughout the soil (Larsson, 2008). Therefore, when applying a load to a soil specimen that is saturated, the compression is not instant. This is due to the soil constituents, the skeletal framework as well as the pore water being

next to incompressible in comparison to structure of the soil (Olsson, 2010). The only way for deformation to take place is by slowly squeezing water from the voids in the soil, see Figure 2.1.

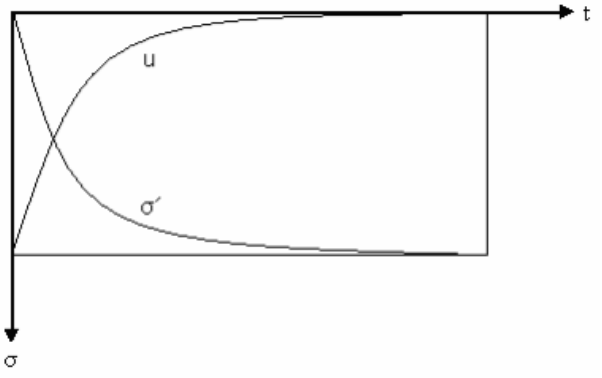

Figure 2.1 The transformation from excess pore pressure to effective stress in soil.

For soft soil, the permeability parameter *k* is used to measure the extent to which the fluid can flow through the soil. The surface area to volume ratio increases as particle dimension of the soil decrease, hence a soil of small particles is most likely to be of low permeability and vice versa (Olsson, 2010). Water within the soil's pores will naturally move from areas with higher excess pore pressures to areas where the excess pore pressures are lower. As illustrated in Figure 2.1, the dissipation of pore pressures will cause shift in the soils effective stress, leading to gradual deformation over time. This process of volume reduction by dissipation of excess pore pressures due to flow is referred to as *consolidation,* which will be described in more detail in section 2.1.1.

2.1.1. Consolidation and creep

The classic consolidation theory was developed and published by Terzaghi (1923). His theory is still what makes out the foundation of 1D consolidation theory today. The theory is developed from the assumption of a relationship between strain and effective stress that is not time dependent.

Other assumptions that validate the theory are:

- Homogenous and fully saturated soil.
- Incompressibility of both soil particle and water.
- Darcy's law is applied.
- During the consolidation process the hydraulic conductivity is a constant parameter.
- Compression and pore pressure developments are in 1D.
- Equal change in pore pressures and effective stress.
- Strain of the soil is only dependent on changes in effective stresses, no secondary consolidation or creep is considered.

Furthermore, the equation for Terzaghi's one dimensional consolidation can be expressed through:

$$\frac{\delta u}{\delta t} = \frac{M}{\gamma_w} \cdot \frac{\delta}{\delta z}\left(k \cdot \frac{\delta u}{\delta z}\right) \tag{2.1}$$

where u = pore pressure [kPa]

M = oedometer modulus [kPa]

t = time [s]

γ_w = unit weight of water [kg/m³]

k = permeability [m/s]

z = depth [m]

Assuming permeability of the soil does not vary with depth:

$$\frac{\delta u}{\delta t} = c_v\left(\frac{\delta^2 u}{\delta z^2}\right) \tag{2.2}$$

where c_v is the coefficient of consolidation, defined as:

$$c_v = \frac{M \cdot k}{\gamma_w} \tag{2.3}$$

Initially, Terzaghi's theory was used for calculating settlements, and the consideration of potential settlements relating to creep began only after all excessive pore pressured had dissipated. Later, Taylor (1942) developed a model applicable for oedometer tests of effective stress vs a general variation of void ratio, *e*, and time, *t*.

The process of consolidation has universally been divided into two distinct behaviours of primary consolidation and secondary consolidation. Primary consolidation refers to when there is an increase in effective stress and simultaneously a decrease in soil volume and pore pressures. On the contrary, secondary consolidation is defined as the process during which the soil volume decreases under constant effective stress. For many years, the development of creep strains in soil were considered as separate from the primary consolidation, and, subsequently, being equal to secondary consolidation.

The first person that suggested clay behaves according to a relation between void ratio, effective stress and strain rate during one-dimensional compression was Suklje (1957). Suklje presented a model where creep strain was assumed to occur continuously throughout the consolidation process. Therefore, the model assumes that creep and primary consolidation are not two separate processes differentiated by the dissipation of excess pore pressures. Thus, Suklje demonstrated that the thickness of the clay layer, the permeability and the drainage conditions all have an influence on the time-dependent strains in the soils (Claesson, 2003; Suklje, 1957).

About a decade later Bjerrum (1967) presented a similar conceptual model, which also assumes creep strains and primary consolidation are not separated processes. The objective of the model was to explain the relationship between geological ageing and the over-consolidations ratio (pre-consolidation pressure) of soft virgin clays. The model provides an explanation and reason for the occurrence of creep effects and settlements over time, despite the pre-consolidation pressure of the soil not being exceeded (Olsson, 2010). Bjerrum stated that strains that occurred should be separated into two distinct components of "delayed" and "instant" compression. Figure 2.2a illustrates how clay compresses over time if the applied loading is instantly supported by the framework structure of the clay in the form of effective stress, and, consequently, causing a reduced void ratio in the soil. This process develops until a point of equilibrium is reached where the soil structure supports the overburden pressure fully and is referred to as "instant" compression. In Figure 2.2a, the dashed line represents the drained behaviour, where compression occurs without the pore water being able to delay it. The gradual rise of effective stresses is attributed to the viscous effect of water, which occurs as excess pore pressures dissipate, and compression follows along the solid line (Bjerrum, 1967). The concept denoted "delayed" compression is a representation of additional volume reduction, i.e., consolidation, taking place while the effective stress (loading) remains constant over time. This causes the soil sate to transition from point A to point B in Figure 2.2b.

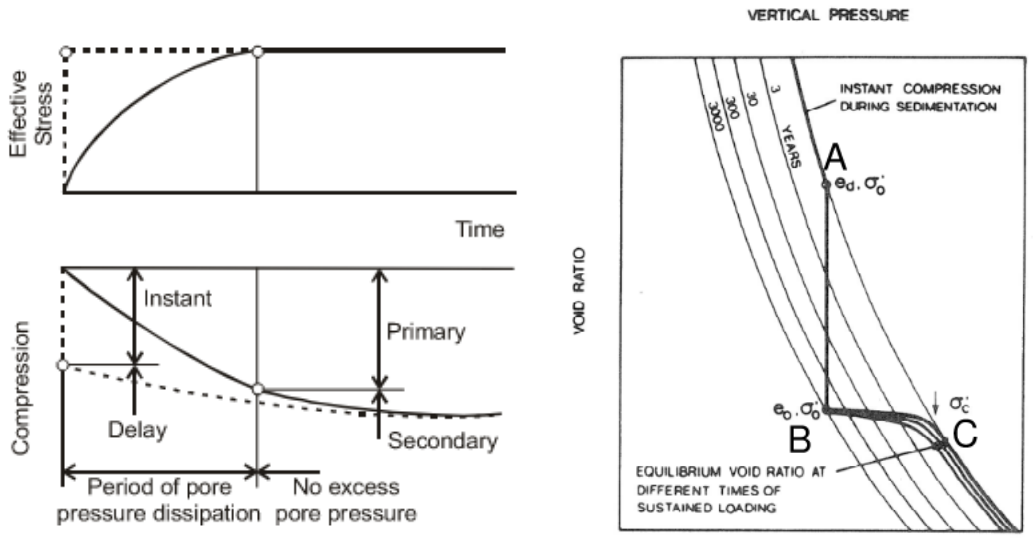

(a) (b)

Figure 2.2. (a) Distinction between "Delayed" and "instant" and "primary" and "secondary" compression behaviour of soil under surcharge loading (Claesson, 2003; Bjerrum, 1967) and (b) secondary compression and its effects on pre-consolidation stress and void ratio in soft clay (Claesson, 2003; Bjerrum, 1967).

These effects are also prevalent in natural soil deposits. This can be observed in Figure 2.2 where the soil reaches an apparent state similar to that of point B, 3000 years after the initial sedimentation. Within laboratory settings, i.e., 1D oedometer tests, this type of soil exhibits minimal strains until the stress state is equal to the pre-consolidation pressure at

point C. Thus, this is where yielding is indicated in the soil, and the trajectory of the curve approaches the initial line representing "instant" compression (Olsson, 2010). The yielding of soil will be further described in section 2.1.3.

Secondary consolidation can normally be characterized by the inclination of the *e-t* curve in an Incremental load, IL oedometer test, where the excess pore pressures in the soil have dissipated, see Figure 2.3 (Olsson, 2010). In order to characterize and quantify creep effects present in the soil, there are multiple commonly used parameters available (C_α, α_s and r_s.), with each essentially describing the same thing and is obtained through similar means.

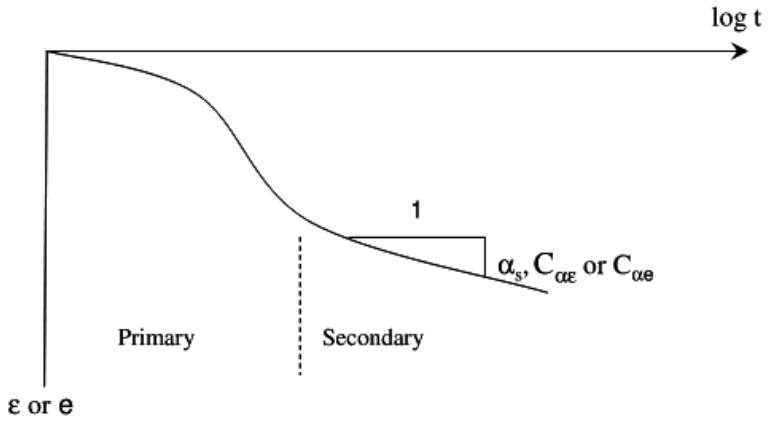

Figure 2.3. Illustration of secondary consolidation (creep) and various associated parameters in an IL laboratory test (Olsson, 2010).

Buisman (1936) first presented a parameter describing creep behaviour defined as the secondary creep index C_α, which can be described using the variation in void ratio Δe or the variation in strain $\Delta\varepsilon$:

$$C_{\alpha\varepsilon} = \frac{\Delta\varepsilon}{\Delta log(t)} \; or \; C_{\alpha\varepsilon} = \frac{\Delta e}{\Delta log(t)} \tag{2.4}$$

In Sweden the coefficient of secondary consolidation α_s is more commonly used, which in turn relates to secondary compression index (Olsson, 2010). The difference is α_s being described as a function of strain, ε, and C_α as a function of void ration, e. The relation between the parameters is expressed as:

$$\alpha_s = \frac{C_\alpha}{1 + e_0} \tag{2.5}$$

Where $1 + e_0$ = the specific volume, V

e_o = initial void ratio

The concept of time resistance, *R*, was developed and presented by Janbu (1969). He claimed it to be a powerful tool to describe time- and stress-dependent behaviour of soft

soil under effects of compression, swelling and recompression. Figure 2.4 describes a single load step during a Oedometer laboratory test. The pore pressure is measured at the impermeable bottom of the sample while the top is drained (Claesson, 2003). Considering time as an action, while the strain as a reaction during creep, the time resistance, *R*, is then defined by Janbu as expressed in equation (2.6).

$$R = \frac{dt}{d\varepsilon} \tag{2.6}$$

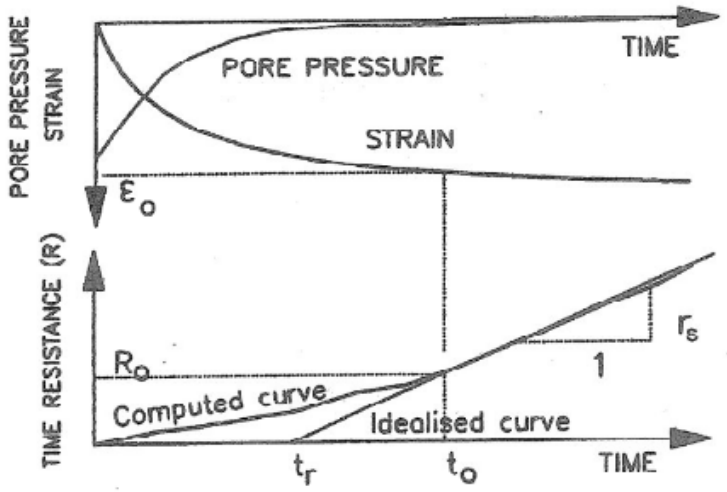

Figure 2.4 Time resistance during a single weighted load step in a 1D Oedometer test (Svanö, et al., 1991).

In Figure 2.4 the time resistance seems to be increasing linearly after a certain time t_0, corresponding to the point when all excess pore pressures in the soil have dissipated (Claesson, 2003). Therefore, the gradient of this relationship, and thus the time resistance r_s can be expressed as:

$$R = r_s(t - t_r) \tag{2.7}$$

Where t is time and t_r is the reference time.

Due to the linear relationship of time resistance an integration from t_0 to t gives a logarithmic creep strain with time, as seen in equation (2.8).

$$\varepsilon_c = \int_{t_0}^{t} \varepsilon \, dt = \int_{t_0}^{t} \frac{dt}{R} = \frac{1}{r_s} \int_{t_0}^{t} \frac{dt}{(t - r_r)} = \frac{1}{r_s} \, ln \left[\frac{t - t_r}{t_0 - t_r}\right] \tag{2.8}$$

2.1.2. In-situ stresses

The total vertical stress at a certain level in natural soil σ_v is composed by the overburden pressure from the overlying soil masses. The vertical effective stress σ'_0 is reduced by the pore pressures u_0 present in the voids of the soil. Their relationship is expressed by:

$$\sigma'_0 = \sigma_0 - u_0 \tag{2.9}$$

The pore pressure in soils can be hydrostatic from a free water table, but it can also have a downward gradient or an upward gradient (artesian) depending on the site conditions (Larsson, et al., 2007).

If a natural soil deposit is currently experiencing the exact amount that is expected from the current pressure exerted by its overburden, and it has never been overloaded, it is *normally consolidated*. If a soil is unloaded after having consolidated under a certain effective surcharge load, i.e., the pre-consolidation pressure, σ'_c, the vertical stress decreases, leading to the soil becoming *over consolidated*. The degree of over consolidation, *OCR*, is expressed as:

$$OCR = \frac{\sigma'_c}{\sigma'_0} \tag{2.10}$$

If OCR ≤ the soil is in a normally consolidated state, and when OCR>1 it is in an over consolidated state.

The relationship between σ'_c and σ'_0 can also be expressed by pre overburden pressure (POP):

$$POP = \sigma'_c - \sigma'_0 \tag{2.11}$$

As evident in the general formulation of OCR and POP, they represent the distribution of σ'_c due to the historical effective stress exerted on the soil in different ways when plotted against depth (see Figure 2.5). Therefore, considerations should be taken to which is more characteristic to the in situ soil conditions. Moreover, the effects of over consolidation can also occur due to drying or ground water fluctuations at the top of the soil profile, weathering effects and creep (Larsson, et al., 2007). The process of defining the pre-consolidation pressure will be described in more detail in the next section.

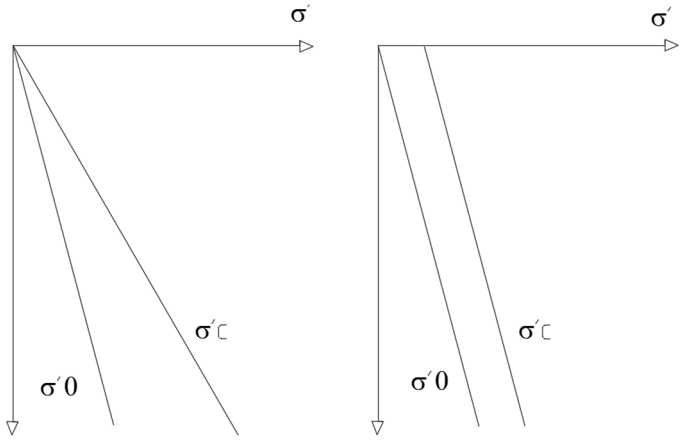

Figure 2.5. Distribution of σ'_c plotted vs depth using OCR (left) and POP (right).

Deformations of fine-grained soils are due to both changes in volume and shape and because of its anisotropic properties it varies in different directions (Olsson, 2010). The relationship between the effective horizontal and vertical stresses is expressed by the coefficient of lateral earth pressure at rest K_0:

$$K_0 = \frac{\sigma'_h}{\sigma'_v} \tag{2.12}$$

For a horizontal ground surface and normally consolidated soil, the vertical stress is equal to the maximum principal stress, and the horizontal stress, σ_h, is equal to the minimum principal stress (Larsson, et al., 2007). The relationship between the vertical and horizontal effective stresses in normally consolidated soil can be uniquely expressed by the coefficient of earth pressure at rest in the normally consolidated region, K_0^{NC}. It depends on angle of internal friction in the soil and can be automatically evaluated by equation (2.13). As the response of the soil depends on the anthropological and geological history, soils are usually not entirely normally consolidated and exhibit some apparent over-consolidation from historical loading/unloading as well as previously described creep effects (Olsson, 2013). In an over consolidated state, the value of lateral earth pressure at rest, K_0 , can be calculated by incorporating the overconsolidation ratio, OCR, into (2.13), through the relationship expressed in (2.14)

$$K_0^{NC} = 1 - sin\ \varphi'_c \text{ (Jaky's formula)} \tag{2.13}$$

$$K_0 = (1 - sin\ \varphi'_c)^{\sin \varphi'_c} \tag{2.14}$$

where ϕ'_c is the friction angle at critical state.

2.1.3. Yielding and rate dependency

The one-dimensional consolidation of soil is an important problem to study and solve for the geotechnical engineer. There is no universal definition of how to define soil yielding (Olsson, 2013). However, the yield stress is usually evaluated from the region where the curve gets steeper in a compression curve plotted in a linear or log scale of stress vs linear strain, see dotted region in Figure 2.6.

Various one-dimensional consolidation test configurations are employed to assess soil deformation and flow properties. The incremental loading test involves a cylindrical test specimen, that is laterally constrained by a rigid ring, and subjected to incremental vertical axial loading or unloading (Larsson, 2008). The constant rate of strain test (CRS) on the other hand, is not performed as a series of discrete stages, but a continuous process (Muir Wood, 2016). The upper surface of a cylindrical sample, like the incremental loading test, is loaded at a displacement rate (strain) that is constant over the duration of the test (Stolle & Stolle, 2011). Using these tests, it is possible to determine the pre-consolidation pressure, σ'_c, which is often considered to be the yielding point of soft soil. Moreover, additional parameters relating to compression and swelling required for calculations and modelling can be determined.

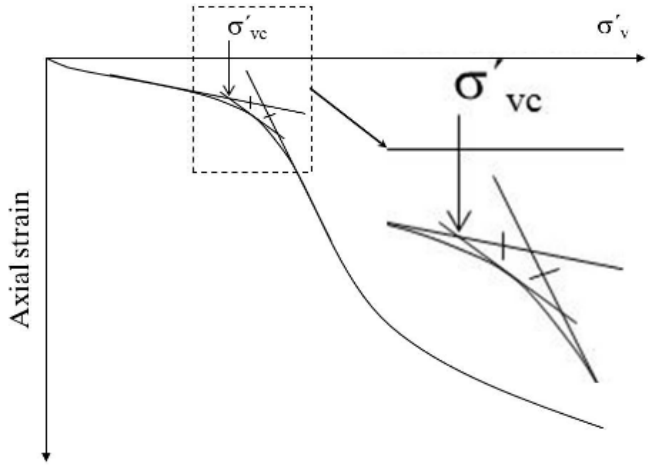

Figure 2.6. *Evaluation of s'$_c$ from a CRS test using the Sällfors (1975) method* (Olsson, 2013)

The value of the pre-consolidation pressure can be derived from a laboratory test and is exceptionally site dependent as it is influenced by anthropological and geological processes. In Sweden it is common practice to define the σ'_c from a standard CRS test using a methodology suggested by Sällfors (1975). The method is illustrated in Figure 2.6 where the correction for strain rate is incorporated through constructing an isosceles triangle that determines the obtained value. This correction is done in addition to the recommended rate of 0.0024 mm/min adopted when conducting the test.

It is considered a common opinion that soft soils are highly rate dependent (Olsson, 2010). Time dependent, long-term deformations in soil, like the previously described creep

effect, must be considered during the design phase to avoid future problems in serviceability and stability (Leoni, et al., 2008). Just as in real-world conditions, strain rate effects are also prevalent and visible in the laboratory as well as in field testing (Claesson, 2003). Considering the rate of deformations in soil is crucial for interpreting test results and accurately predicting soil behaviour in the short term, as well as the long term.

It is generally believed that when conducting a one-dimensional laboratory test, the higher the adopted rate of strain, the higher the pre-consolidation pressure (Olsson, 2010). This effect is especially evident in the normally consolidated region and can be observed in Figure 2.7, showing CRS and incremental loading tests conducted by Sällfors (1975) and Claesson (2003).

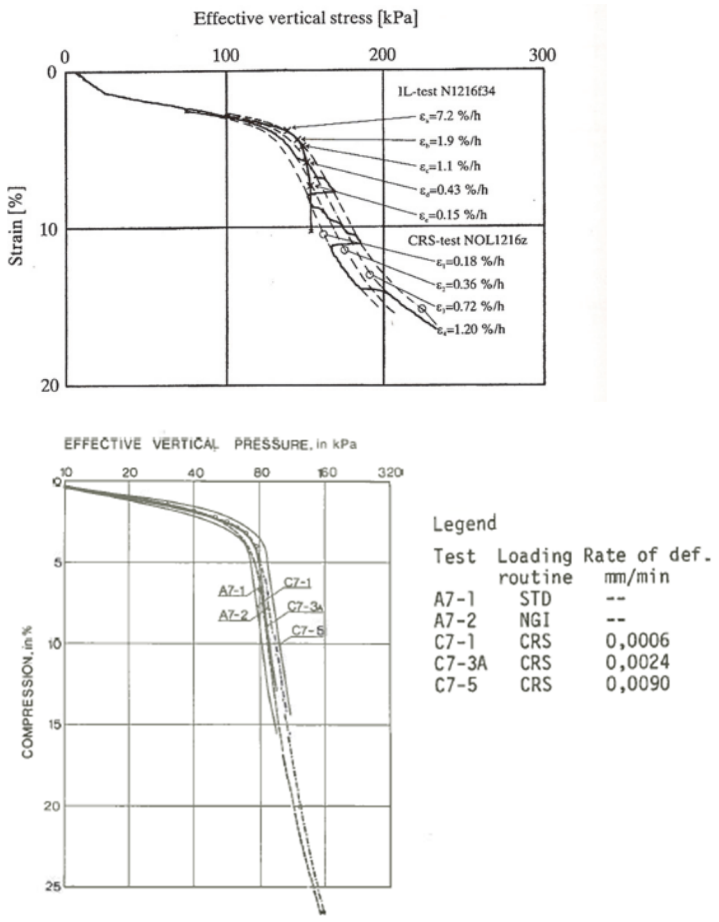

Figure 2.7. One-dimensional CRS and IL tests by Claesson (2003) (top) and Sällfors (1975) (bottom) conducted using different strain rates.

Moreover, the pre-consolidation pressure, $\sigma'_{c,}$ is often a crucial input parameter when modelling the behaviour of soft soil (Karstunen & Amavasai, 2017). As previously stated, the value of the pre-consolidation pressure can be influenced by the rate of strain of the conducted test. Thus, especially, when using derived parameters for modelling creep behaviour of soil this has large implications, as expressed by Karstunen & Amavasai (2017). As different clays have different tendencies to express creep behaviour (especially

clays with big variations in sensitivity and mineralogy) a universal method for correcting values of σ'_c derived from CRS tests is not possible. The method like the one described by Sällfors (1975) can be useful and work well for clay extracted from the same corresponding depths and location that was used in his work but is not accurate and applicable in all cases of soft soil. In later years it has been highlighted by Muir Wood (2016) that for more advanced non-linear, elasto-plastic modelling the interpreted results of laboratory CRS tests need to be used at system level (Karstunen & Amavasai, 2017).

2.1.4. Sample disturbance

Soil characterisation through field and laboratory testing is conducted to obtain information about soil properties and behaviour and is essential for the geotechnical design process. Field tests provide information about in-situ conditions, while laboratory tests determine the physical and mechanical properties of soil. Thus, obtaining reliable test data is paramount to making accurate predictions of soil behaviour. This is particularly relevant when making long-term predictions of deformation in rate dependent sensitive soil (Karlsson, et al., 2016). If the material properties of the investigated soil are not clearly identified there is little to no point in doing refined analysis. Moreover, the cost of laboratory testing is something that must be recovered during the design phase in terms of increased design confidence, savings, or improved performance (Graham, 2006).

The disturbance of soil samples often takes place during the initial sampling process. According to Amundsen (2017) the main contributor to disturbance is the type of sampler used. The disturbance is minimal for large diameter samples, such as 160-250mm block samples, but it may be critical for small diameter tube and piston samples. In addition to the sampling process itself, it is important to acknowledge the potential impact of secondary disturbance on extracted soil samples. Factors such as temperature, humidity, transportation, and time stored can influence the clay structure and subsequently affect the outcomes of the tests (Amundsen et al., 2017).

The disturbance of soil samples has a notable impact on important design parameters. Disturbance generally leads to a decrease in pre-consolidation pressure and the (initial) stiffness, while causing an increase in the stiffness post yielding (Larsson, 2008). To assess the quality of obtained soil samples, and therefore the influence of sample disturbance, there are several methods available.

Karlsrud and Hernández-Martinez (2013) introduced the method of assessing sample quality by the oedometer stiffness ratio. The ratio is a comparison between the maximum constrained modulus (M_0) within the OC stress range and the minimum constrained modulus (M_L) obtained in the NC range. When the soil undergoes disturbance, reloading it into in-situ stresses results in a significant volumetric change. Therefore, a higher ratio of M_0/M_L would indicate a better soil sample quality, and vice versa. The criteria for

which to determine the soil sample quality using the oedometer stiffness ratio is presented in Table 2.1.

Table 2.1. Soil sample quality assessment criteria according to the oedometer stiffness ratio.

Ratio M_0/M_L	Soil sample quality
>2	Very good to excellent
1.5 - 2	Good to fair
1 – 1.5	Poor
<1	Very poor

Lunne et al. (1997) proposed a method of evaluating the sample quality using the void ratio of the soil. This approach involves normalising the change in void ratio, $\Delta e/e_0$, which represents the amount of recompression required to restore the specimen to its in-situ, σ'_{v0}, stress conditions. The sample quality is determined using the criteria in Table 2.2.

Table 2.2. Soil sample quality assessment criteria using void ratio (Lunne et al., 1997).

$\Delta e/e_0$	Soil sample quality
< 0.04	Very good to excellent
0.04 – 0.07	Good
0.07 – 0.14	Poor
> 0.14	Very poor

Andresen & Kolstad (1979) introduced the Specimen Quality Designation, SQD, which involves assessing the volumetric strain of a soil sample using multiple laboratory tests. In oedometer as well as triaxial compression tests, the volumetric (recompression) strain for the sample to reach the assumed in-situ vertical and horizontal effective stress is evaluated. The measured values are compared against the criteria presented in Table 2.3 to assess the quality.

Table 2.3. Soil sample quality assessment according to the Specimen Quality Designation (SQD) (Andresen & Kolstad, 1979).

Volumetric strain (%)	Soil sample quality
< 1	Very good
1 – 2	Good
2 – 4	Fair
4 – 10	Poor
> 10	Very poor

Another method for assessing soil sample quality by measuring the recompression strain to in-situ vertical effective stress is the one presented by Larsson et al. (2007). The method is grounded in the work by Lunne et al. (1997), but instead of void ratio, uses volumetric

strain in combination with the initial water content, w_N, to assess the soil sample quality. The classification criteria used for the method is presented in Figure 2.8

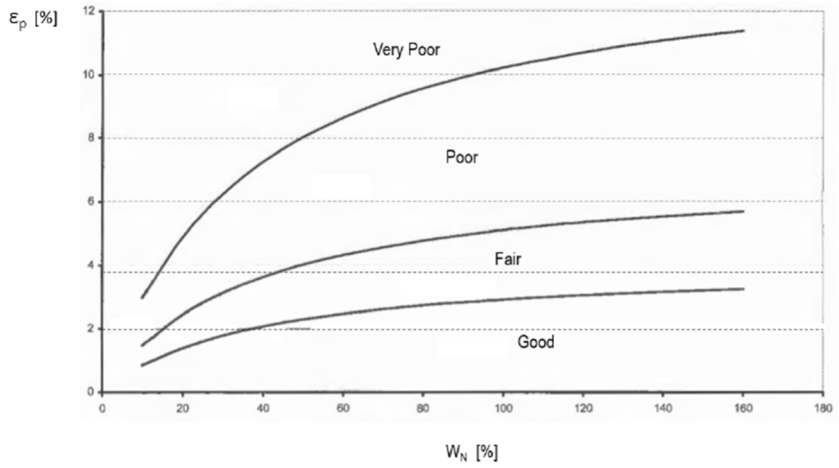

Figure 2.8. Soil sample quality assessment by using volumetric strain, together with the water content of the soil, as by (Larsson, et al., 2007).

2.2. Embankments on Soft Soil

Constructing an embankment on soft soil if often challenging due to the compressibility, low hydraulic conductivity, and low undrained shear strength of the underlying soil deposit. The inherent properties of the soil can cause stability and settlement issues in both the short and long term. Consequently, careful consideration must be given to address these concerns during the design process. Understanding soil behaviour and fundamental principles of primary and secondary consolidation is essential for competent serviceability limit state (SLS) design (Almeida & Marques, 2013).

When constructing an embankment on very soft soil it is anticipated that most of the settlements will occur after construction, as the excess pore pressures dissipate. However, it is crucial to give special consideration to time-dependent creep behaviour as well. By implementing an appropriate SLS design long-term maintenance costs of the construction can be avoided (Krenn, 2008). Furthermore, implications of creep is often just considered in relation to SLS design. Although, it may also affect the ultimate limit state design (ULS) of an embankment. In the case of a gradual accumulation of excess pore pressures due to ongoing creep under embankment loading, the mean effective stress will decrease as the pore pressures increase. This process can occur until the effective stress approaches the undrained shear strength in the soil (Krenn, 2008). Thus, the shear forces that previously offered resistance no longer provide any support and potentially leading to failure along a slip surface.

Achieving the required factor of safety (FoS) for stability or limiting settlements to an acceptable degree becomes challenging, various ground improvement or reinforcement methods can be employed. By effectively implementing such techniques, engineers can mitigate the challenges associated with soft soil and ensure the long-term stability and

performance of embankment structures. Almeida & Marques (2013) highlights a number of factors that should be considered when selecting the appropriate construction method for a specific project. These include the geotechnical properties of the soil, intended use of the area, construction deadlines and cost considerations. Figure 2.9 illustrates different construction methods, ground improvement and reinforcement techniques utilized when constructing embankments on soft soil. These address aspects such as settlement and stability control, with many approaches addressing both aspects simultaneously. In cases when the soil is exceptionally soft, it is common to incorporate geosynthetic reinforcement in combination with the alternatives in Figure 2.9.

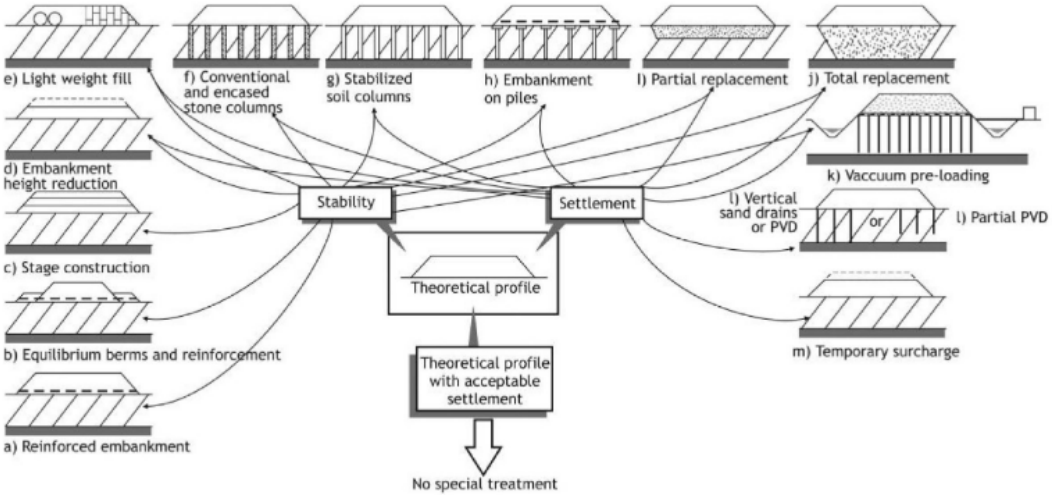

Figure 2.9. Different construction methods, ground improvements and reinforcements utilized for constructing embankments on soft soil (Almeida & Marques, 2013)

According to Almeida & Marques (2013), an embankment constructed without employing any specific measures to mitigate settlement or stability control is referred to as a conventional embankment. A conventional embankment can be constructed by utilizing a *temporary surcharge* (see Figure 2.9m) with the purpose of accelerating the primary settlements induced and counteract all or some of the secondary settlements in the soil. One disadvantage of this method is the considerably large amount of earthworks required. Moreover, if the soil deposit is not very thick, *removal of the soil* may be a viable option (i, j in Figure 2.9), especially if the excavated material can be reused during the project and transport distances are manageable. However, in urban areas, finding suitable locations for the disposal of excavated material, can be challenging due to environmental concerns and possible contamination.

Using lightweight materials, such as expanded polystyrene (EPS), is an effective approach to mitigate settlements induced by embankment loading (Almeida & Marques, 2013). This technique, known as *lightweight fill* (Figure 2.9e), involves replacing the original fill material with one with significantly lower unit weight, allowing for a fast construction process. The lightweight fill materials, however, come at a cost.

Furthermore, a *reduction of embankment height* (Figure 2.9d) can be considered if the undrained shear strength, c_u, is very low in the top layers of the deposit. Although, depending on the project, this may not be possible due to geometry requirements of the road or railway. Hence, if the height of the embankment cannot be altered, and the projected safety factor against failure is low, it may be an alternative to *construct the embankment in stages* (Figure 2.9c), allowing an incremental increase of stability (Almeida & Marques, 2013). Another useful technique that can be implemented if stability problems are prevalent and the FoS need to be increased, is *equilibrium berms* (Figure 2.9b). However, using berms will increase the settlements, and, particularly in densely populated areas, space constraint may restrict potential use.

Furthermore, constructing e*mbankments on vertical drains* can be used as a ground improvement method where challenges related to settlements are prevalent, especially when combined with temporary surcharge loading. The technique is further explored in this thesis and a comprehensive description will be provided in the following section.

Embankments that are constructed on *pile-like elements* (Figure 2.9f, g, h) work by transferring the load of the embankment to a stronger soil layer or bedrock beneath the soft soil deposit (Almeida & Marques, 2013). This is achieved through using a platform with caps, geogrid, or slabs that distribute the load from the embankment to the piles or columns. One notable advantage of this approach is that it helps to shorten the construction schedule due to relatively fast installation procure. However, solutions with pile-like elements often come with high embodied *CO_2-eq* emissions.

Specifically in Scandinavian countries, *deep mixing* is a widely used method for improving the strength and deformation properties of soft soil. This technique involves the creation of columns or small wall panels by blending a binding material, such as cement, lime, or gypsum, into the soil to achieve stabilisation (Krenn, 2008). However, it is important to carefully consider the environmental implications associated with the method when considering the design.

Evidently, different solutions have clear perks and disadvantages associated. When discussing solutions such as the aforementioned conventional embankment types (Figure 2.9a, b, c, d, m), or embankments with vertical drain-improvements (Figure 2.9k, l), an important aspect to consider is the time consuming nature of most of these solutions (Almeida & Marques, 2013). Hence, they may not be suitable if time limitations are strict. In such cases, solutions using pile-like elements (see Figure 2.9 f, g, h) may be preferred options. However, it is important to note that the latter may come at a higher monetary and environmental cost.

Ultimately, the geometry of the embankment and the geotechnical characteristics of the site are highly variable factors that need to be carefully analysed on a case-by-case basis. Each project requires a thorough assessment on the specific conditions to determine the most suitable design.

2.3. Prefabricated Vertical Drains

Construction of an embankment using temporary surcharge loading is a widely adopted approach for addressing challenges associated with slow, long-term consolidation in soft soils. However, the implementation of this procedure on its own does, in practice, often present a challenge due to its time-consuming nature — something that is rarely an abundant commodity in modern design projects.

The shortened drainage path introduced by the installation of PVDs will considerably reduce the consolidation time when applying a load to the soil. Thus, preloading, in combination with the installation of prefabricated vertical drains (PVDs), has been widely used by engineers as an effective ground improvement method to accelerate the consolidation process of soft soils under surcharge loading. The significant accelerating impact of vertical drains on the consolidation process of soft soil can be seen in Figure 2.10 using an illustration of the settlement developments against time, with and without vertical drains installed. Moreover, by removing the surcharge after the preloading period, the creep settlements can also be reduced.

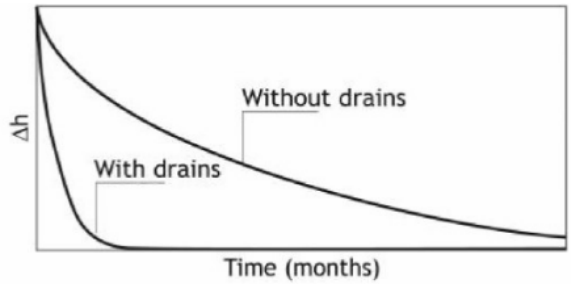

Figure 2.10. Development of settlements under surcharge loading with and without the use of vertical drains. (Almeida & Marques, 2013)

The first vertical drains adopted were sand drains in the early 1900s, which were subsequently replaced by PVDs (Almeida & Marques, 2013). PVDs are made of corrugated plastic drainage cores that make up geosynthetic elements (see Figure 2.11). These are installed in the soil to effectively provide decreased horizontal drainage paths in natural soil deposits (Rowe & Taechakumthorn, 2008). Therefore, designs that consider both radial and vertical drainage are often complicated. The solutions used in practice are usually those that ignore the effects of vertical drainage, such as the analytical 1D unit cell solutions of Barron (1948) or Hansbo (1981). Barron (1948) presented a solution that incorporated, and was fundamentally built on, the legitimacy of Darcy's law. The theory included two alternatives, with one assuming free vertical strains and the other assuming equal vertical strains, together with the combined effect of vertical and radial flow towards the drains. However, today, most designs today are based on the subsequent, simpler, and more practical, additions made by Hansbo (Müller, 2010; Hansbo, 1981).

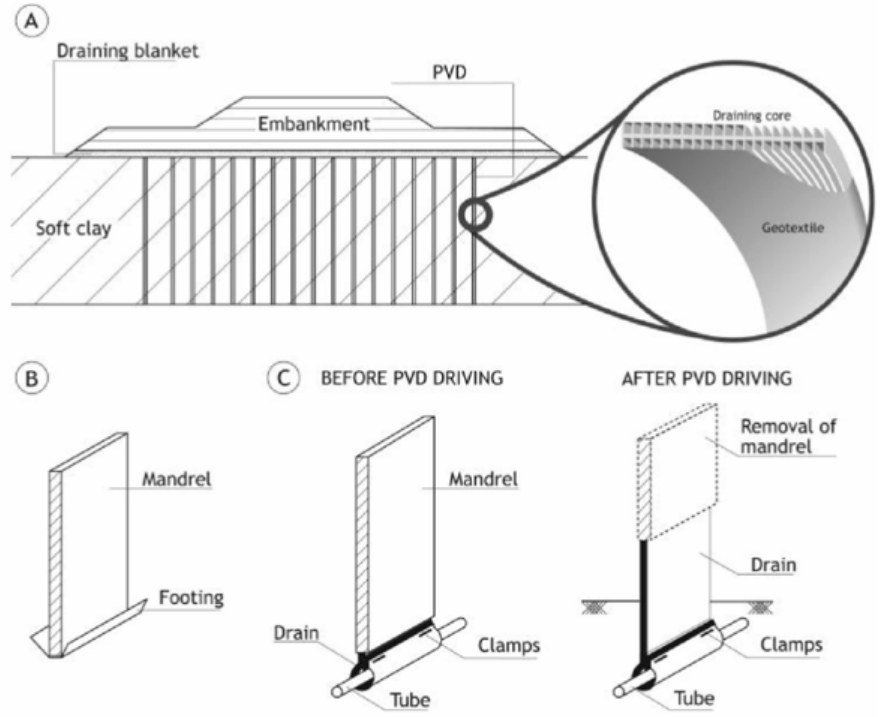

Figure 2.11. (a) Schematic figure of an embankment on PVDs (and equilibrium berms) (b) detail of mandrel and footing adopted for installation and anchoring of the PVD (c) detail of driving mandrel and tube for anchoring (Almeida & Marques, 2013)

Hansbo (1981) elaborated on the principles of Barron (1948) regarding the analysis of enhanced consolidation in soil improved by vertical drains. His method based on equal vertical strain assumption and included a zone of smear and reduced well resistance. Other important assumptions in his theory are drainage in the soil is entirely restricted to the horizontal direction, the soil is totally uniform and homogenous and has constant compressibility and permeability.

In practical use, the discharge capacity of a drain is naturally limited. Therefore, physical aspects like well resistance will have a delaying effect on the consolidation process of the soil, leading to degree of consolidation, expressed in (2.15), often being overestimated. Although, when using modern types of band-drains, the well resistance effect can generally be disregarded entirely in the design, due to their high enough discharge capacity (Hansbo, 1997). This can be seen in equation (2.17) where a simplified version of Hansbo's (1981) original expression for resistance effects in the vertical drains, μ, is expressed, where the well resistance is ignored. Moreover, as this type of drains are pushed, driven, or vibrated into the soil by means of a mandrel, the effect of smear introduced during installation must also be considered (Hansbo, 1981). However, it is challenging to estimate the extent of the disturbance caused by this. Different contractors utilize different techniques and equipment (penetration velocity, mandrel size and shape) and there are multiple ways of conducting the design process (Amavasai, et al., 2018). An illustration of a PVD installed in the soil, and the surrounding smear zone can be seen in Figure 2.12.

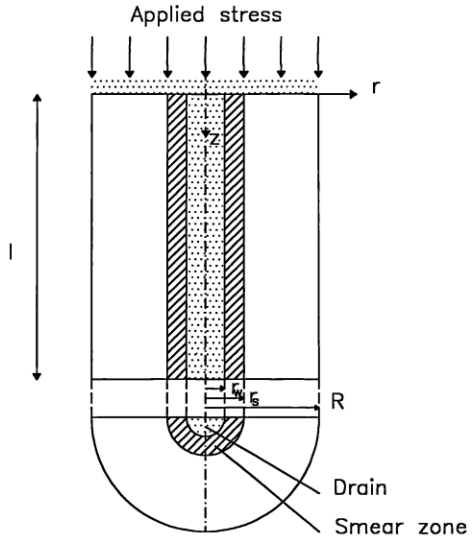

Figure 2.12. Vertical drain unit cell with surrounding smear zone (Hansbo, 1981).

Hansbo (1981) accounted for the smear effect by introducing a zone around the drain with lower hydraulic conductivity (see Figure 2.12). Assuming that Darcy's law is valid, the average degree of consolidation due to radial drainage can be expressed as:

$$U_r = 1 - \exp\left(-\frac{8}{\mu} \cdot T_h\right) \tag{2.15}$$

where the time factor T_h is defined as:

$$T_h = \frac{c_h \cdot t}{D_e^2} \tag{2.16}$$

where c_h = coefficient of consolidation in the horizontal direction [m²/year]

D_e = diameter of unit cell [m]

t = time [year]

and the value of μ can be expressed as:

$$\mu = ln\frac{n}{s} + \frac{k_h}{k_s}\, ln(s) - \frac{3}{4} + \pi\frac{2l^2 k_h}{3q_w} \tag{2.17}$$

where k_h = horizontal hydraulic conductivity [m/day]

k_v = vertical hydraulic conductivity [m/day]

k_s = horizontal hydraulic conductivity in smear zone [m/day]

d_w = diameter of drain [m]

d_s = diameter of smear zone [m]

$n = D_e/d_w$

$s = d_s/d_w$

In more recent years, Basu et al. (2010) revealed that the rate of consolidation is influenced by both the extent of soil disturbance near the drain and the variability of hydraulic conductivity withing the disturbed zone. Therefore, accurately predicting the rate of consolidation requires identifying the hydraulic conductivity profile surrounding the drain.

As soil is rarely homogenous and often has multiple layers with varying properties and drain installation causes disturbance in the soil, it is not always justifiable to consider PVD-improved soil to be under 1D conditions (Chai, et al., 1995). Hence, as the analytical unit cell theory, (2.15) - (2.17), is not always able to account for all aspects of PVDs, methods of numerical analysis (typically FEM) are often required for accurate predictions. However, considering the potential numerical challenges involved and uncertainty surrounding the properties and varying magnitude of the smear zones, comprehensive efforts of modelling isolated drains may yield limited benefits. In contrast, employing a simplified approach can be key for achieving effective and precise predictions of performance of PVD-improved soil, as emphasized by Amavasai et al. (2018).

From a macro perspective, the installation of vertical drains enhances the vertical hydraulic conductivity of the underlying soil. As a result, it is reasonable to attempt to determine an approximate value for the hydraulic conductivity that encompasses both the influence of natural vertical drainage and the radial drainage caused by the presence of prefabricated vertical drains (PVDs). Chai et al. (2001) introduced an approach that enables the user to analyse soil that has been improved with PVDs in a similar way to the unimproved case. The method incorporates an equivalent vertical hydraulic conductivity, k_{ve}, derived through a process based on the assumption of equal average degree of consolidation under the initial conditions. Using to the method introduced by Carillo (1941) the effects of horizontal and vertical drainage are combined through the relationship in equation (2.18).

$$U_{vr} = 1 - (1 - U_v)(1 - U_r) \tag{2.18}$$

where U_{vr} is the average degree of consolidation of drain improved soil, and U_v equals the average degree of consolidation in the vertical direction. The degree of consolidation due to radial drainage U_r should be calculated by Hansbo's solution (1981), defined previously in equations (2.15) - (2.17).

To arrive at a simple expression for equivalent hydraulic conductivity in the vertical direction, k_{ve}, Chai et al. (2001) proposed an approximation of Terzaghi's general expression for the average degree of vertical consolidation:

$$U_v = 1 - \exp(-C_d T_v) \tag{2.19}$$

where the time factor T_v is defined as:

$$T_v = \frac{c_v \cdot t}{D_e^2} \tag{2.20}$$

Where c_v = coefficient of consolidation in vertical direction

H = vertical drainage length [m]

C_d = constant [-]

t = time [year]

Furthermore, Chai et al. (2001) specified a number of factors that need to be considered to determine the value of the constant C_d.

- Equation (2.19) is specifically utilized to determine value of k_{ve}. Once k_{ve} has been determined, U_v is calculated using Terzaghi's theory for one dimensional problems and Biot's theory (1941) for cases in 2D and 3D.
- As depicted in Figure 2.13, when U_v equals 50%, equation (2.19) produces the same outcome as Terzaghi's theory if the constant C_d is assumed as 3.54. However, equation (2.19) underestimates the average degree of consolidation for $U_v < 50\%$ and overestimates for $U_v > 50\%$, with a maximum error of less than 10% (Chai, et al., 2001). Consequently, when converting the apparent effects of PVDs into k_{ve}, and ignoring the vertical drainage of natural soil, $C_d = 3.54$ is the most appropriate value.
- It is possible minimize errors in the average degree of consolidation by accounting for both the vertical drainage of the natural soil as well as the radial drainage of the installed PVDs. However, adopting the value of $C_d = 3.54$ will result in the range of underestimation being more than half (Chai, et al., 2001).
- The optimal value of C_d depends on the relative significance of vertical and radial drainage, which varies form one case to another.

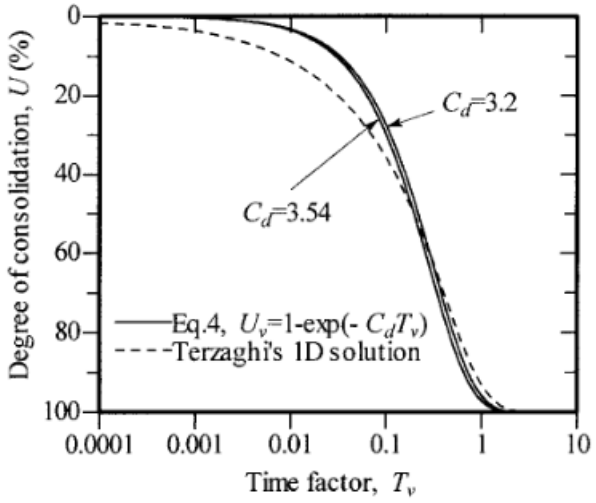

Figure 2.13. Influence of constant C_d on degree of consolidation (Chai, et al., 2001).

As (2.19) takes the same form as (2.15) (Hansbo's solution) the equivalent hydraulic conductivity in the vertical direction, k_{ve}, can be defined through a simple expression:

$$k_{ve} = \left(1 + \frac{2.5l^2 k_h}{\mu D_e^2 k_v}\right) k_v \tag{2.21}$$

where all parameters are previously defined.

For conditions where the soil stratigraphy is interpreted with multiple layers, and (2.19) is used to calculate k_{ve}, it can simply be assumed that the length of the drainage l equals the thickness H of the zone with PVDs installed. Consequently, $l = H$ for one-way drainage and $l = H/2$ when considering two-way drainage. In a case where the soft soil deposit is experiencing drainage on two fronts, but the installed drains are not installed all the way to the permeable layer, as seen in figure Figure 2.14, one-way drainage should be applied.

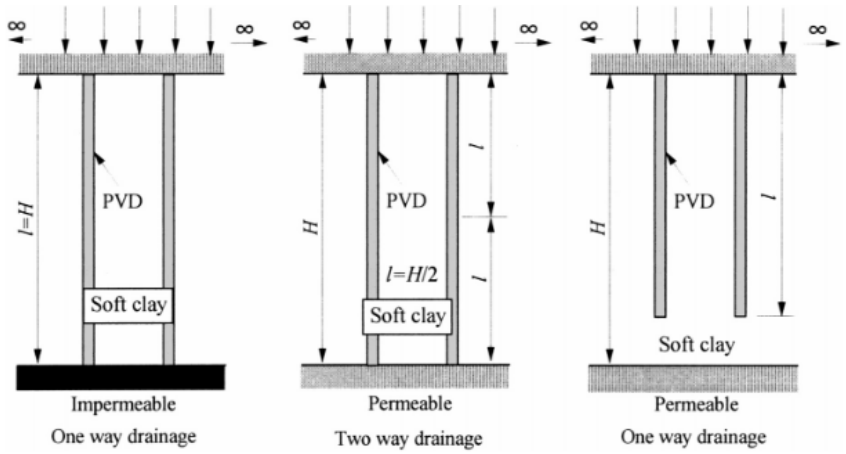

Figure 2.14. Different drainage conditions of PVD-improved soil (Chai, et al., 2001).

Ultimately, Chai et al. (2001) highlighted the fact that one-dimensional conditions are used to arrive at the k_{ve} value. However, this does not mean the proposed method is only applicable in cases for 1D analysis. A vertical drain-improved zone hydraulic conductivity of k_{ve} in vertical direction and k_h in horizontal direction can be used in 2D and 3D, depending on the requirements of the situation.

2.4. Plane Strain and PVD Performance

Typically, numerical analyses of embankments are conducted using plane strain conditions (Figure 2.15b) for a cross-section perpendicular to the centreline of the embankment. However, this approach becomes problematic when attempting to model the impact of PVDs, as the consolidation conditions around each drain are closer to that of the axial symmetry (Figure 2.15a) (Hird, et al., 1995). To incorporate the influence of drains, methods for matching their effect under axisymmetric and plane strain conditions needs to be used.

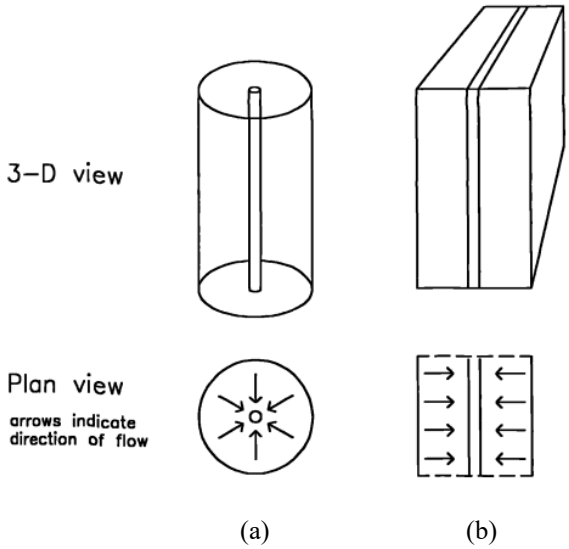

Figure 2.15. Direction of flow for PVDs in (a) axisymmetric conditions (b) plane strain conditions (Almeida & Marques, 2013).

There are several methods available to numerically model the effects of PVDs in plane strain, including the mathematical matching procedure introduced by Hird et al. (1992) and the homogenisation method using equivalent vertical permeability by Chai et al. (2001) described in the previous section. Various techniques can be employed, but the key factor common to all is the need for parameters that accurately represent the physical performance of the vertical drains being modelled.

One of the most important parameters that influences the consolidation rate of PVD-improved soil is the horizontal permeability (Chai & Miura, 1999). However, there is no satisfactory method available to test this parameter in a laboratory. Other influential parameters relating to PVD performance are:

- Diameter and spacing between drains
- Discharge capacity (well resistance)
- Drainage boundaries
- Overall smear effects

Except for the spacing between drains, there exist some uncertainties for quantifying these factors. In general, larger equivalent drain diameters result in smaller well resistance (greater discharge capacity) and a smaller smear effect gives a more effective vertical drain. The equivalent drain diameter, d_w, for a band shaped drain initially relied on the assumption of equal drainage perimeter. However, further research has shown that the presence of corner effects results in a smaller equivalent diameter (Chai & Miura, 1999). The equivalent drain diameter, d_w, depends on the width, w, and thickness, t, of the drain, according to equation (2.22).

$$d_w = \frac{w + t}{2} \tag{2.22}$$

The discharge capacity of PVDs have significant impact on drain behaviour. However, they require experimental determination and should be included by the provider of the drain. Moreover, according to Chai & Miura (1999), it is reasonable to assume a circular boundary of the smear zone, based on the rectangular shape of the mandrel and equal area assumption.

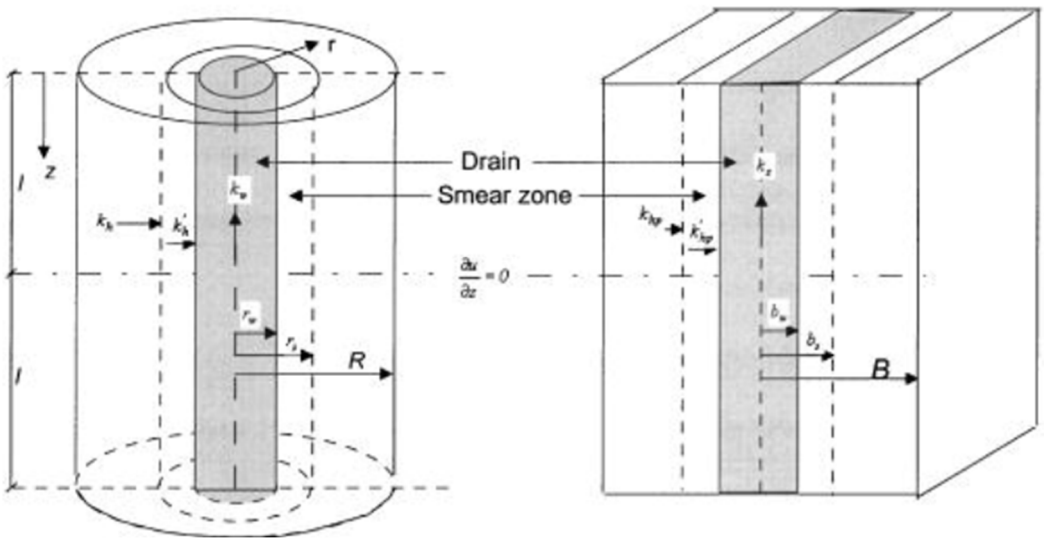

Figure 2.16. (a) Axisymmetric and (b) plane strain view of a PVD unit cell (Chai, et al., 1995).

To quantify the effect of the smear zone surrounding the drains on soil permeability, two parameters are required: the diameter of the smear zone (d_s) and the hydraulic conductivity ratio (k_h/k_s), which represents the ratio of horizontal hydraulic conductivity in the undisturbed zone (k_h) to that in the smear zone (k_s) (see illustration of parameters in Figure 2.16). An estimation of the diameter of the smear zone (d_s) can be made through equation (2.27).

$$d_s = (2\ to\ 3)d_m \tag{2.23}$$

Where d_m is the equivalent diameter of the mandrel. For the value of k_h/k_s there are many uncertainties. It is possible to determine the parameter in a laboratory, although the results are often underestimated due to sample disturbance and sample size (Chai & Miura, 1999). Moreover, as described in the previous section, the smear effect decreases with the radial distance from the drain. The value of k_h/k_s can be approximated by:

$$\frac{k_h}{k_s} = \left(\frac{k_h}{k_s}\right)_l \cdot C_f \tag{2.24}$$

Where l is determined using laboratory tests and C_f is the ratio of hydraulic conductivity when comparing laboratory and field values.

2.5. Numerical Modelling of Soft Soil

Numerical modelling provides a valuable tool for the geotechnical engineer in providing insights, predictions and allows for informed decision-making. It allows for explorations of different scenarios and evaluations of potential risks and mitigation measures, testing innovative solutions and assessing the long-term performance of geotechnical systems during the design phase.

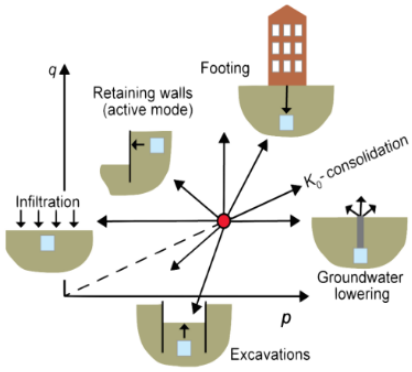

Figure 2.17. Typical loading paths associated with construction projects in urban areas (Karstunen, 2021).

In geotechnical design, situations where we have limited control over the applied loads and the resulting stress paths that develop from the coupled hydro-mechanical response of natural soil often emerge (Karstunen, 2021). This is especially true for underground projects in poulated areas, as depicted in Figure 2.17., where various total stress paths associated with different types of construction are represented by means of stress p and deviatoric stress q. Naturally, it is impractical to conduct extensive testing in every single project for all the possible stress paths. Thus, a representative constitutive model is needed (Karstunen & Amavasai, 2017).

A constitutive model is a generalized representation of the stress-strain relationship in soil when under surcharge loading (Potts, 2003). An instance familiar to most geotechnical engineers where a constitutive model is applied is when conducting slope stability analyses using the limit equilibrium method. In this method, a rigid-perfectly plastic behaviour is assumed in the soil implying it remain completely undeformed until a failure occurs (see Figure 2.18) (Karstunen & Amavasai, 2017). Furthermore, elasto-plastic perfectly plastic constitutive models include, i.e., the Mohr Coulomb model. The model assumes a purely linear elastic response until a point of failure is reached after which perfect plastic deformations are calculated, with the points being the principal stresses that define the yield surface.

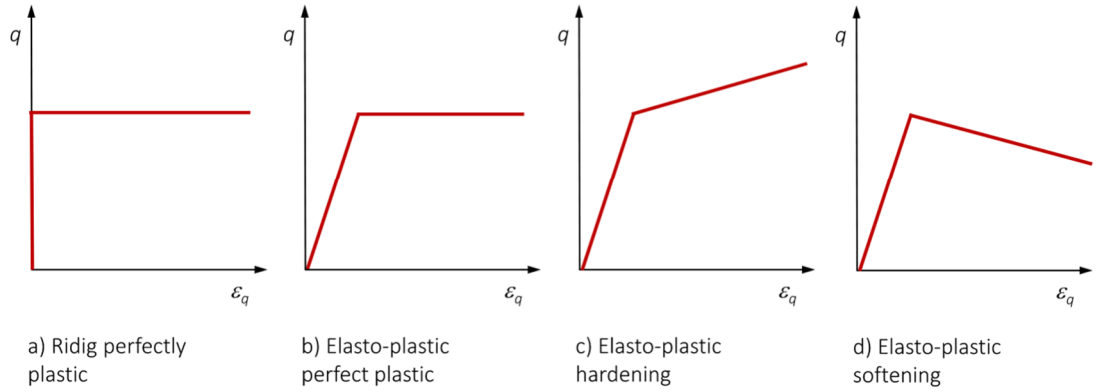

Figure 2.18. Various classifications of elasto-plastic models (Karstunen & Amavasai, 2017).

Rate-independent elasto-plastic constitutive models encompass several fundamental properties, including: an elastic law, yield surface, flow rule and hardening law.

An *elastic law* defines the stress-strain relationship under elastic conditions and determines the calculation of elastic (recoverable) strains.

The *yield surface* is what defines the boundary of small, recoverable (elastic) strains, and the larger irrecoverable (plastic) strains (Phillips & Sierakowski, 1965). Mathematical formulations utilized to describe the yield surfaces vary among different models.

A *flow rule* is essential as it determines the direction of the stress path during plastic flow, thus, defining the magnitude of calculated incremental strains. In generalized elasto-plastic models, the ratio of incremental strains varies depending on the type of loading must be defined accordingly (Amavasai, et al., 2017).

As described previously in section 2.1, soft soils commonly experience substantial contraction or volumetric reduction when under surcharge loading. Hence, an elasto-plastic perfectly plastic constitutive model proves totally inadequate for accurately representing the stress-strain behaviour of soft clays that are normally consolidated or lightly over consolidated. For soft soil conditions, models that exhibit an elasto-plastic

hardening or softening behaviour are more appropriate (see Figure 2.18) (Karstunen & Amavasai, 2017).

Hardening laws characterize the evolution and size of the yield surface based on the increments of plastic strains. The hardening models have the capability to provide explanations for several observed occurrences in soil, including the influence of stress history on soil stiffness and the increase of undrained shear strength during the consolidation process (Ti, et al., 2009). One example of such models is the hardening soil model. On the other hand, if the effect of degradation of mobilised shear strength in the soil needs to be accounted for, as would be necessary for sensitive soft clays, models that enable strain softening are required (see Figure 2.18).

Rate-dependent (creep) models, such as the Creep-SCLAY1S model explored in this thesis, are built on similar concepts but with but with modifications. The most significant distinction being that it does not have a purely elastic region, like the Mohr-Coulomb or the Hardening Soil model. Creep-SCLAY1S is a rate-dependent enhancement of the Modified Cam Clay (MCC) model. Instead of a yield surface, the Creep-SCLAY1S model, and similar rate-dependent models such as Soft Soil Creep, introduce the idea of a Normal Compression surface (NCS). The surface constitutes the boundary between small, recoverable, strains and more significant, irrecoverable creep strains. This concept will be elaborated on in the following section.

2.6. Creep-SCLAY1S Model

Creep-SCLAY1S is a constitutive model for soft clays capable of simulating features of soil behaviour like anisotropy, structural degradation, and rate-dependency (Amavasai, et al., 2017). The model is a further developed version of the Creep-SCLAY1 model introduced through a collaboration between, Chalmers University of Technology, Plaxis bv and NGI (Karstunen & Amavasai, 2017). Creep-SCLAY1 originated from the Modified Cam Clay model but was further extended on the ideas by Wheeler et al. (2003) and Karstunen et al. (2005), with adaptations for application on sensitive natural clays. For the sake of simplicity, the model is mathematically formulated in the triaxial stress space, see Figure 2.19. Therefore, it can only be used to model samples vertically cut form the soil deposit (cross-anisotropic) which are subjected to triaxial or oedometric loading (Sivasithamparam, et al., 2015).

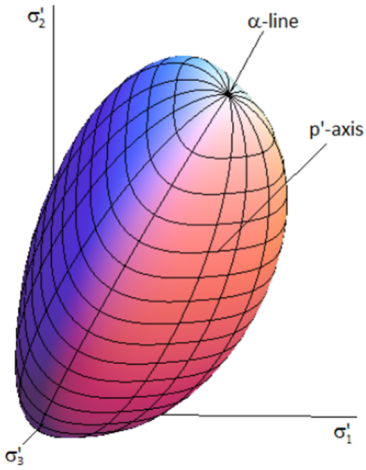

Figure 2.19. General stress space of Creep-SCLAY1S model (Karstunen, et al., 2013)

The fundamental assumption in the Creep-SCLAY1S model is that a purely elastic region does not exist (Amavasai, et al., 2018). Consequently, viscoplastic (creep) deformations take place at all stress levels. The total strain rate is mathematically represented through an additive law combining both the elastic and viscoplastic components, as demonstrated in equations (2.25) & (2.26) (Sivasithamparam, et al., 2015).

$$\dot{\varepsilon}_v = \dot{\varepsilon}_v^e + \dot{\varepsilon}_v^c \tag{2.25}$$

$$\dot{\varepsilon}_q = \dot{\varepsilon}_q^e + \dot{\varepsilon}_q^c \tag{2.26}$$

where ε equals strain and dot over symbol refers to rate (differentiation with respect to time). The superscript e refers to the elastic component and c to the viscoplastic component. Subscripts v refer to the volumetric part and q refer to the deviatoric part.

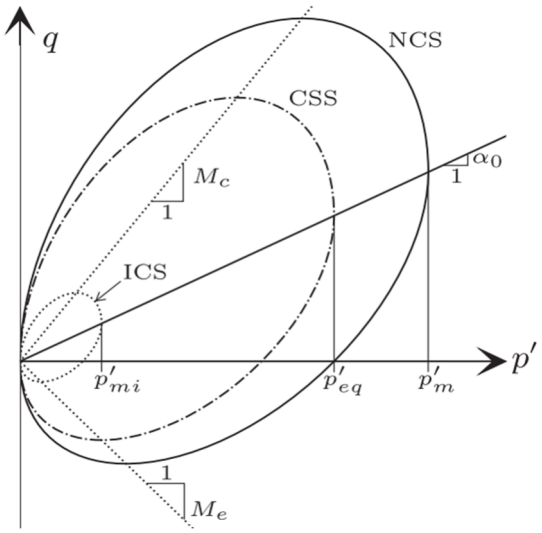

Figure 2.20. Constitutive yield surfaces for the Creep-SCLAY1S model (Tornborg, et al., 2021).

The model comprises thee yield surfaces which are defined simplistically in the triaxial stress space, see Figure 2.20 (Amavasai, et al., 2017). The Normal Consolidation Surface (NCS) is analogous to, and serves as, a boundary surface between small and large creep strains. Here, the apparent pre-consolidation pressure of natural clay is used to determine the size of the surface (denoted by p'_m in Figure 2.20). The second surface CSS, or the Current Stress Surface, represents the present effective stress state of the soil. Consequently, the modified over-consolidation ratio (OCR^*) is determined by the ratio between the size of the CSS (defined by p'_{eq} in Figure 2.20) and the size of the NCS. To incorporate the effects of structural degradation, an Intrinsic Compression Surface (ICS) is introduced (Sivasithamparam, et al., 2015). The size of the ICS (denoted as p'_{mi} in Figure 2.20) is defined and related to the size of the NCS using equation (2.27). Moreover, NCS, ICS and CSS have similar orientation and shape and are defined using equation (2.28).

$$p'_m = p'_{mi}(1 + \chi) \tag{2.27}$$

$$p'_s = p' + \frac{(q - \alpha p')^2}{(M(\theta_\alpha)^2 - \alpha^2)p'} \tag{2.28}$$

where p' represents the mean effective stress and q the deviatoric stress. χ represents the current amount of bonding present in the soil. The term p'_s can be substituted with p'_m p'_{eq} p'_{mi} to define the respective surface, see Figure 2.20. α is a scalar state variable which corresponds to the orientation of the yield surface in the simplified triaxial stress space, see, indicating the change in soil anisotropy (Karstunen & Amavasai, 2017). $M(\theta_\alpha)$ represents the formulation of the modified Lode angle of the critical state, which governs the inclination of the critical state in triaxial compression (M_c) and extension (M_e) (see Figure 2.21). By incorporating a Lode angle dependency, a smooth yield surface is obtained by avoiding sharp corners and thus simplifies numerical computations (Sivasithamparam, et al., 2015). The formulation of (2.29) the critical slope dependent Lode angle is expressed as:

$$M(\theta_\alpha) = M_c \left(\frac{2m^4}{1 + m^4 + (1 - m^4)\sin 3\theta_\alpha} \right)^{1/4} \tag{2.29}$$

and

$$\sin 3\theta_\alpha = -\left[\frac{3\sqrt{3}}{2} \frac{(J_3)_\alpha}{(J_2)_\alpha^{3/2}} \right] \tag{2.30}$$

In Figure 2.21 the Lode angle is depicted for variations in the value of m, where m is defined as M_e/M_c. Further, $(J_2)_\alpha$ and $(J_3)_\alpha$ define invariants of the modified deviatoric stress tensor.

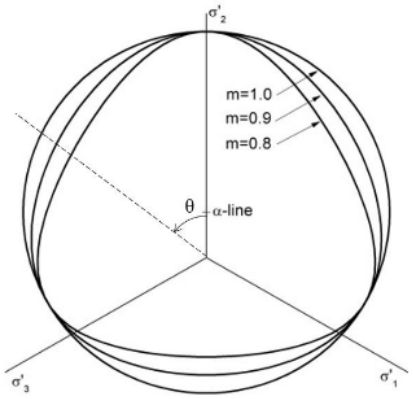

Figure 2.21 Lode angle dependency of the stress state in Creep-SCLAY1S model in π -plane (Sivasithamparam, et al., 2015).

Three different hardening laws are accounted for in the Creep-SCLAY1S model (Karstunen & Amavasai, 2017). The first rule of isotropic hardening is related to the variation of the intrinsic isotropic pre-consolidation pressure p'_{mi} as well as the viscoplastic volumetric strain rate $\dot{\varepsilon}_v^c$ though equation (2.31).

$$p'_m = \frac{p'_{mi}}{\lambda_i^* - \kappa^*}\dot{\varepsilon}_v^c \tag{2.31}$$

where λ_i^* is the modified compression index and represents the stiffness in the soil, with the subscript i indicating an intrinsic material state, derived at large strains where complete loss of structure has occurred. κ^* is the modified compression index.

The second hardening law express the variation of the orientation of the reference surface due to the viscoplastic strain rate as formulated by (Leoni, et al., 2008), see equation (2.32).

$$\dot{\alpha}_d = \omega\left(\left[\frac{3\eta}{4} - \alpha_d\right]\langle\dot{\varepsilon}_v^c\rangle + \omega_d\left[\frac{\eta}{3} - \alpha_d\right]\dot{\varepsilon}_d^c\right) \tag{2.32}$$

where η is the stress ratio ($\eta = q/p'$) and ω and ω_d are model constants that are related to evolution of anisotropy. ω controls absolute effectiveness of rotational hardening while ω_d controls the relative effectiveness of rotational hardening due to viscoplastic strain rate in the deviatoric plane (Amavasai, et al., 2017).

The third hardening rule addresses the degradation of bonding to the increase of viscoplastic strains. The variation in the parameter χ is determined by the rates of volumetric and deviatoric viscoplastic strain, and is influenced by the two parameters ξ_v and ξ_d as expressed in (2.33) (Karstunen & Amavasai, 2017). ξ_v governs the absolute rate of structural degradation while ξ_d regulates the impact of deviatoric viscoplastic strain rate on relative effectiveness of structural degradation.

$$\dot{\chi} = \xi_v([0-\chi]|\dot{\varepsilon}_v^c| + \xi_d[0-\chi]|\dot{\varepsilon}_d^c|) = -\xi_v\chi(|\dot{\varepsilon}_v^c| + \xi_d|\dot{\varepsilon}_d^c|) \tag{2.33}$$

In the Creep-SCLAY1S model, an associated flow rule is assumed, as is reasonable due to evolution of anisotropy being included in the formulation (Sivasithamparam, et al., 2015). Thus, the creep related strain rates are defined as (2.34), where $\dot{\Lambda}$ is the viscoplastic multiplier, defined in (2.35), incorporated to capture the rate dependent behaviour (creep) in the soil (Grimstad, et al., 2010)

$$\dot{\varepsilon}_{ij}^c = \dot{\Lambda}\frac{\delta {p'}_{eq}}{\delta {\sigma'}_{ij}} \tag{2.34}$$

$$\dot{\Lambda} = \frac{\mu_i^*}{\tau}\left(\frac{{p'}_{eq}}{(1-\chi){p'}_{mi}}\right)^{\beta}\left(\frac{M_c^2 - \alpha_{K_0^{NC}}^2}{M_c^2 - \eta_{K_0^{NC}}^2}\right) \text{ and } \beta = \frac{\lambda_i^* - \kappa_i}{\mu_i^*} \tag{2.35}$$

where μ_i^* is the intrinsic modified creep index, corresponding to intrinsic material properties as all internal structure of the soil is erased. τ is the reference time which describes at what duration (time increment) the incremental loading laboratory test, used for determining the pre-consolidation pressure, is conducted at. $\alpha_{K_0^{NC}}$ is an expression of the inclination of the constitutive ellipses that correspond to the initial K_0 conditions, while $\eta_{K_0^{NC}}$ refers to its stress ration while in the normally consolidated state.

As evident, the Creep-SCLAY1S model is designed to comprehensively address multiple aspects of natural soil behaviour, which necessitates the utilization of an extensive array of input parameters. In the following section the individual parameters used in the model are described.

2.6.1. Parameters

The following sections includes a description of the various input parameters for the Creep-SCLAY1S model. In Table 2.4 a summary of the parameters is presented along with required laboratory tests for determination of the parameter.

Table 2.4 Summary of input parameters and required laboratory test.

Parameter type	Parameter	Symbol	Required laboratory test
Conventional parameters	Modified swelling index	κ^*	Oedometer IL or CRS test
	Poisson's ratio	ν'	Triaxial test
	Modified intrinsic compression index	λ_i^*	Oedometer IL or CRS test
	Stress ratio at critical state in triaxial compression	M_c	Triaxial compression test
	Stress ratio at critical state in triaxial extension	M_e	Triaxial extension test
Anisotropic parameters	Absolute effectiveness of rotational hardening	ω	Triaxial extension test
	Relative effectiveness of rotational hardening	ω_d	Calculated (see equation (2.43)
	Initial anisotropy	α_0	Calculated (see equation (2.42)
Bonding and destructuration parameters	Absolute rate of destructuration	ξ_v	Back calculated from Triaxial and IL/CRS test
	Relative rate of destructuration	ξ_d	Back calculated from Triaxial and IL/CRS test
	Initial bonding	χ_0	Estimated using sensitivity (S_t)
Viscous parameters	Modified intrinsic creep index	μ_i^*	Oedometer IL (creep) test
	Reference time (days)	τ	Oedometer IL average time step
Initial stress parameters	Pre-overburden pressure	POP	Oedometer IL or CRS test
	Over consolidation ratio	OCR	Oedometer IL or CRS test
	Lateral earth pressure at rest	K_0	K_0-triaxial test or calculated (see equation (2.12)
	Lateral earth pressure at rest for normally consolidated state	K_0^{NC}	Calculated (see equation (2.13)

2.6.1.1. Initial stress state parameters

The apparent pre-consolidation pressure is a crucial parameter in geotechnical analysis and has a large influence on predictions of creep models in general (Karstunen, 2021). As described in section 2.1.3 the value of σ'_c is affected by anthropological and geological processes and is thus very site-specific. For the Creep-SCLAY1S model the interpretation is best done in linear scale, as anisotropy may influence yielding when plotting in a semi-logarithmic scale (Karstunen & Amavasai, 2017). Moreover, as touched upon in sections 2.1.3 and 2.1.4, the derived values of σ'_c from laboratory tests is severely influenced by strain rate effects and sample disturbance and, consequently, as is the results of the conducted prediction. Thus, for the Creep-SCLAY1S model, it not advised to use CRS

tests when deriving the pre-consolidation pressure, rather, incremental loading tests (IL) are recommended (Karstunen & Amavasai, 2017). After determination of σ'_c POP and OCR can be calculated according to equations (2.10) and (2.11). Moreover, either a constant POP or a constant OCR should be selected as input for the model.

The values of the coefficient of lateral earth pressure at rest for the normally consolidated state, K_0^{NC}, and K_0 for the over consolidated state, are estimated with the friction angle at critical state φ'_c, using previously defined equations (2.13) and (2.14). In this case, the values of K_0 and K_0^{NC} are directly dependant on the value of M_c . However, these can also be calibrated and, if available, determined using advanced K_0-triaxial tests (Gras, et al., 2017).

2.6.1.2. Conventional parameters

Five of the total 10 parameters for the Creep-SClay1S model that can be defined using standard laboratory test data have similarities with the Modified Cam-Clay model (Sivasithamparam, et al., 2015). The conventional isotropic soil constants used in the model include ν', λ_i^*, κ^*, M_c and M_e.

Poisson's ratio for unloading - reloading, denoted as ν', is a purely elastic soil constant. In the case of soft soils, like clay, it is commonly assumed at a constant value ranging between 0.1 and 0.2 (Karstunen & Amavasai, 2017).

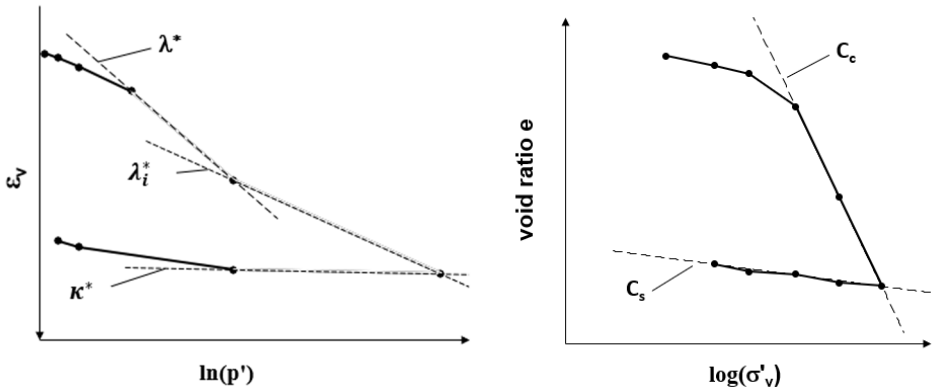

Figure 2.22. Illustration of determination of stiffness parameters (a) λ^*, λ_i^*, $\kappa^*$and (b) C_c and C_s (Gras, et al., 2017).

In the Creep-SCLAY1S model, one of the parameters relating to the stiffness in the soil is the modified intrinsic compression index, λ_i^*. This can be determined from an oedometer IL test but using reconstituted samples, or analogously to the similar modified compression index, λ^*, but from a high enough stress state in the test that all inter-particle bonds are erased (see Figure 2.22) (Karstunen & Amavasai, 2017). The modified swelling index, κ^*, also relating to the stiffness of the soil, is not defined as a constant used for natural clays with high sensitivity. However, for the purpose of modelling the highest gradient from an incremental loading test can be used (Sivasithamparam, et al., 2015).

The parameters λ^* and κ^* correspond to a radial stress path in a $p' - q$ plane as they are determined in a semi-logarithmic $\varepsilon_v - \ln(p')$ scale (see Figure 2.22), where ε_v is the volumetric strain and p' is the mean effective stress. Moreover, as seen in Figure 2.22, they can be related to their 1D equivalents in an $e - \log(\sigma'_v)$ (or $\varepsilon_v - \log(\sigma'_v)$) plot, i.e., the compression index, C_c, and swelling index C_s respectively. The relationship is defined by equations (2.36)-(2.38).

$$C_c = \frac{\Delta e}{\Delta \log(\sigma'_v)} \qquad C_s = \frac{\Delta e}{\Delta \log(\sigma'_v)} \tag{2.36}$$

$$\lambda^* = \frac{\lambda}{1 + e_0} \qquad \kappa^* = \frac{\kappa}{1 + e_0} \tag{2.37}$$

$$\lambda^* = \frac{C_c}{2.3(1 + e_0)} \qquad \kappa^* \approx \frac{2\,C_s}{2.3(1 + e_0)} \tag{2.38}$$

where e_0 is the initial void ratio.

The parameter M denotes the stress ratio at critical state (q/p'), where M_c correspond to the critical state line in triaxial compression and M_e for triaxial extension. M_c is determined using anisotropically consolidated undrained triaxial tests in compression (CAUC). In, i.e., excavation problems, it is preferable to have an additional test with shearing in extension (CAUE) for determination of M_e (Karstunen, 2021). The method for determination of M_c and M_e are presented in equations (2.39) and (2.40) (Muir Wood, 1990).

$$M_c = \frac{6\,sin\varphi'_c}{3 - sin\varphi'_c} \tag{2.39}$$

$$M_e = \frac{6\,sin\varphi'_c}{3 + sin\varphi'_c} \tag{2.40}$$

where ϕ'_c is the friction angle at critical state.

If triaxial extension tests are unavailable, M_e, can be calculated using M_c, by assuming an equal friction angle in extension and compression by using the Mohr-Coulomb failure criterion, see equation (2.41).

$$sin\,\varphi'_c = \frac{3\,M_e}{6 - M_e} \tag{2.41}$$

2.6.1.3. Anisotropic parameters

During deposition, sedimentation, consolidation history and any subsequent straining, natural soft clays develop a substantial degree of anisotropy (Yin & Karstunen, 2011). This has a significant influence on the stress-strain behaviour of soft clays, particularly in terms of their viscous behaviour and deformations. Consequently, this need to be considered in analysis and predictions related to the mechanical response of the soil (Leoni, et al., 2008). The Creep-SCLAY1S model accounts for this phenomenon though including the state parameter α_0 that characterise the anisotropy of the soil deposit by describing the initial rotation of the yield surface. An approximation for the initial rotation can be expressed using equation (2.42) α_0 depends on M_c and the normally consolidated stress ratio η_{K_0} (Wheeler, et al., 2003).

$$\alpha_0 = \frac{\eta_{K_0}^2 + 3\eta_{K_0} - M_c^2}{3} \text{ where } \eta_{K_0} = \frac{3(1 - K_0^{NC})}{(1 + 2K_0^{NC})} \tag{2.42}$$

If advanced K_0-triaxial tests are not available, K_0^{NC} can be determined by Jaky's formula, see equation (2.13). In generalised 2D and 3D form the scalar α_0 is replaced by a deviatoric fabric tensor that is analogous to the deviator stress tensor (Wheeler, et al., 2003).

Furthermore, the value of ω_d determines the relative effectiveness of rotational hardening and depends on M_c and η_{K_0}. It can be evaluated using equation (2.43) (Wheeler, et al., 2003).

$$\omega_d = \frac{3}{8}\frac{\left(4M_c^2 - 4\eta_{K_0}^2 - 3\eta_{K_0}\right)}{\left(\eta_{K_0}^2 - M_c^2 + 2\eta_{K_0}\right)} \tag{2.43}$$

The initial value obtained for the parameter representing the absolute effectiveness of rotational hardening, ω, can be determined using equation (2.44). ω is also possible to calibrate through simulation of a triaxial test that is anisotropically consolidated to in-situ conditions and sheared to failure in extension (Karstunen & Amavasai, 2017).

$$\omega \approx \frac{1}{(\lambda_i^* - \kappa^*)} ln\left(\frac{10M_c^2 + 2\alpha_0\omega_d}{M_c^2 + 2\alpha_0\omega_d}\right) \tag{2.44}$$

where other parameters are previously defined.

2.6.1.4. Bonding and destructuration

In addition to anisotropy, it is common for natural soils to display some form of apparent bonding. Furthermore, as natural clays undergo deformation, the initial apparent bonding gradually diminishes. Thus, at significant strains, the soil begins to exhibit behaviour similar to fully reconstituted material, see Figure 2.23 (Yin & Karstunen, 2011). In the

Creep-SCLAY1S model the effects of bonding and destructuration is incorporated using a scalar quantity, χ, representing the amount of bonding between particles. χ_0 is a state parameter defining the initial amount of bonding in the soil, relating intact soil samples to reconstituted samples where all bonding of the soil is erased, see Figure 2.23 (Yin & Karstunen, 2011). The initial amount of bonding is expressed using the sensitivity of the soil through:

$$\chi_0 = S_t - 1 \tag{2.45}$$

where he sensitivity S_t represents the relationship between the undisturbed peak strength and the remoulded strength of the soil and can be determined using various measurement methods. Some common approached include field or laboratory vane tests and the Swedish fall-cone test (Gras, et al., 2017).

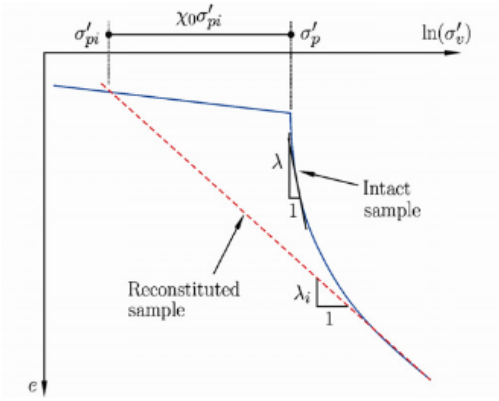

Figure 2.23. Relationship between intact and reconstituted soil samples of sensitive clay (Yin & Karstunen, 2011)

Furthermore, the model parameters ξ_v and ξ_d govern the degradation of bonds in the soil due to volumetric and deviatoric strains respectively. However, these parameters are not derived directly from standard laboratory test and require optimisation.

2.6.1.5. Viscous parameters

The intrinsic modified creep index, μ_i^*, is determined by the inclination of the curve in the $\varepsilon_v - ln(\mathrm{t})$ plane at the end of the consolidation phase in an oedometer test, see Figure 2.24. The notation i determines it is an intrinsic parameter and should subsequently be derived at large stresses, or reconstituted samples, where all internal structure of the soil is erased (Gras, et al., 2017).

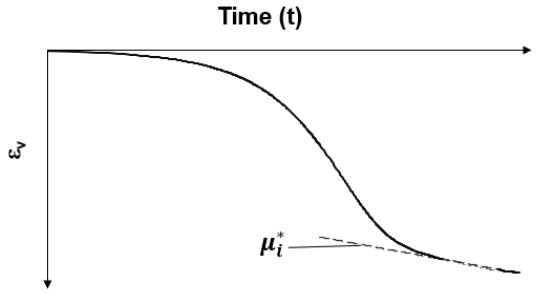

Figure 2.24. Procedure for determination of μ_i^* at high stress levels where all soil structure is erased.

Moreover, it is also possible to derive the parameter μ_i^* using the intrinsic secondary compression index $C_{\alpha i}$ (corresponding to high enough stress levels) described in section 2.1.1 using the relation:

$$\mu_i^* = \frac{C_{\alpha i}}{2.3(1+e_0)} \tag{2.46}$$

Where $C_{\alpha i} = \Delta e / \Delta \log(t)$

The reference time, τ, represents the duration, in days, of the load step in the oedometer test that is conducted to determine the initial pre-consolidation pressure. If the test is done using 24-hour loads step the reference time is set to 1 (Gras, et al., 2017).

3. Ballina Trial Embankments

The case study for this thesis relates to the Ballina trial embankment. Ballina is a test site with full-scale trial embankments constructed at the National Field-Testing Facility (NFTF) for soft soils in Ballina, New South Wales. The concept was brought forward by the Ballina Bypass Alliance after facing challenges during the construction of a nearby highway. Over a span of 3 years, a maximum settlement of 6.4 m settlements occurred (up to 14 m embankment fill) (Kelly, et al., 2017). Currently, there is around 150 km of highway under construction in the general area of Ballina, of which about 25 km consists of soft soils. Accurately predicting the settlement, the rate at which it occurred and the horizontal movements in the soil proved to be difficult. This led to the field-testing facility being established after the Australian Research Council Centre of Excellence for Geotechnical Science and Engineering (CGSE) took up on the idea. The overall motivation of the research project was to improve the process of design and construction of infrastructure on naturally deposited soft soil (Pineda, et al., 2019). The site in Ballina offered an ideal location for a test facility due to its convenient access, favourable ground conditions, and close proximity to ground conditions of the planned projects.

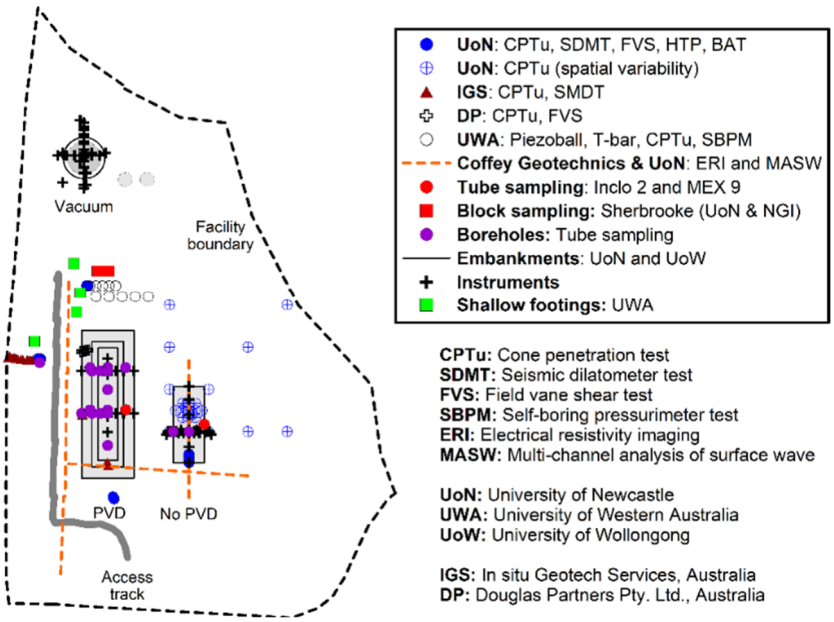

Figure 3.1. Plan view of the Ballina National Field-Testing Facility including location of in-situ tests conducted at the site (Kelly, et al., 2017).

Two embankments were built at the site in 2013. A plan view with location of conducted in-situ tests and boreholes can be seen in Figure 3.1. One of the embankments was constructed with conventional PVDs (Prefabricated Vertical Drains), as well as biodegradable jute drains, and the other without any drains installed (Kelly, et al., 2017). In this thesis, both embankments will be modelled. However, only the embankment modelled with drains is compared with measurement data (class C prediction). The

embankment without drains will be modelled as a class A prediction, as there are currently no published results available.

Before construction, soil samples of high quality were obtained and subjected to advanced laboratory testing and the site was instrumented extensively. Installed instruments gathered data on deformations in vertical and horizontal direction as well as pore pressures and vertical- and horizontal soil pressures. Measurements were recorded at the site for 3 years.

3.1. Geological Setting

Situated in the northwestern area of Ballina, the site spans across 6.5 hectares of land that was previously utilised for agricultural purposes. Figure 3.2 provides an illustration of the sites position within the regional context (Pineda, et al., 2019).

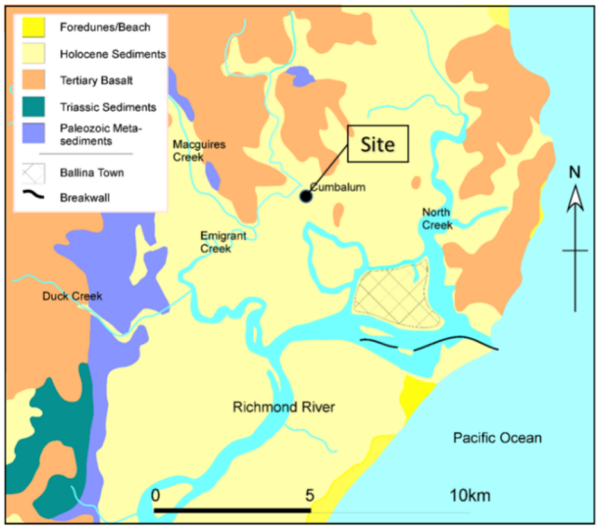

Figure 3.2. Geological setting of the Ballina National Field-Testing Facility (NFT) (Pineda, et al., 2019).

The ground surface at the Ballina site is situated at 0.5 m Australian height datum (AHD). The geological composition of the area corresponds to the infilling materials found in the Richmond River Valley in northern New South Wales with specifically consisting of estuarine quaternary sediments. According to Kelly et al. (2017) the area can be classified into three different stages of deposition. The first stage primarily comprises deep deposits of dense, heavily altered fluvial sandy gravels which are knows as South Casina Gravel, accompanied by highly compacted and eroded clays referred to as Dungarubba Clay. The second and third stage consist mainly of gravels, sandy clays (at lower levels) and prevalent grey shelly muds along the strata. In the lower levels, the clay is referred to as Gundarimba Clay (Pineda, et al., 2016). The upper estuarine clays, including the soft soil at Ballina, form the Pimlico Clay unit, with variable thickness ranging from 10-40 meters. South Casino Gravel, Dungarubba Clay, and Gundarimba Clay are believed to date back to the Pleistocene age, while the deposition of Pimlica clay is associated with the

Halocene age. The Pimlica clay, also known as soft Ballina clay, consist of mainly illite and kaolinite, indicating the clay has low potential for swelling (Amavasai, et al., 2018). Furthermore, based on results from oedometer tests, Kelly et al. (2017) states that the clays in the are above 4 m depth exhibit some structure as they were deposited flat tidal environment. On the other hand, clays located at a depth below 4 m were deposited in a less dynamic deep-water environment, allowing for a more open structure to form in the soil. In general, the observed behaviour of Ballina soft Clay, is remarkably consistent with those of most soft clay deposits. Therefore, the geographical location of a trial embankment in Ballina was well selected (Kelly, et al., 2017).

3.2. Embankment with PVDs

The embankment with PVDs is 3 m high, 80 m long and 14 m wide with slopes of inclination 1:1.5. For the construction of the embankment and installation of PVDs a working platform (95m long, 25 m in width and 0.6 m high) was placed beneath the footprint of the embankment. Between the working platform and the embankment fill a horizontal sand drainage layer was constructed. The PVDs were installed in a square grid with a nominal centre-to-centre distance of 1.2 m. Two types of drains were used at the site. One area with conventional CeTeau PVDs and one area with biodegradable Jute drains. The embankment fill consists of gravel and the construction schedule is presented in APPENDIX A. An illustration of the PVD-improved embankment, including an initial approximate soil profile can be seen in Figure 3.3.The geometry of the embankment without PVDs is unknown and is assumed to have the same cross-section as the improved embankment.

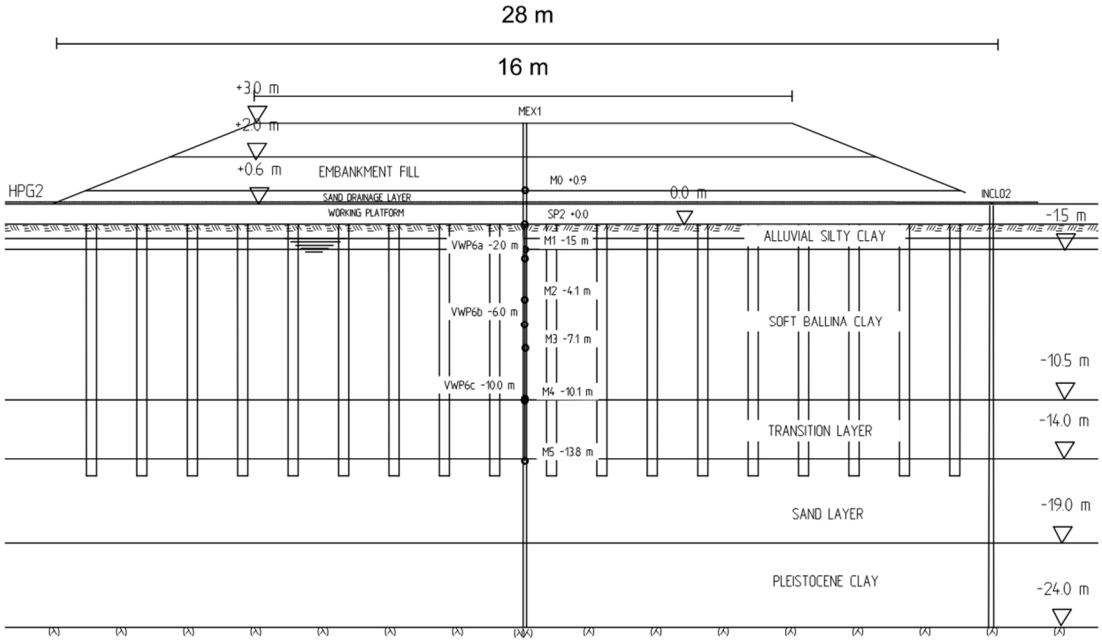

Figure 3.3. Illustration of the Ballina trial embankment, approximate soil profile and most relevant instrumentation in cross section 2 (not to scale).

Two primary sets of instruments (cross section 2 & 3) were deployed at the embankment with PVDs: one in the section containing Jute drains and another in the section with conventional Wick drains (Kelly, et al., 2017). A plan view of the site and instrumentation can be seen in Figure 3.4. Before the construction, four settlement plates (SP) were positioned along the embankment centreline to monitor the ground surface settlement beneath it. Each of the two instrument lines has a hydrostatic profile gauge installed. These gauges provided continuous measurements of settlement across the entire width of the embankment. To assess deformations in various layers of the soil, spider magnets were installed near the upper and lower boundaries of the sand, within the transition layer, as well as in the estuarine clay and alluvial clay layer. Additionally, an extra plate magnet was placed within the embankment fill after constructing the working platform. To measure pore water pressures, vibrating wire piezometers (VWPs) were installed in the centreline of the embankment. At each location, three piezometers were installed at nominal depths of 2 m, 6 m, and 10 m. To measure the loads imposed by the embankment on the ground surface, six total pressure cells (TPCs) were installed along the embankment at ground level. To monitor lateral deformations of the soil, four inclinometers were installed on each side of every instrumentation line. These inclinometers were positioned within the working platform at the toe of the embankment (Kelly, et al., 2017).

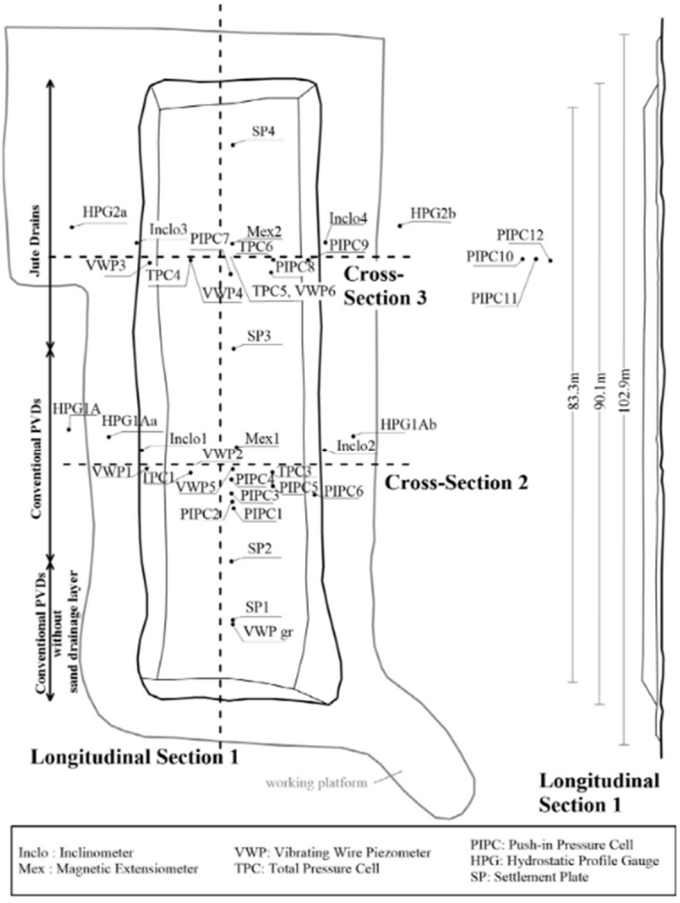

Figure 3.4. Plan view of instrumentation at the PVD-improved embankment in Ballina (Kelly, et al., 2017).

3.3. Soil Profile

The first layer beneath the embankment up to 1.5 m depth consists of a heterogenous layer of different compositions of alluvial silt, clay, and sand with high organic content. The soft Ballina clay (Pimlico clay) is found between around 1.5 m to 10.5 m depth. This layer will be characterised and described in more detail in the next section. From 10.5 to 14 m depth is a transition layer with gradually higher sand content, followed by a permeable sand layer up to 19 m depth. Above the bedrock lies the stiff Pleistocene clay deposit.

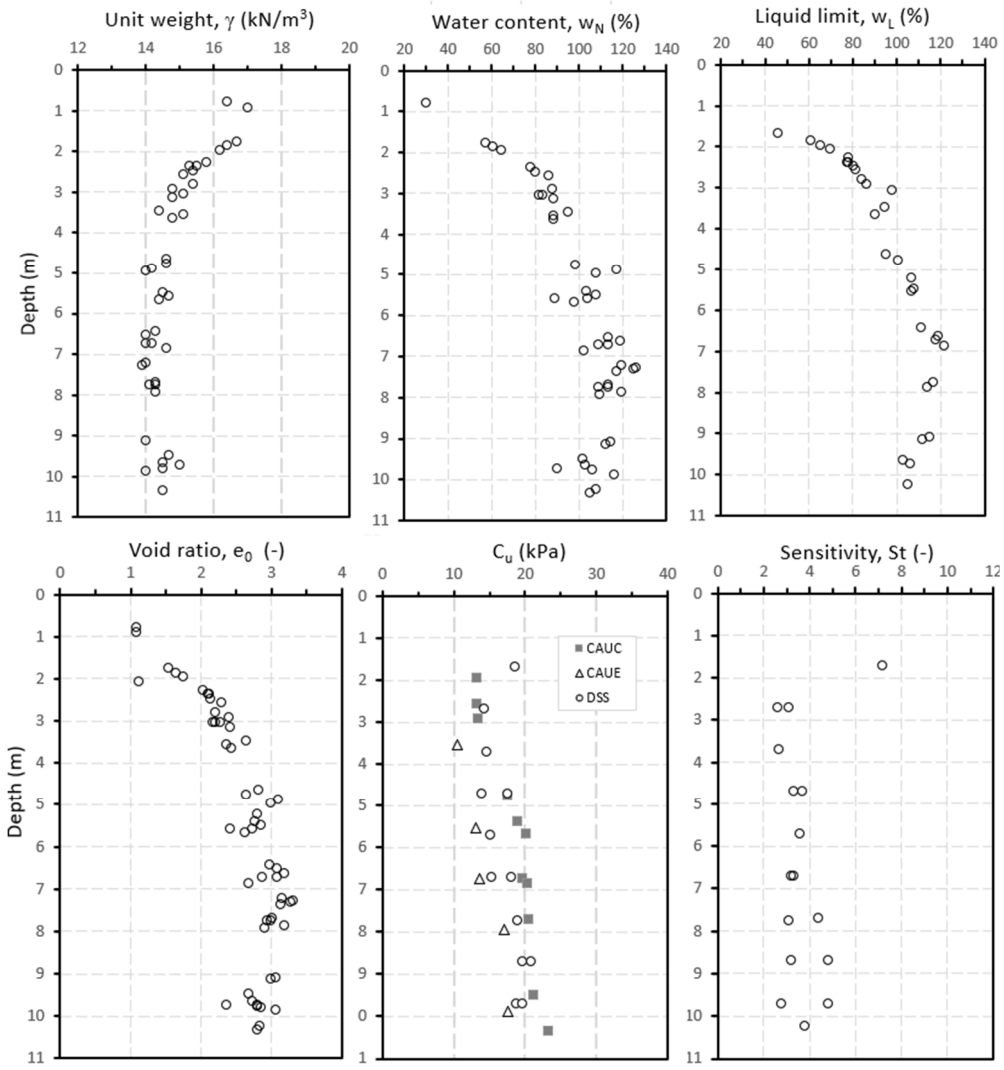

Figure 3.5. Soil properties at the site for the Ballina trial embankment

As when establishing any geotechnical analysis, an often most crucial step involves analysing soil index properties and partitioning the soil into sequential, representative layers. This is especially true when setting up for a numerical analysis for a boundary value problem. Ideally, this is done to accurately interpret in-situ soil conditions, and to simplify the process of parameter derivation, as soft soil is rarely homogenous. However,

this process is often restricted by amount of field- and laboratory tests available. As field and laboratory testing is extensive at the Ballina site, the process of interpreting layers is relatively straight forward. Especially the soil unit weight, water content, liquid limit and void ratio exhibit some grouping along the depth of the soil deposit.

For the Ballina Trial Embankment, an initial approximation of soil layers is obtained by analysing soil index properties using the in-situ water content, w_N, unit weight, γ, and initial void ratio, e_0. Additionally, results from conducted field tests, i.e., CPTU were used. Obtained soil properties for the Ballina embankment are presented in Figure 3.5.

The unit weight of the soil varies between 13.9 – 17.1 kN/m³ with the highest values in the shallow alluvium layer and the top of the soft clay, see Figure 3.5. The maximum measured clay content in the deposit is 70 – 80% observed around 6-8 m depth. The water content generally varies from 60 – 130% with lower values in the shallow parts of the deposit and increase with depth. A clear correlation between water content and the liquid limit can be observed as the water content is roughly equal or less throughout. However, the dry crust exhibit considerably lower water content of around 30%. This could be due to natural ground water fluctuations or desiccation from high temperatures. Desiccation can lead to crack propagation and swelling of the soil, subsequently leading to a reduction in void ratio in the shallow layer, which can be observed in Figure 3.5. Furthermore, the undrained shear strength of the soil is approximately 13 kPa in the first 4 meters, from where it increases linearly. The sensitivity of the soil typically ranges between 2 and 5, with a higher value of 7 at 1.5 m depth.

When a preliminary estimation of layers is established, results from conducted laboratory tests can be used to assist in process of layering. In the case for the Ballina embankment there are 23 available CRS tests form borehole INCLO2. Using the preliminary layers, the CRS data with similar initial void ratio e_0 is plotted on top of each other in a $e - \log(\sigma'_v)$ plot to confirm the layers (see Figure 3.6). Generally, a good agreement is found. Moreover, plotting pre-consolidation pressure from laboratory tests against depth can be used for confirming the layers. The process of deriving σ'_c will be described in the next section.

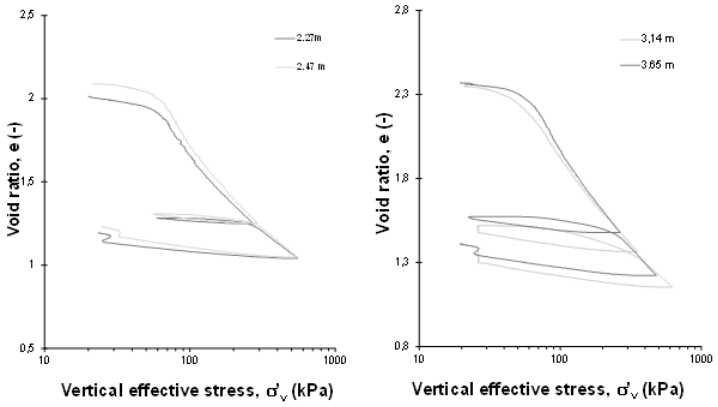

Figure 3.6. Example of layering procedure using CRS tests.

When soil layers are estimated through field tests and index properties, and confirmed through laboratory test results, the soil, and the parameters previously mentioned are divided into layers. Figure 3.7 shows the results of the soft soil characterisation process where soft soil deposit that precedes the transition layer is divided into 5 sublayers at different depth with varying properties. Representative values for unit weight, γ, the in-situ water content, w_N, liquid limit, w_L, initial void ratio, e_0, undrained shear strength, c_u, and sensitivity, s_t are presented.

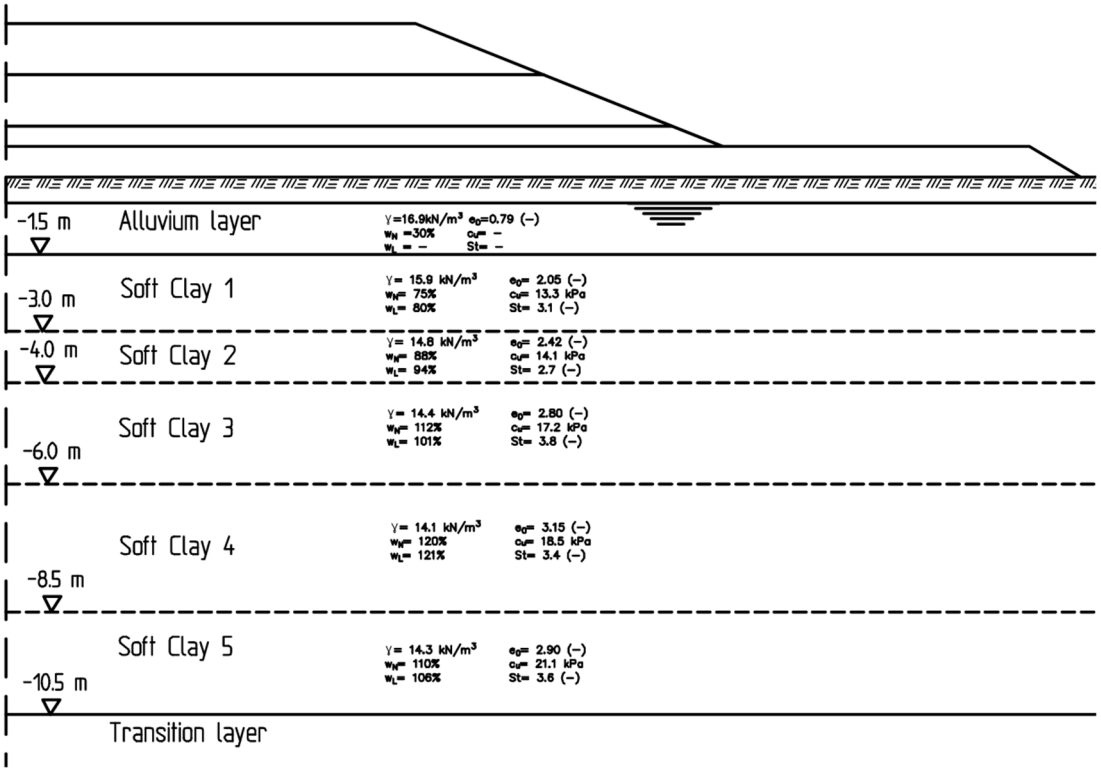

Figure 3.7. Illustration of soft Ballina clay layer with assigned soil properties for each layer respectively.

4. Modelling of Embankment

The following chapter includes a detailed description of the methodology behind the determination of model parameters, determination of hydraulic properties of the soil and calibration of model parameters against laboratory tests for the Creep-SCLAY1S model. Additionally, the setup of the numerical model in Plaxis 2D is presented, including geometry and design properties for both embankment as well as PVDs.

4.1. Parameter Determination

A crucial part of numerical analysis is the measurement and analysis of soil properties in a laboratory. If the material properties of the investigated soil are not clearly identified there is little to no point in doing refined analysis (Graham, 2006). As a foundation for the numerical analysis, extensive effort is put into deriving, calibrating, and optimizing required model parameters from the available laboratory data. An overview of the methodology of parameter derivation is presented in Figure 4.1

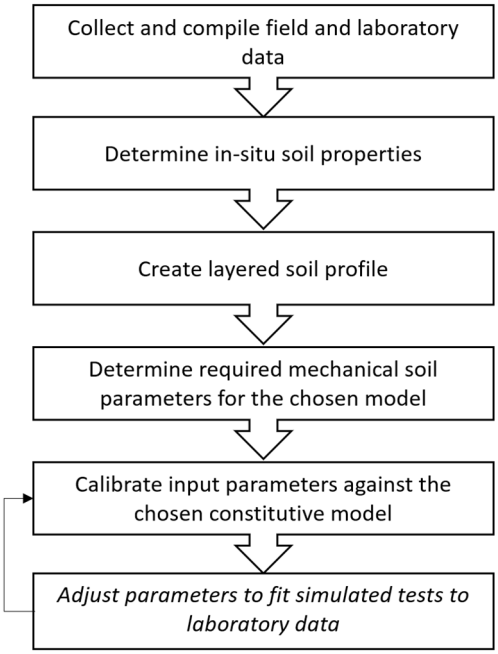

Figure 4.1. Methodology of parameter derivation.

As described in section 2.6.1.6 the Creep-SCLAY1S model requires a high number of parameters that are manually derived. The mechanical properties of the Ballina soil deposit are estimated using 23 constant rate of strain (CRS) oedometer tests, 6 incremental loading (IL) oedometer tests. Values for pre-consolidation pressure, soil stiffness and water permeability are estimated from CRS tests, whereas creep properties are derived from the IL tests.

The pre-consolidation pressure is obtained directly form the CRS and IL-tests using a straightforward, consistent, and easily replicable methodology. The procedure involves plotting the change in void ratio, *e,* against the logarithmically scaled effective vertical stress, σ'_v, and identifying the using the intersection point between an extrapolated linear fit of the over consolidated region and a similarly fitted extrapolated line of the normally consolidated region. In order to maintain consistency and repeatability. this intersection point is considered as the apparent pre-consolidation pressure. It should be noted that adjustments for potential sample disturbance or strain rate, as discussed in section 2, are not attempted during this process. Another important remark is that this method comes with a permissible margin of error. However, in this case where the amount of laboratory tests is high, consistency and repeatability of the approach is prioritized. Furthermore, values of POP or OCR are subsequently calibrated and optimized for the Creep-SCLAY1S model used. As σ'_c is determined, OCR and POP are calculated through equations presented in section 0 and plotted against depth, see Figure 4.2. The determined pre-consolidation pressures demonstrate a clear discrepancy between the values derived from the CRS oedometer test and IL oedometer tests respectively. This is likely due to the high strain rate adopted for the CRS tests (0.004 mm/min) and the long time-duration (5 days) of each load increment during the IL oedometer tests. As evident in Figure 4.2, even by adopting a correction factor of $0.84 \cdot \sigma'_c$ (recommended by Pineda et al. (2016) to account for the high strain-rate used in the CRS-tests) there is a significant difference between values from the two tests – demonstrating the difficulty of correcting strain-rate effects in CRS-tests.

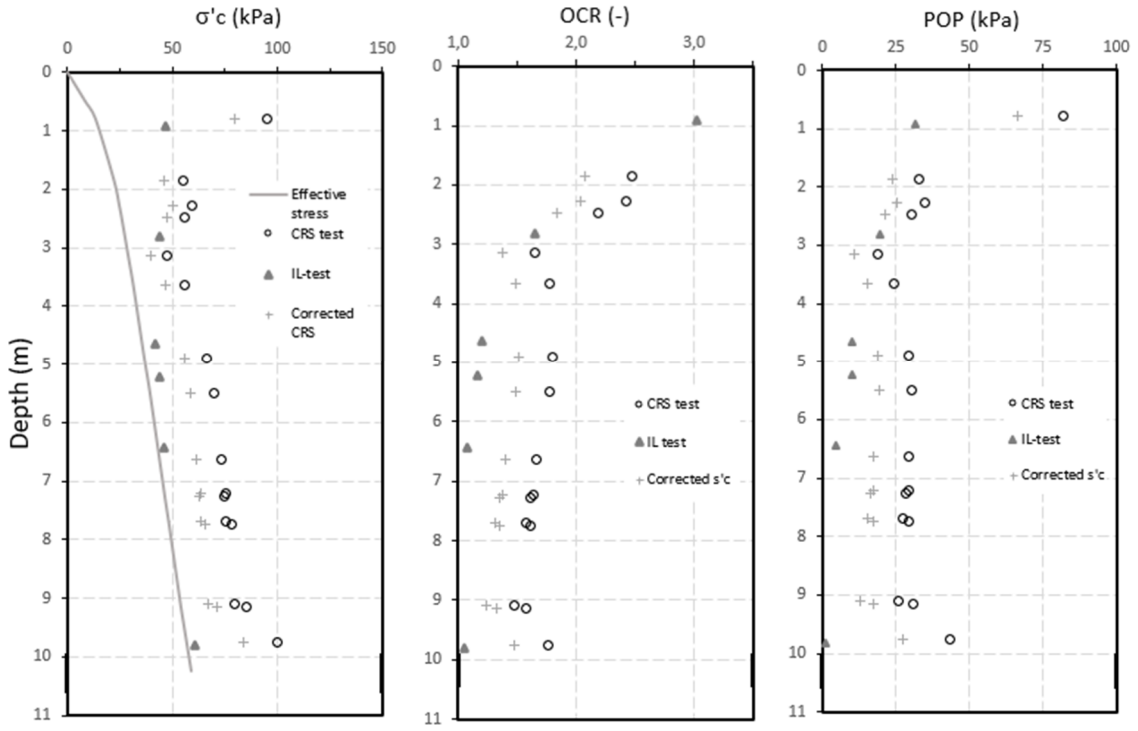

Figure 4.2. OCR and POP plotted vs depth using pre-consolidation pressure from CRS and IL-tests.

Figure 4.3 include the distribution of the derived conventional stiffness parameters λ^*, λ_i^* and κ^* derived directly from CRS and IL oedometer tests using the procedures described in section 2.6.1.2. There is a clear overall variation of the parameter λ^*, as well as variation between derived values from CRS test compared to IL tests. Derived values for λ_i^* show less variation, and similar values are derived from CRS tests and IL tests, indicating better predictions for the model using this parameter. However, it is likely that the CRS tests were not done at a high enough stress level to bring the soil into an intrinsic state. Therefore, values derived from IL tests were prioritized. Furthermore, the obtained values of κ^* in Figure 4.3 show substantial variation, indicating that the loading rates for conducted CRS and IL tests are highly variable for the samples used. The modified intrinsic creep index, μ_i^*, was derived from available IL oedometer tests at the highest possible load increment for each test respectively, and the result can be seen in Figure 4.3.

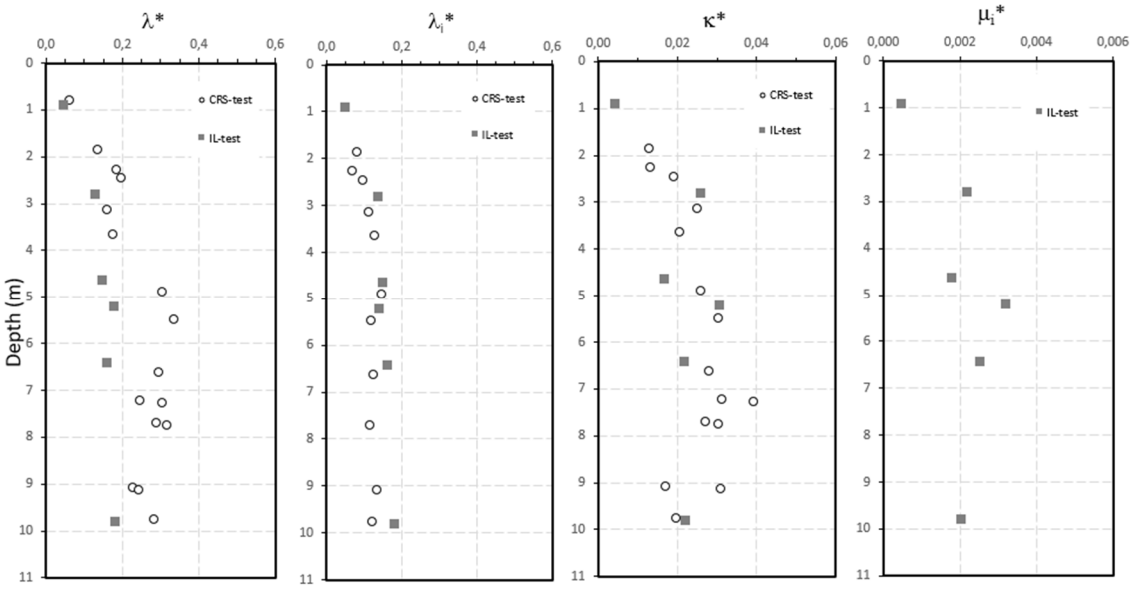

Figure 4.3. Derived values of λ^*, λ_i^* and κ^* and μ_i^* plotted against depth.

The inclination of the critical state line M is a highly important parameter for the Creep-SCLAY1S model due to its influence on other calculated parameters in the model. The concept of critical state refers to the ultimate state, at constant stress ratio η, where shearing can persist indefinitely, without any significant variations in volume or effective stress (Muir Wood, 1990). The critical state line acts as a boundary restricting variations in effective stress (p'), deviator stress (q) and specific volume during a test. The parameter M_c represent the critical state line in triaxial compression, while M_e represents the critical state line in triaxial extension. For the Ballina trial embankment there are 24 available undrained triaxial compression tests and 5 undrained triaxial extension tests from 2 boreholes. Figure 4.5 illustrates that borehole INCLO2 exhibits three main compressive inclinations, while borehole MEX9 (Figure 4.5) demonstrates two compressive inclinations and two primary extension inclinations. Following that, the assigned values

of M_c and M_e were attributed to the respective soft soil layers involved in the conducted tests.

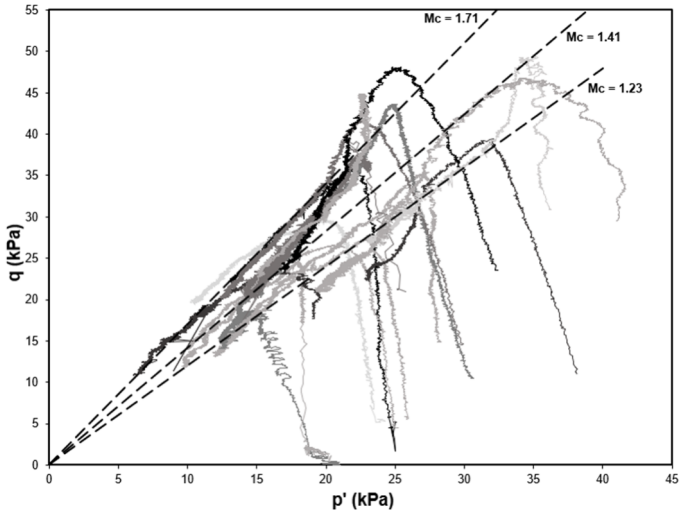

Figure 4.4. Critical state line in triaxial compression from boreholes INCLO2.

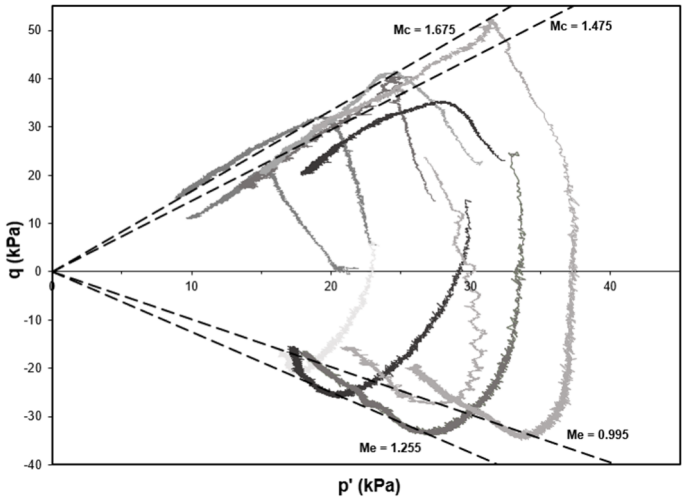

Figure 4.5. Critical state line in triaxial compression and extension from borehole MEX9.

After determination of the pre-consolidation pressure and the conventional parameters from laboratory data the coefficient of earth pressure at rest for in-situ conditions (K_0), and normally consolidated conditions (K_0^{NC}), can be calculated using the equations in section. However, for the Ballina embankment, undrained *K₀*-consolidated triaxial tests were available for determination of in-situ *K₀*. Furthermore, with the aforementioned parameters available it is possible to calculate the parameters relating to anisotropy in the Creep-SCLAY1S model, namely α_0, ω and ω_d , using corresponding equations (2.42) – (2.44) in section 2.6.1.3. The parameters relating to bonding and destructuration are χ_0, ξ_v, and ξ_d. The initial amount of boding, χ_0, is calculated using the sensitivity of the soil and equation (2.45). ξ_v and ξ_d which controls the absolute and relative rate of destructuration in the model respectively, cannot be determined through laboratory data and require an optimization process. However, according to Yin & Karstunen (2011),

typical values lie in the range of 8 – 12 for ξ_v and 0.20 – 0.30 for ξ_d, from where an initial approximation was obtained. A final summary of the initially determined parameters can be found in APPENDIX B.

All analysed soil samples were classified in regard to soil sample quality, using the methodology by Lunne et al. (1997) described in section 2.1.4. The soil speciemns are generally of good quality according to the classification method. The result is presented in Figure 4.6, where the majority (53) of the soil specimens used for laboratory testing are of very good to excellent quality, 7 are of good to fair quality and 1 specimen is of poor quality. The CRS specimen from INCLO2 borehole at 10.23 m depth was disregarded from the analysis.

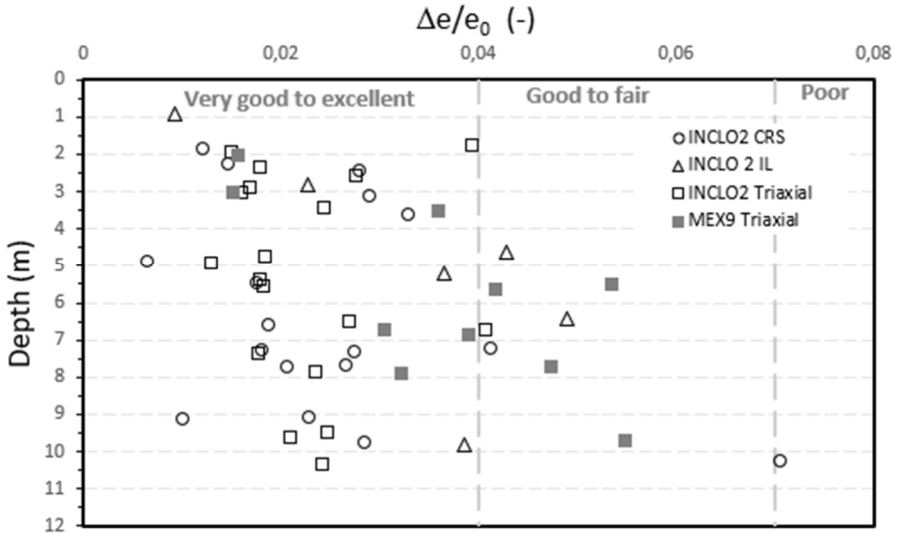

Figure 4.6. Soil sample quality of conducted CRS, IL and triaxial tests from borehole INCLO2 and MEX9 classified according to method by Lunne et al. (1997).

4.1.1. Hydraulic properties

The hydraulic properties of the soil were evaluated through available CRS and IL tests. The derived values are presented in Figure 4.7. Both the permeability and consolidation coefficient are high in the shallow layers. This could be due to potential occurrence of soil desiccation, like previously described, as swelling and cracking also can lead to an increase of hydraulic properties. From around 2 m depth and below, both the hydraulic conductivity and consolidation coefficient decreases considerably and exhibits more linear behaviour. Typical values for Ballina soft clay are around 10^{-9} (m/s) for k_v and around 2.5 for c_v (m²/year) (see Figure 4.7).

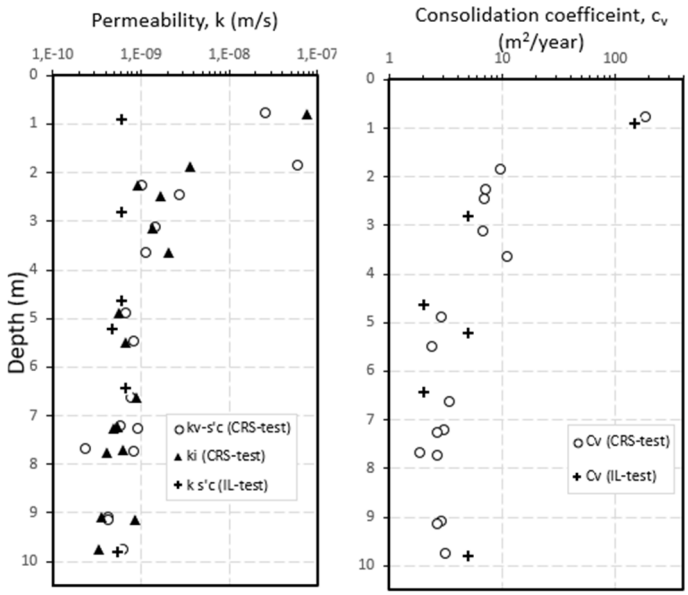

Figure 4.7. Hydraulic properties of soft Ballina clay.

From the derived values a representative value of vertical permeability, corresponding to the chosen soil stratification, was chosen for each layer. Moreover, as recommended by Pineda et al. (2016), a ratio of $k_h = 1.5 \cdot k_v$ was adopted to account for the horizontal permeability being higher than the vertical one. The calculated values of horizontal permeability are presented in Table 4.1.

Furthermore, to account for the PVDs, an equivalent hydraulic conductivity k_{ve} was calculated according to the simple homogenisation method by Chai et al. (2001) presented in section 2.3, by representing the global impact of prefabricated vertical drains on the soil hydraulic properties. The equivalent values presented in Table 4.1 were used in the numerical analysis. For the transition layer the permeability was set at a high value of 0.7 m/day such that a new equivalent value is not required when modelling the drains. The permeability of the sand layer was set to 0.9 m/day and was modelled as a drained layer to allow water to flow throughout the layer. For the stiff Pleistocene clay layer, the permeability was set to 0.005 m/day.

Table 4.1 Initial and calculated hydraulic conductivity values.

		10^{-4} m/day		
Depth (m)	Soil strata	k_h	k_v	k_{ve}
0-1.5	Alluvium	23.3	15.2	360
1.5-3.0	Soft clay 1	1.8	1.2	29
3.0-4.0	Soft clay 2	1.3	0.84	20
4.0-6.0	Soft clay 3	0.69	0.46	11
6.0-8.5	Soft clay 4	0.59	0.39	9.3
8.5-10.5	Soft clay 5	0.47	0.31	7.4
10.5-14.0	Transition layer	7000	7000	-
14.0-19.0	Sand layer	9000	9000	-
19.0-24	Pleistocene clay	50	50	-

Note: For the soft clayey soil layers a ratio between horizontal and vertical hydraulic conductivity of $k_h=1.5xk_v$ was set, where k_h and k_v is hydraulic conductivity in the horizontal and vertical direction respectively.

4.1.2. Parameter calibration

To ensure accurate predictions of soil response by the adopted constitutive model, the laboratory tests are simulated using the Creep-SCLAY1S model and the Soil Test Tool in PLAXIS. A number of IL oedometer tests, CRS oedometer tests and triaxial compression and extension tests were simulated to calibrate the first setup of manually derived soil parameters against the model. 5 CRS oedometer tests from depths 2.26 m, 3.14 m, 4.89 m, 7.22 m, and 9.09 m below ground surface and 5 IL oedometer tests form depths 2.81 m, 4.64 m, 5.22 m, 6.46 m, and 9.81 m below ground surface are simulated. The results of the simulated IL oedometer tests did not show an acceptable initial agreement with laboratory tests, and some adjustments of high influence parameters was required. Parameters that were altered are mainly POP, λ_i^* and κ^* where all included parameters were somewhat overestimated for the different tests. Moreover, the parameters relating to destructuration needed adjusting for the IL oedometer tests, as the initial assumption for ξ_v, and ξ_d was clear to be an overestimation. Figure 4.8.b shows an example of a calibrated IL oedometer test from 2.81 m depth. The initial agreement between simulated CRS tests using manually derived parameters, and the laboratory tests was somewhat lacking. Furthermore, there were inconsistent results observed among the simulations conducted at different depths. However, these outcomes can be deemed reasonable since the manual process prioritized IL oedometer tests while deriving the conventional parameters. Figure 4.8.a displays an example of the outcome after calibration of a CRS tests from 4.89 m depth where an excellent fit is achieved.

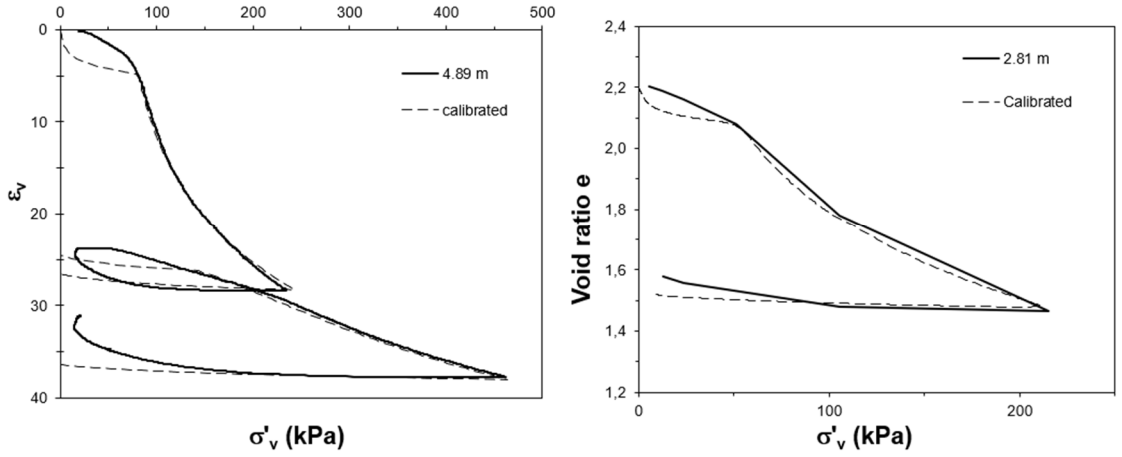

(a) (b)

Figure 4.8. Calibrated (a) CRS oedometer test at 4.89m depth and (b) IL oedometer test at 2.81 m depth using Soil Test Tool in PLAXIS.

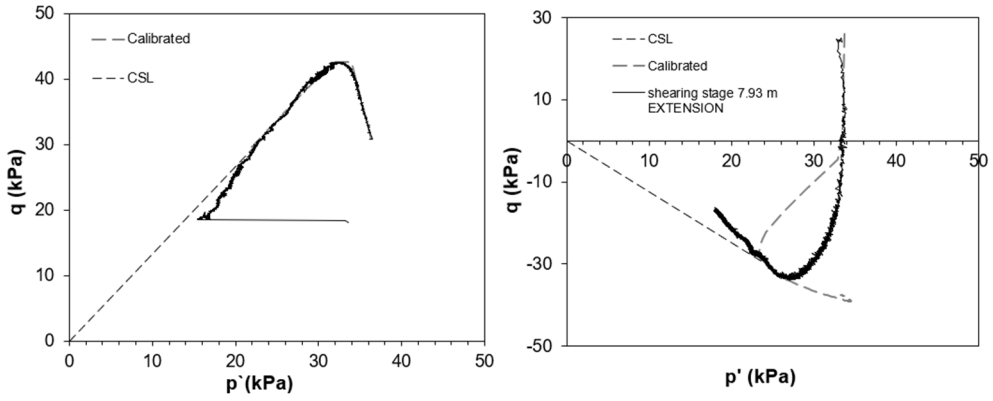

(a) (b)

Figure 4.9. Calibrated triaxial (a) compression test at 9.49 m depth (b) extension test at 7.93 m depth.

A total of 5 triaxial compression tests were calibrated from depths of 2.57 m, 3.05 m, 5.40 m, 6.87 m, 9.49 m below ground surface. Generally, an acceptable agreement was found with the manually derived parameters. However, the main parameter that had to be adjusted significantly was in-situ K_0, especially for layers 1-2. Other parameters that were moderately changed are M_c and α_0. Figure 4.9a shows an example of a calibrated undrained triaxial compression test at 9.49 m depth. For triaxial extension tests all 5 available tests from depths 3.55 m, 5.53 m, 6.73 m, 7.93 m, and 9.87 m were calibrated against the model. Overall, for most of the layers, there was not a good fit between simulated tests using manually derived parameters and the laboratory tests and adjustments of the parameters had to be made. The main parameters changed to fit the curves were M_e, ω, ω_d. Figure 4.9 shows a calibrated undrained triaxial extension test at 7.93 m depth. Calibrated and final parameters subsequently adopted for the boundary value analysis are presented in Table 4.2.

Table 4.2. Final calibrated input parameters for the Creep-SCLAY1S model.

		Layers (m)				
Parameter type	Parameter	1.5-3.0	3.0-4.0	4.0-6.0	6.0-8.5	8.5-10.5
Conventional parameters	κ^*	0.011	0.013	0.0145	0.0123	0.0102
	v'	0.2	0.2	0.2	0.2	0.2
	λ_i^*	0.097	0.112	0.098	0.095	0.098
	M_c	1.47	1.72	1.59	1.55	1.38
	M_e	1.13	1.22	1.15	1.15	0.952
Anisotropic parameters	ω	29	28	25	28	23
	ω_d	0.94	0.993	1.02	1.02	0.84
	α_0	0.69	0.624	0.625	0.723	0.485
Destructuration parameters	ξ_v	5.1	5.5	5.5	7.8	6.1
	ξ_d	0.31	0.324	0.291	0.21	0.304
	χ_0	3.5	4.2	3.5	4.3	3.8
Viscous parameters	μ_i^*	0.0026	0.0023	0.0029	0.0028	0.0031
	τ	5	5	5	5	5
Initial state parameters	ρ	1.59	1.48	1.44	1.41	1.43
	e_0	2.05	2.42	2.80	3.15	2.90
	POP	17	11	7	4	3
	K_0	0.86	0.83	0.55	0.50	0.48
	K_0^{NC}	0.41	0.33	0.37	0.38	0.44

4.2. Numerical Model

The Ballina trial embankment described in section 3 is modelled in PLAXIS 2D under 2D plane strain conditions. To reduce computational requirements, the embankment is modelled using symmetry along the embankment centre line. As a result, only the right side of the embankment is considered in the model. Details and measurements of the modelled embankment are described in section 3.2. To ensure that the results are not affected by boundary effects such as groundwater flow, the geometry of the model is extended a total of 40 m from the embankment centre line. 15-node triangular elements are used in order to discretize the embankment and soil below. The model consists of a total 1043 elements and 8543 nodes. According to Krenn (2008), prediction of vertical settlements using plane strain modelling of embankments on soft soil, that are not close to failure, are not significantly impacted by mesh coarseness. Figure 4.10 shows the generated mesh in PLAXIS, refined locally only in the embankment and PVD-improved area. Moreover, due to expected large strains the functions "updated mesh" and "updated water pressure" functions in PLAXIS are used to account changes in embankment geometry and accounting for buoyancy effects due to deformations over time.

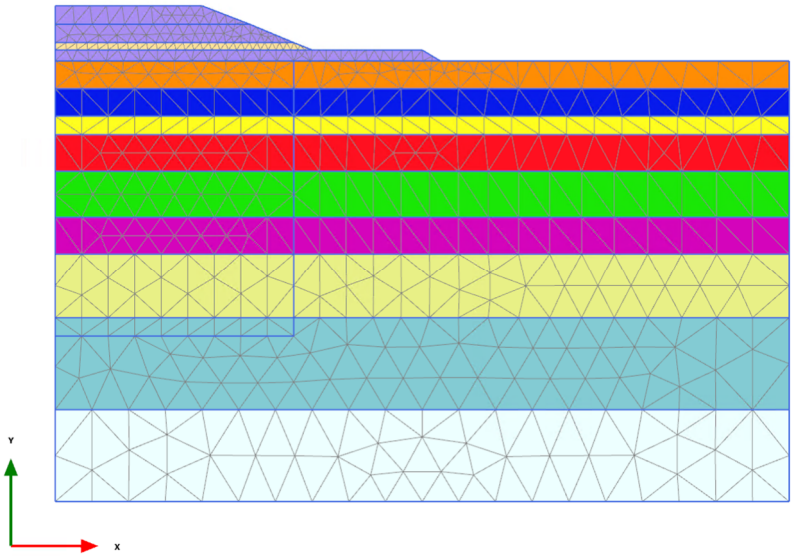

Figure 4.10. Finite element mesh of the modelled embankment.

Phreatic level in the model is set to 0.5 m below ground surface based on available pore pressure measurements. Embankment fill and sand layer are set as drained layers while the other layers are modelled as undrained. Drainage boundaries are closed at left and bottom side and open at the top and right side of the modelled geometry. The embankment is constructed in stages. The construction sequence is presented in APPENDIX A. The soft Ballina clay deposit between 1.5 and 10.5 m is modelled using the Creep-SCLAY1S model with the input parameters described in the previous section.

The embankment fill, alluvium layers and layers below the clay deposit (transition layer, sand layer and Pleistocene clay) are modelled using the simple Mohr-Coulomb model with corresponding properties described in Table 4.3.

Table 4.3. Table of adopted material properties using Mohr-Coulomb model.

	γ [kN/m³]	E [MPa]	υ' [-]	c' [kPa]	φ' [deg]
Embankment fill	20	40	0.35	2	40
Sand drainage layer	18	30	0.25	2	30
Alluvium layer	18	12	0.3	2	26
Transition layer	18	30	0.3	2	30
Sand layer	18	40	0.3	1	34
Pleistocene clay layer	18	30	0.3	4	28

In order to compare simulation results with measured data calculation points are selected in corresponding points to selected measurement instruments. These include settlement plates SP2 & SP3, magnetic extensometers M0-M4 in borehole MEX1, and Hydrostatic Pressure Gauge 1 (HPG1) for measurements of vertical settlements. Moreover, points corresponding to Vibrating Wire Piezometer (VWP) instruments 6a, 6b and 6c are selected for pore pressure measurements. Horizontal deformations are simulated and compared to measurements in INCLO 2 borehole.

The model is simulated both with and without PVDs installed in the subsoil. However, both simulations are carried out in the same cross section where the conventional CeTeau drain are installed, as results for the unimproved embankment are not yet published. The unimproved embankment is modelled for comparison and will be considered more as a Class A type of prediction. The PVDs are modelled using the simple homogenisation method described in section 2.3 using the equivalent hydraulic conductivity k_{ve} calculated according to the equations in section 2.3. Moreover, the parameters adopted relating to PVD performance are presented in Table 4.4. The drains were installed in a square pattern with a centre-to-centre distance of 1.2 m. The mandrel used for the drains had a 120 x 60 mm cross section and an area equivalent diameter of 96 mm. Moreover, the size of the anchor plate used was 190 x 90 mm and an area equivalent diameter of 147 mm. The diameter of the unit cell, d_e, adopted is 1.356 m, the diameter of the smear zone, d_s, 0.4 m, and diameter of drain, d_w, 51.5 mm. The overall smear effect is assumed at 10 for the initial simulation. Additionally, the discharge capacity, q_w, is assumed at 100 m³/year, as recommended by Indraratna et al. (2018)

Table 4.4. Parameters relating to PVD performance.

	Symbol	Unit	CeTeau PVD
Length	l	m	7.5
Diameter of unit cell	d_e	m	1.356
Diameter of smear zone	d_s	m	0.4
Diameter of drain	d_w	mm	51.5
Overall smear effect	k_h/k_s	-	10
Discharge capacity	q_w	m³/s	$8x10^{-5}$

5. Results

In the following section the results of vertical displacements, horizontal displacements, and pore pressures from the numerical analysis of the Ballina trial embankment are presented. Simulation results are compared to measurement data from installed instruments at the site as well as a comparison with the simulated case of no PVDs. Subsequently, the results of the sensitivity analysis conducted on a number of selected input parameters is presented.

5.1. Vertical Displacement

Figure 5.1 displays the time settlement curve for settlement plates SP2-4, in comparison to the simulation performed using Creep-SCLAY1S model at a node located at the centreline of the embankment. Overall, the simulation results align well with the measured data, albeit slightly underestimating the settlement. It should be noted that none of the settlement plates are in the simulated cross section as all are positioned at various cross sections along embankment centreline which likely has an influence on the results. Plates SP2 and SP3 are located with the shortest distance to the cross-section used for the model.

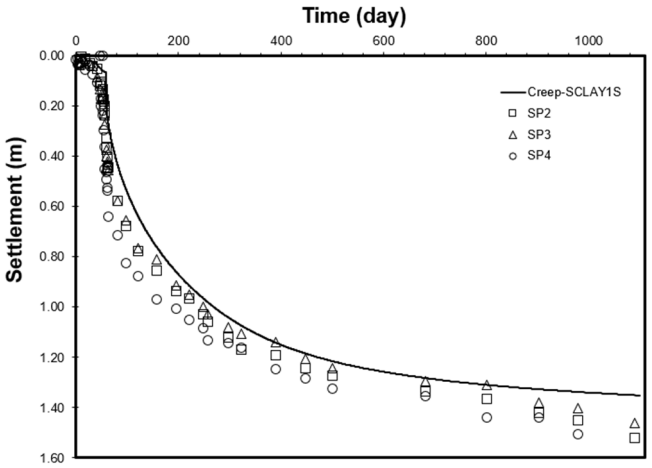

Figure 5.1. Time settlement curve for settlement plates SP1-4 compared to simulation results using Creep-SCLAY1S model.

Figure 5.2 shows a comparison between the settlement predictions obtained from the simulation and the measurements acquired from 5 magnetic extensometers in borehole MEX1 (labelled as magnets M0 to M4). The magnets were installed beneath the embankment centre line of the PVD improved area. Magnets M0 to M3 demonstrate a good agreement between the simulation results and field measurements. However, magnet M4, positioned at a depth of 10.5 m at the base of the soft clay layer, exhibits some measured settlements while the model prediction suggests minimal settlement. This discrepancy can be attributed to the utilization of high stiffness properties for the

transition layer. As the primary focus is on the behaviour of the soft clay layer this was done to minimize the impact on prediction results. For the shallow magnets M0 and M1 there is a small disparity of the rate of the primary settlements during the first 200 days or so. This could be explained by stiffness in the embankment and the alluvium layer somewhat mitigating the initial settlements. Moreover, for magnets M0-M3, the rates of the simulated settlements after around 700 days in Figure 5.2 are somewhat lower than the measured values with a slightly higher inclination, likely indicating that the tendencies for creep in the soil are underestimated.

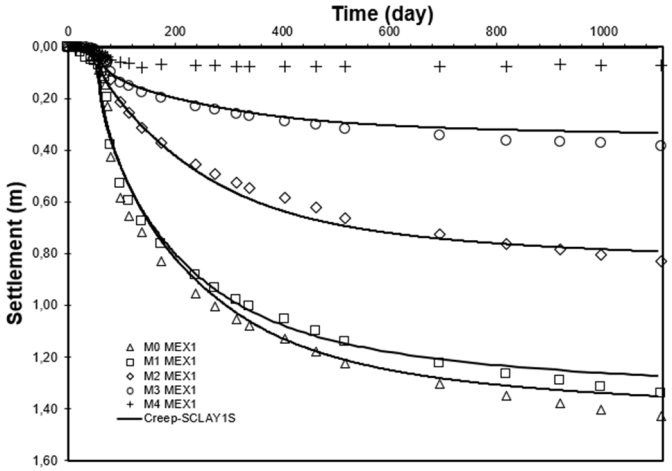

Figure 5.2. Time settlement curve for magnetic extensometers M0-M4 in MEX1 borehole compared to simulation results using Creep-SCLAY1S model.

Figure 5.3 displays the measured and simulated settlement profile for the hydrostatic pressure gauge (HPG1) installed under the embankment centreline. Settlements are presented for total time periods of 60 days, 260 days, 686 days, and 1100 days. There is generally a closer agreement of settlements at the embankment centreline than close to the toe of the embankment. Moreover, the simulation exhibits some heave at the edge of the working platform.

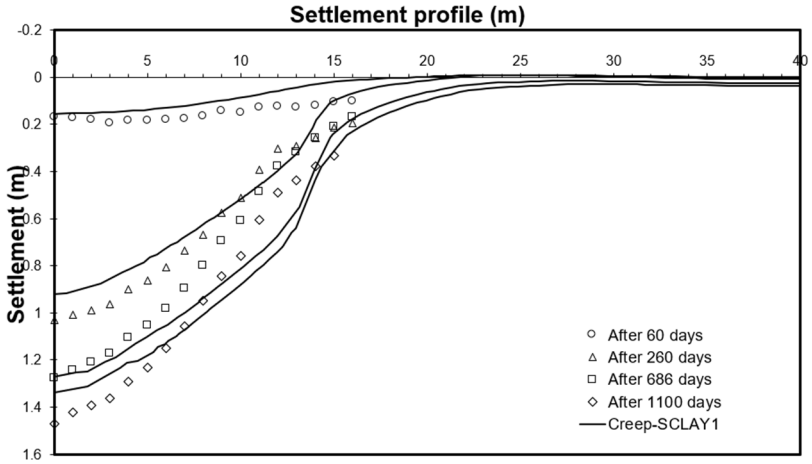

Figure 5.3. Settlement profile in HPG1 instrument for different time periods compared to simulation results using Creep-SCLAY1S model.

5.2. Horizontal Displacements

Figure 5.4 shows the horizontal displacements in INCLO 2 instrument compared to Creep-SCLAY1S simulation results. Displacements at four different time periods are presented, including 60 day, 240 day, 700 day and 1100 day time periods. There is a clear tendency of high lateral movement in the first layer (1.5-3.0 m depth) in all simulated time-periods. However, especially for the third to fifth layer, the simulation exhibits a significant drop off in lateral movement from around 3 m depth after 700 days and 1100 days. This could be due to the significant difference in in-situ K_0-values between the layers 1-2 and 3-5. Moreover, the immediate horizontal displacements after embankment construction are overpredicted compared to field measurements. The simulation after 240 days shows the best agreements between simulation and measurements. Although, the displacements in the middle of the soft clay layer are still underpredicted. All simulated time-periods show some negative horizontal movements in the shallow part of the cross section where top layers are "dragged" towards embankment centre. Moreover, it can be observed that Figure 5.4d shows the same, or less, order of magnitude of settlements when comparing to Figure 5.4c. This observation suggests a change in the direction of horizontal displacements within the soil. It is likely that this change is influenced by the same phenomenon, i.e., significant vertical settlements occurring in the central regions of the embankment, in combination with increased undrained shear strength over time. As a result, the soil in the deeper layers is caving towards the centre instead of expanding outward, leading to this altered behaviour in the deformation pattern, instead of a linear increase.

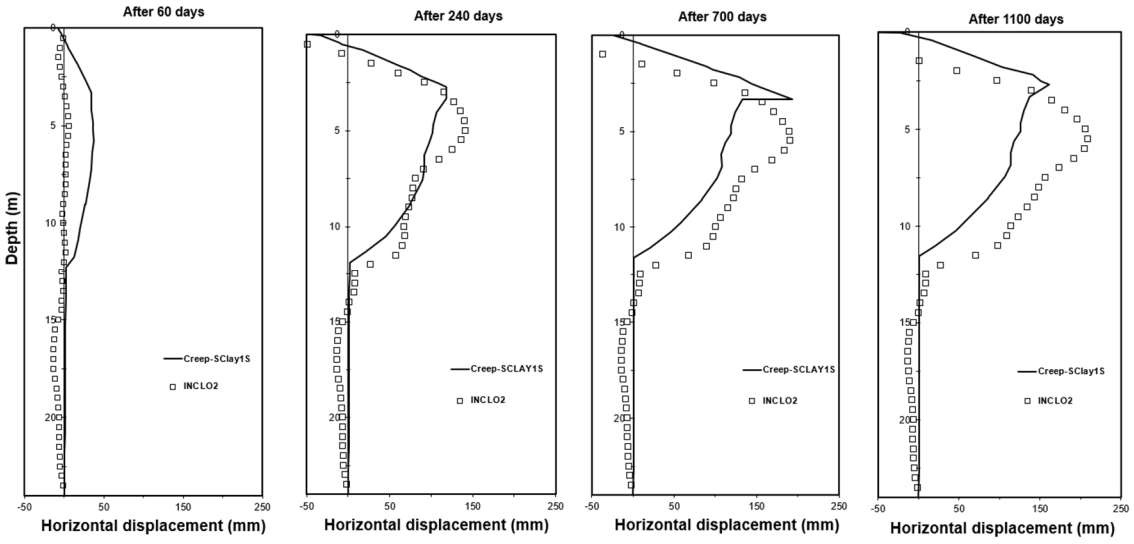

(a) (b) (c) (d)

Figure 5.4. Horizontal displacements vs depth for INCLO2 instrument and Creep-SCLAY1S instrument after (a) 60 days (b) 140 days (c) 700 days (d) 1100 days.

5.3. Pore Pressures

Figure 5.5 shows simulated total pore pressures and their dissipation with time, compared to measured values from installed Vibrating Wire Piezometers (VWP) 6a, 6b and 6c. VWP 6a installed at a shallow depth displays an increase of excess pore pressures up to around 60 days when construction of embankment is finished for both simulated and measured case. The excess pore pressures in VWP 6a dissipate quickly, which is reasonable as vertical drainage paths are shorter in shallow layers. It is important to remember that the homogenisation method drastically increases the vertical hydraulic conductivity throughout the soil. Furthermore, the curve for measured values is flat from 200 days onward, while the curve for simulated case exhibits a slight increase from 200 up to 1100 days. This could be attributed to creep effects in the layer, as the volume of the voids filled with water decreases when soil particles rearrange. VWP 6b and 6c show similar behaviour as 6a, although with slower dissipation of pore pressures as vertical drainage paths are longer. Moreover, the measured values of total pore pressure are generally higher for VWP 6b and 6c compared to simulated values. This is likely due to the fact that actual field instruments are placed between the drains, and consequently show maximum obtained pore pressures in the subsoil. However, the numerical model uses homogenised values for hydraulic conductivity, and thus, exhibit average values of pore pressures at arbitrary points in the area with PVDs. Another reason for the high pore pressures seen in the measured data could be clogging of the filter tips of the VWP or sensor movements due to settlements. As can be seen in Figure 5.5, the simulated and measured values approach similar magnitudes over time.

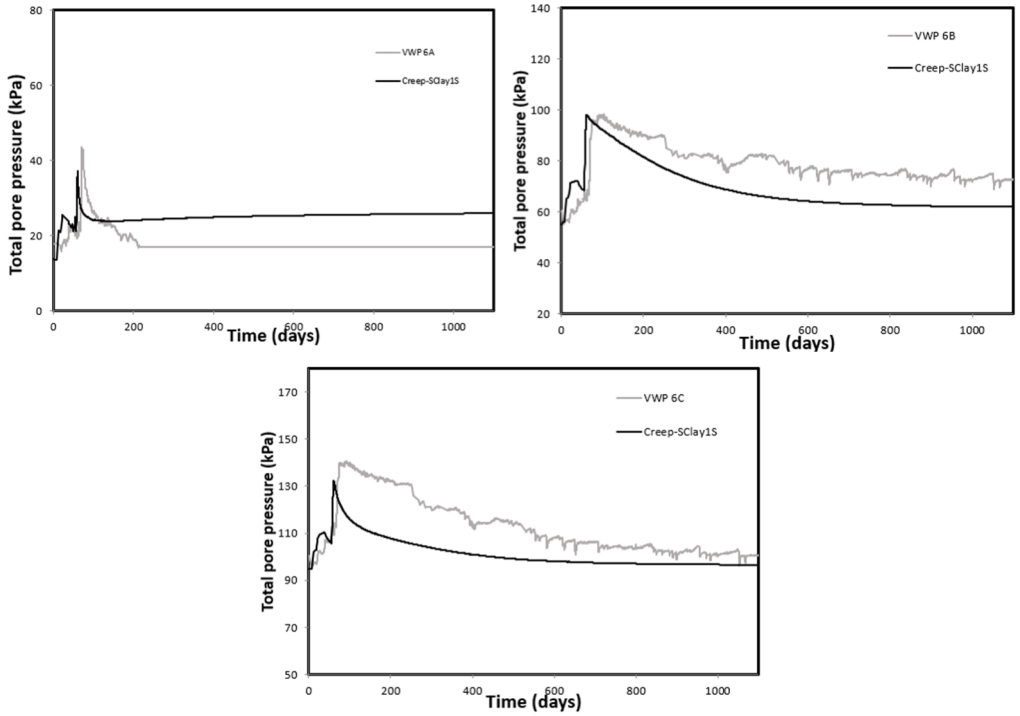

Figure 5.5. Time vs total pore pressure curves for VWP instruments 6a, 6b and 6c compared to simulation results using Creep-SCLAY1S model.

5.4. Embankment without PVDs

Figure 5.6 presents the time settlements curves for the simulation of the Ballina trial embankment without PVDs. Figure 5.6a shows a comparison of the unimproved case with the improved case with corresponding measured values in magnetic extensometer M1 over 1100 days. As expected, there is major difference in order of magnitude of consolidation settlements between the cases. Figure 5.6b displays the time settlement curve for an increased time period of 40 years, which can be considered the general lifespan of the embankment. The results illustrate the difference in development rate of the consolidation settlements. There is negligible difference in settlements after around 3 years for the PVD-improved case, whereas, for the unimproved case, the total time period required to reach equivalent vertical settlements is more than 40 years.

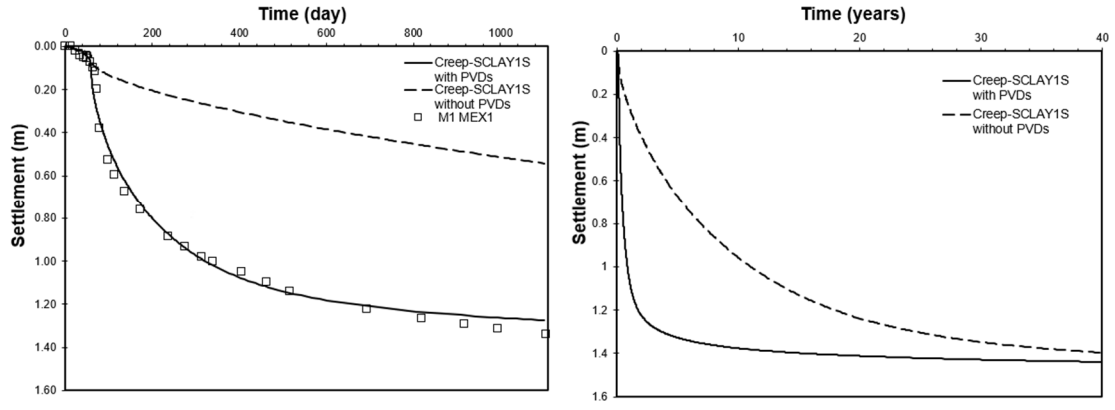

(a) (b)

Figure 5.6. Time settlement curves for the case with and without PVDs for a time period of (a) 1100 days (b) 40 years.

Figure 5.7 displays horizontal displacements for the simulation of the embankment without PVDs compared to the simulated PVD-improved case. The order of magnitude after 60 days, 240 days and 700 days are rather similar. Although, for simulation after 1100 days the horizontal displacements are larger for the unimproved case. During a 40-year simulation of the improved and unimproved embankment, the disparity in lateral movement is even more pronounced, as illustrated in Figure 5.7. In the case of the improved embankment, there is only a slight increase in displacements between the 3-year and 40-year periods. Conversely, for the unimproved embankment, the deformations nearly double after 40 years. This observation suggests a clear enhancement in soil stability due to the presence of PVDs. However, this apparent increase in stability is likely time-dependent in nature as the improvement for the PVD-case during the initial 3-year period is minimal. And finally, the unimproved case shows a different settlement distribution and does not exhibit as much negative displacements at shallow layers, as is reasonable when magnitude of vertical settlements are much smaller at the corresponding time periods.

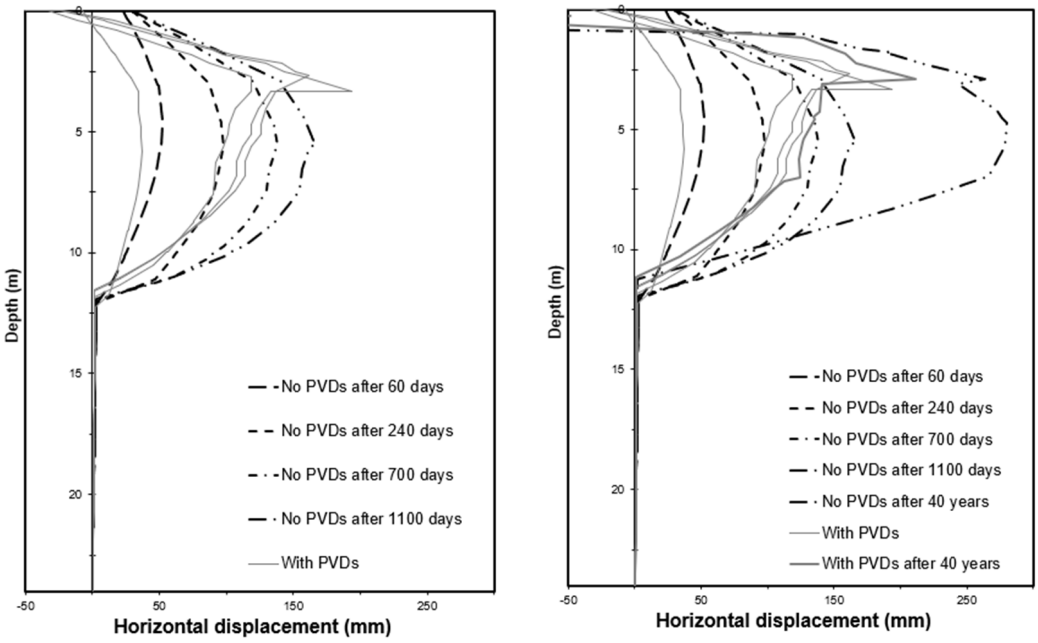

(a) (b)

Figure 5.7. Comparison of horizontal displacements for case with and without PVDs after (a) 60 days, 240 days, 700 days, and 1100 days (b) 40 years.

Figure 5.8 presents the total pore pressures of the simulation without PVDs, compared to simulation of improved case as well as measurement data in VWP6. The build-up of excess pore pressures shows similar behaviour between the improved and unimproved case. However, there is a significant difference in rate of pore pressure dissipation as the curves for the unimproved case stay at high levels for the duration of the simulation up to 1100 days. VWP6a show diminutive dissipation behaviour, VWP6b negligible dissipation behaviour and VWP6c exhibit some dissipation and is very similar to the measured values during the first 200 days after embankment constructions. This further reinforces the assumption for the improved case where the homogenisation method gives average values of pore pressures in the soil, compared to the "maximum" values experienced by the VWPs installed between drains where hydraulic properties are similar to the unimproved case (if the soil is undisturbed).

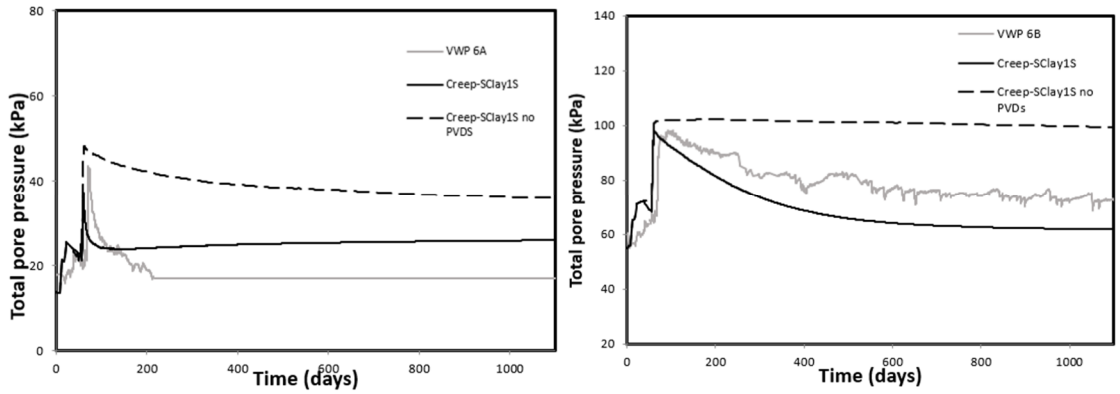

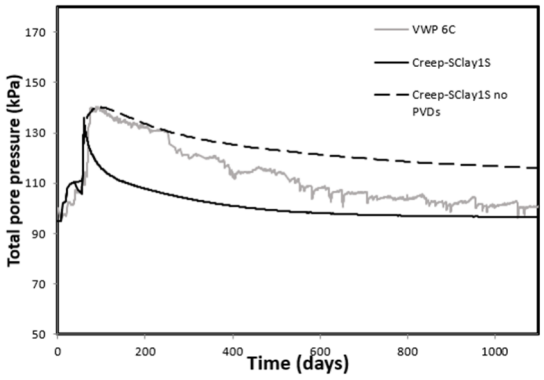

Figure 5.8. Time vs total pore pressure curves for simulation of embankment without PVDs, compared to the improved case and instruments VWP6a, b and c.

5.5. Sensitivity Analysis

A sensitivity analysis was conducted on the results from the numerical analysis to assess the influence of various parameters on settlement results and their relative importance.

5.5.1. Sensitivity of POP and OCR

The Creep-SCLAY1S constitutive model (as most creep models) is very sensitive to the yielding point of the soil. Thus, the influence of pre-consolidation pressure, σ_c, and subsequently OCR and POP, on simulation results was analysed. Moreover, as particularly significant for the Ballina case, where CRS-tests with a high strain-rate, and IL-tests with a very low strain rate (5-day loading increments) are conducted, the impact of using derived values of σ_c from each test respectively is investigated.

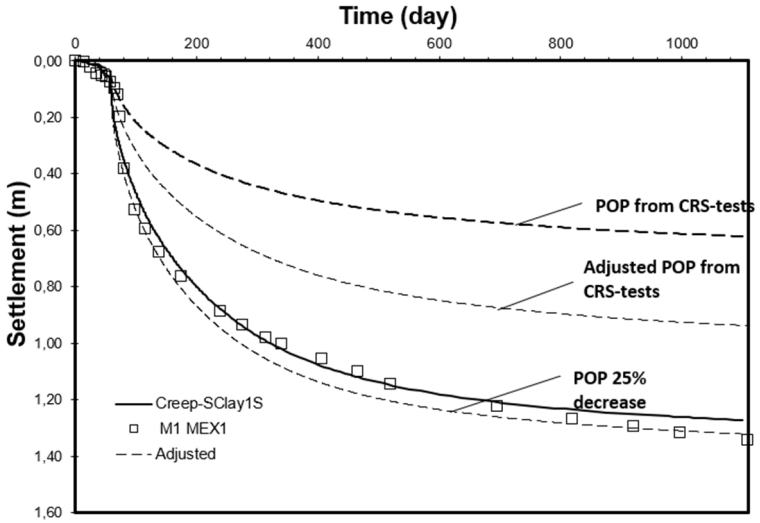

Figure 5.9. Influence of Pre-Overburden Pressure (POP) on vertical settlements over 1100 days.

Figure 5.9. presents the results of the conducted sensitivity analysis on values Pre–Overburden Pressure (POP) and their impact on the simulation with the Creep-SCLAY1S

model. The final values of POP used in the simulation were derived from available IL-tests and then calibrated using the soil test tool in PLAXIS and gives a total vertical settlement of about 1.27 m after 1100 days in M1 instrument. As illustrated in Figure 5.9, using values of POP derived directly from available CRS-tests would give a total settlement of about 0.62 m, while using POP with adjusted values of $0.84 \cdot \sigma_c$ according to recommendation by Pineda et al. (2016), would produce a total settlement of about 0.94 m after 1100 days. Consequently, a 16% decrease in σ_c results in about 48% increase in vertical settlements. Moreover, a reduction of adopted POP by an additional 25% for each layer would result in result in merely 4% increase of settlement.

5.5.2. Sensitivity of stiffness parameters

Figure 5.10 presents the result of the conducted sensitivity analysis on parameters relating to soil stiffness, namely the modified swelling index, κ^*, and the modified intrinsic compression index, λ_i^*. It is evident that the simulation is sensitive to variations of the modified compression index, λ_i^*, as changing this parameter has large implications on the vertical settlements. A 25% increase of λ_i^* gives a 25% increase in vertical settlements, whereas a 25% reduction of λ_i^* gives 47% less settlements over 1100 days. A 25% increase of κ^*resulted in 3.2% less settlements, whereas a 25% decrease of the parameter resulted in 2.3% more settlements at 1100 days, with a substantial increase in computation time required in PLAXIS. Moreover, a 25% increase in both κ^* and λ_i^* simultaneously resulted in a total 23% increase in vertical settlements after 1100 days. Consequently, the numerical simulation is overall more sensitive to the modified intrinsic compression index, λ_i^*, than the modified swelling index, κ^*, as is logical when conducting an analysis of an embankment, where compression, as opposed to swelling, is the most prevalent behaviour in the soil.

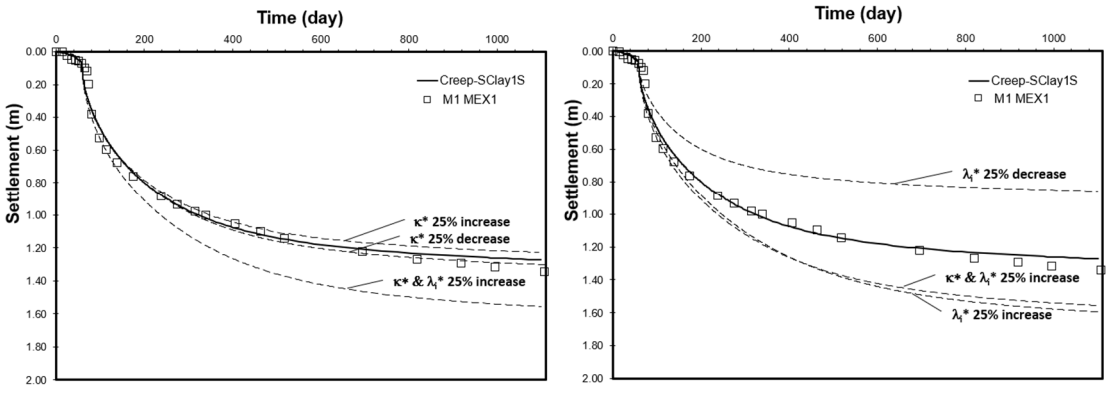

(a) (b)

Figure 5.10. Influence of stiffness parameter κ^* (a) and λ_i^* (b) on vertical settlements over 1100 days.

5.5.3. Sensitivity of lateral earth pressure

A sensitivity analysis was conducted on coefficient of lateral earth pressure at rest, in-situ K_0 and K_0^{NC}, to investigate their influence on vertical and horizontal settlements. Initial values of K_0 for the simulation were chosen in the region of 0.83–0.86 for the shallow clays 1–2 and in the region of 0.48–0.55 for the deeper clays 3–5, after calibration of triaxial tests against the Creep-SCLAY1S model using the soil test tool in PLAXIS. To observe the impact on results by using a more homogenous, and representative of field conditions, K_0-profile throughout the clay deposit the values of clay 3-5 were increased by 50%. The adopted values of K_0 are presented in APPENDIX C. As seen in Figure 5.11, the simulation using increased K_0-values had little impact on the magnitude of vertical settlements, with a reduction of about 3%.

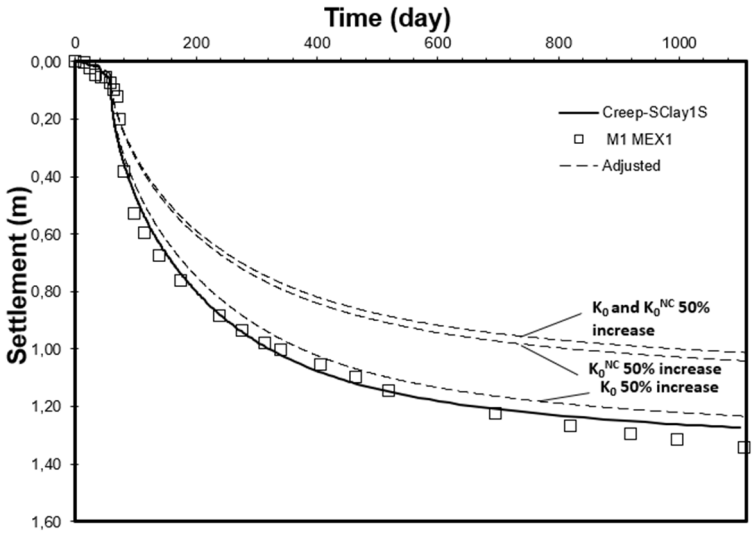

Figure 5.11. Influence of anisotropy parameters coefficient of lateral earth pressure at rest, in-situ K_0 and K_0^{NC}, on vertical displacements over 1100 days.

Figure 5.12 displays the impact of increased K_0-values on horizontal displacements, where a slight reduction can be observed for all four time periods investigated. After 240 days, at the "peak" around 3.3 m depth, the horizontal displacements are larger than for the initial simulation. Furthermore, to investigate the impact on the coefficient of lateral earth pressure at rest for the normally consolidated region, K_0^{NC}, a simulation was run where K_0^{NC}-values were increased by 50%. Figure 5.11 shows the influence on vertical displacements, where a 22% reduction in settlements can be observed. Figure 5.12 displays the impact on horizontal displacements, where a reduction in horizontal settlements is evident for all time-periods. Additionally, as seen in Figure 5.11, an increase of both K_0 and K_0^{NC} resulted in a total of 25.7% reduction in vertical settlement and, as seen in Figure 5.12, a reduction in horizontal displacements for all time-periods simulated. Overall, it is evident that an increase of K_0 and K_0^{NC} throughout the soil profile decreases the horizontal displacements. Higher K_0-values would indicate presence of more lateral stresses in the soil and, thus, lead to less tendency for soil movement in the

horizontal direction. Furthermore, another observation in Figure 5.12 is the "drop off" in lateral displacements around 3 m depth still occurs with a more homogenous K_0-profile, but is more prevalent after 240 days, instead of after 700 days.

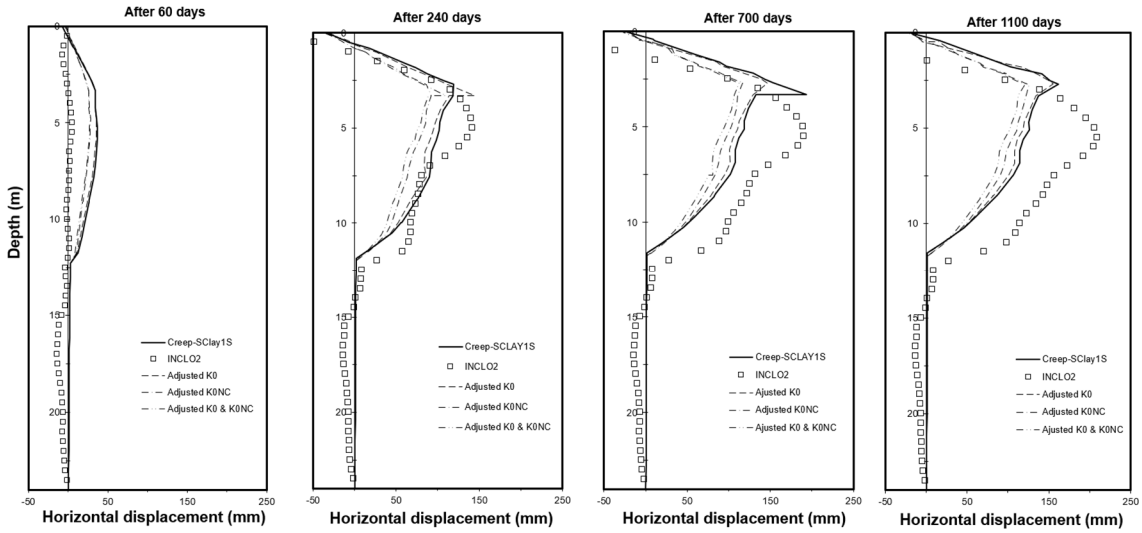

(a) (b) (c) (d)

Figure 5.12. Influence of coefficients of lateral earth pressure at rest, in-situ K_0 and K_0^{NC}, on horizontal displacements over time periods of (a) 60 days (b) 240 days (c) 700 days (d) 1100 days.

5.5.4. Switching off anisotropy

Due to Creep-SCLAY1S being a hierarchical model is it possible to switch off some model features by appropriate choice of certain material parameters. This method can be useful if the features are deemed unimportant or if there is not sufficient experimental data available to the user. The anisotropy of the model was switched off in order to analyse its influence on the results. The anisotropy in the model can be switched off by setting both the initial anisotropy, α_0, and the evolution of anisotropy, ω, equal to 0, resulting into a rate dependent isotropic model. In addition, the model can be set to using only fixed anisotropy, by switching only the evolution of anisotropy (ω) to zero. Doing this will result in the Creep-SCLAY1S model becoming an anisotropic model with a fixed NCS (Sivasithamparam, et al., 2015).

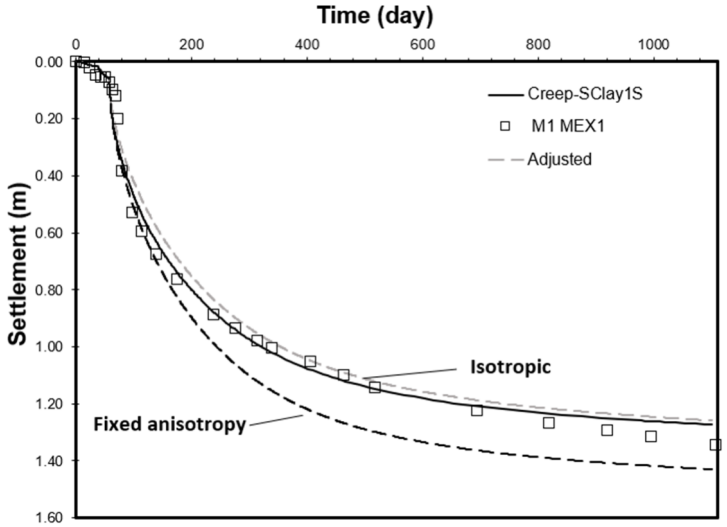

Figure 5.13. Influence on vertical displacements when simulating with Creep-SCLAY1S model as isotropic and with fixed anisotropy.

Figure 5.13 shows the influence on vertical settlements by exploiting the hierarchy of the model by simulating the embankment with PVDs with an isotropic version and fixed anisotropy version of the Creep-SCLAY1S model for 3 years. Negligible difference is observed in vertical settlements for the isotropic case, and the same is true for the horizontal displacements in Figure 5.14, where the order of magnitude is similar to the initial case. However, simulating the soil response with fixed anisotropy, but ignoring the evolution of anisotropy, clearly overestimates the vertical settlements (see Figure 5.13). The reason for the overprediction is likely due to the lower stiffness predictions by the model when evolution of anisotropy is not considered. When anisotropy evolves, energy dissipates as the soil fabric rotates, leading to the development of larger settlements. This response is also evident during the initial days of simulation in Figure 5.14, where lateral deformations are larger than for the initial case, indicating similar behaviour. Moreover, the observed change in lateral movement after 1100 days, along with the increased similarity in deformations between the two cases, can likely be attributed to the same phenomenon of contraction resulting from significant vertical settlements, as explained earlier.

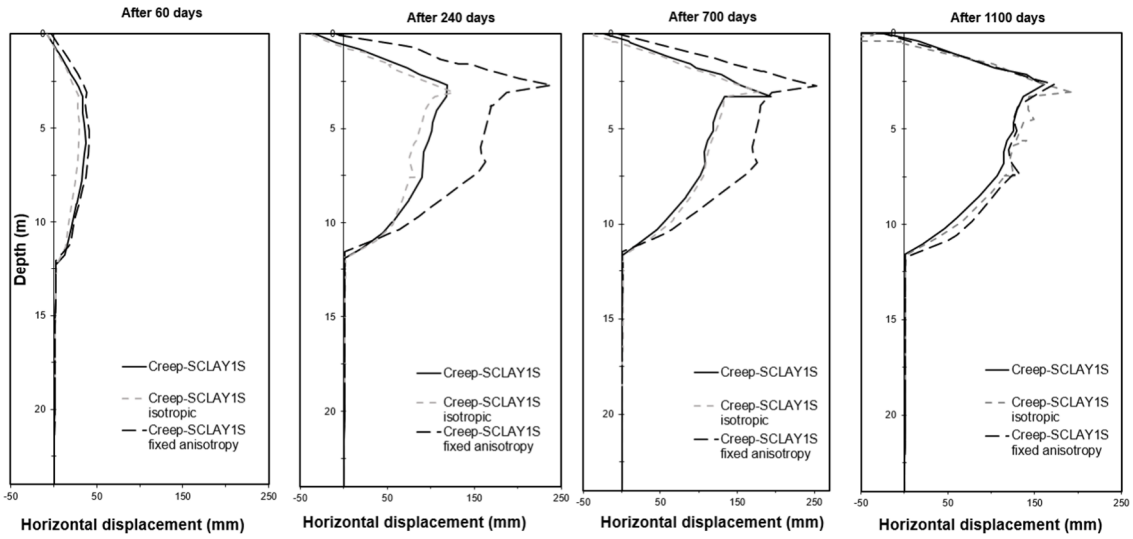

Figure 5.14. Horizontal displacements when simulating with Creep-SCLAY1S model as isotropic and with fixed anisotropy.

5.5.5. Sensitivity of permeability

An important factor when conducting consolidation analysis is the hydraulic properties of the soil. This becomes especially important when modelling behaviour of vertical drains, as their purpose is to speed up the consolidation process. Figure 5.15a shows the result of a sensitivity analysis conducted on the hydraulic conductivity used when modelling the vertical drains. A 5-fold reduction of the hydraulic conductivity in the horizontal direction, and the hydraulic conductivity in the vertical direction, yielded a significantly lower development rate of the vertical settlements over 1100 days. On the other hand, a 5-fold increase yielded negligible difference in vertical settlements over the time period. However, there is a clear change in the rate of which the settlements develop. It can be observed in Figure 5.15 that the same magnitude of displacements is reached after about 300 days (with a 5-fold increase), compared to around 800 days in the initial case. Additionally, to resemble 1D consolidation conditions, a simulation was carried out with setting the hydraulic conductivity in the horizontal direction, k_h, to 0. The result, as seen in Figure 5.15, shows that consolidation in the horizontal direction has negligible impact on the vertical settlements, when the averaging technique is used for the vertical permeability.

As touched upon in section 2.3, a clear agreement on the size of the smear zone does not exist in literature. Different contractors utilize different techniques and equipment (penetration velocity, mandrel size and shape) and the impact of the smear zone consequently varies from case to case. Therefore, a sensitivity analysis on the overall smear effect, k_h/k_s, and its impact on the calculated equivalent hydraulic conductivity, and consequently on the modelling on the vertical drains was conducted. Figure 5.15b shows simulation results where four different ratios of k_h/k_s ranging from 3, 10 (adopted value for initial simulation), to 12 and 20. The results indicate that the adopted value of

k_h/k_s has a relevant impact on the ability to accurately predict settlements when utilizing vertical drains. Moreover, it is evident from Figure 5.15 that a large reduction of the ratio k_h/k_s merely has an impact on the rate at which the consolidation settlements develop and not hugely influential on the magnitude of the final settlements.

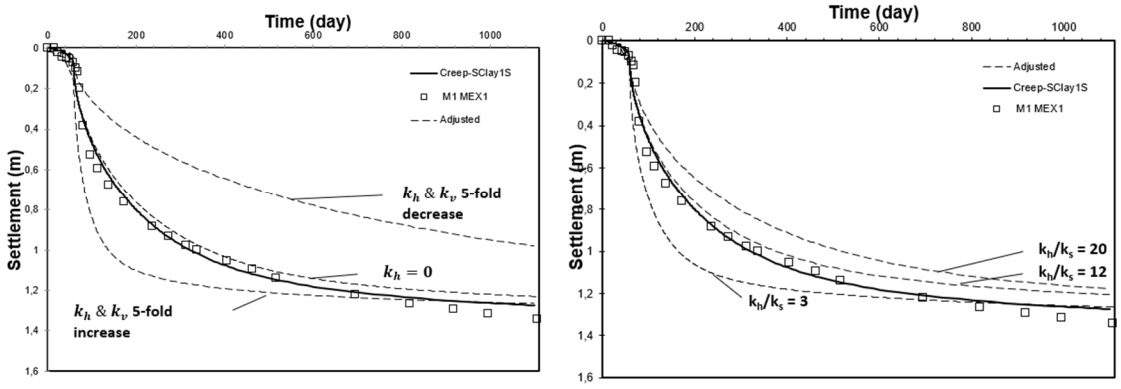

(a) (b)

Figure 5.15. Influence on vertical displacements by adjusting (a) horizontal and vertical permeability (b) overall smear effect of PVDs.

5.5.6. Sensitivity of absolute rate of destructuration

Figure 5.16 shows the influence of the absolute rate of structural degradation, ξ_v, on vertical settlements. Increasing ξ_v yields around 12.5% increase of settlements over a period of 1100 days, while a 25% decrease of ξ_v yields around 15.5% less settlements over the same time-period. Consequently, increasing and decreasing the parameter ξ_v has virtually the same effect on order of magnitude of vertical settlements.

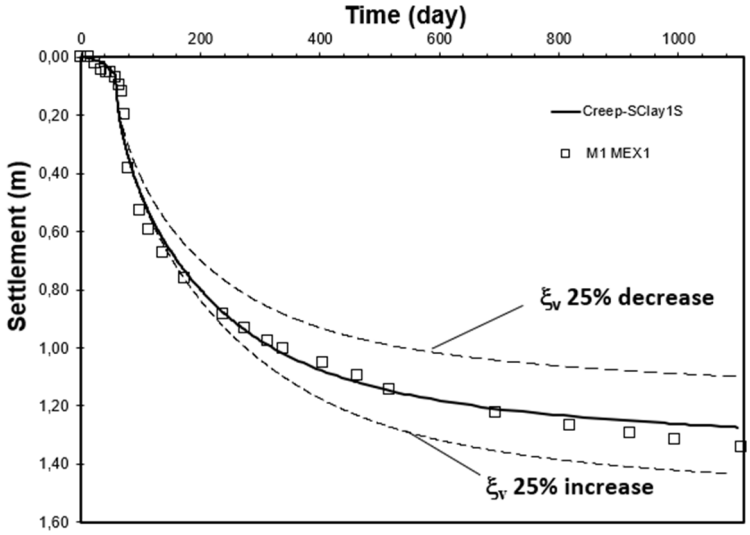

Figure 5.16. Influence of absolute rate of structural degradation, ξ_v, on vertical settlements over 1100.

5.5.7. Sensitivity of modified intrinsic creep index

In the initial simulation, the inclination of the time-settlement curve at 1100 days slightly diverged from measurement data, indicating that impact of creep behaviour in the model could be somewhat underestimated and yielding a larger underestimation of vertical settlements over a longer time-period than 1100 days. Therefore, the modified intrinsic creep index, μ_i^*, which governs the rate at which creep settlements develop in the model, was increased by 15%. Figure 5.17 displays the impact on vertical settlements over time by adjusting the parameter μ_i^*. To enable observation of creep behaviour over a longer time-period the analysis was extended to 3000 days in total. Ultimately, as seen in Figure 5.17, the rate of creep settlements shows a better agreement than the initial case. However, the rate of creep settlements is likely still underestimated compared to measurements in the field.

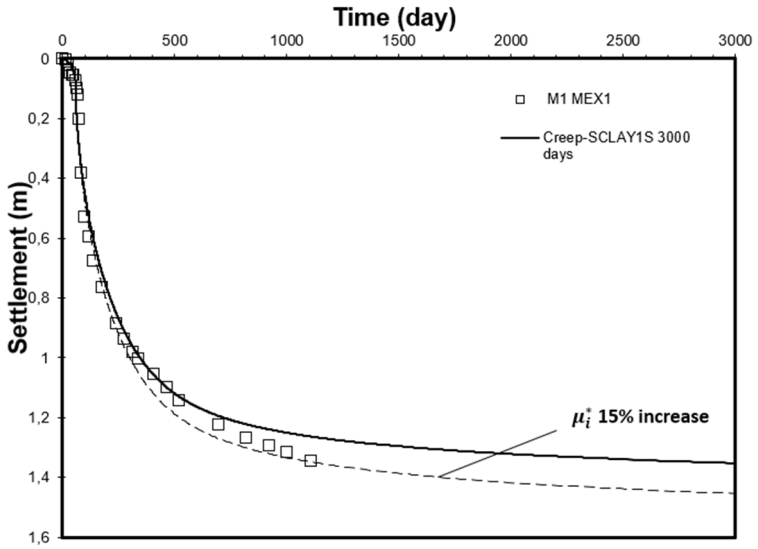

Figure 5.17. Influence of the modified intrinsic creep index, μ_i^*, on vertical settlements over 3000 days.

6. Discussion

Based on the results obtained from the numerical analysis, it is clear that there is an overall reasonable agreement between the measured data and the prediction. Comparing the vertical displacements for the PVD-improved embankment with the results for the unimproved case, there is a substantial difference in the rate at which the settlements develop, as well as the final settlements over a 3-year period. The PVD-improved embankment demonstrates significantly larger consolidation settlements during the first 700 days, aligning with field-measurements. Thus, indicating the effectiveness of the PVDs, and the homogenisation method used to model their behaviour.

When analysing a PVD-improved embankment on soft clay, it is paramount to get an accurate representation of the initial, short-term, consolidation settlements. As the method is often utilized in combination with pre-loading in time-constrained projects, being able to predict the rate of the settlements over a certain time-period enables the engineer to make well informed decisions on the adequacy of the method.

In Figure 5.6, the benefits of employing PVDs as a ground improvement-technique is demonstrated. For the unimproved case, it takes approximately 40 years to achieve vertical settlements of similar magnitude as those achieved in just 2 years for the improved case. In this perspective, the improvement of accelerated settlements is significant. However, during design projects, 2 years is often a lot more time than what is available.

In the case of the PVD-improved embankment, the consolidation settlements are developed within approximately 700 days, as the majority of the excess pore pressures have dissipated. Therefore, a model that accounts for rate-dependency and incorporates creep effects is essential for long-term predictions. As indicated in Figure 5.1 and Figure 5.2, the creep settlements are somewhat underestimated compared to measurement data. Thus, larger discrepancies are likely from a long-term perspective.

Simulation of horizontal displacements for the PVD-improved and the unimproved embankment demonstrate similar order of magnitude between the two cases during the first 2 years, where no clear improvement of stability is observed. However, as shown when simulating both cases for an extended period of 3-40 years, horizontal displacements for the unimproved embankment are significantly larger. Indicating an improvement in soil stability, attributed to the accelerated consolidation settlements introduced by the PVDs. Moreover, an important note is that undrained shear strength is not possible to treat as a soil constant. The predicted increase of shear strength due to consolidation of numerical models is dependent on adopted initial state parameters and the size of the yield surface. Therefore, it is important that an accurate interpretation of the initial stress state and initial state parameters is achieved.

As explored in the literature review, and clearly demonstrated in the sensitivity analysis, the factor with the largest impact on vertical settlements is the pre-consolidation pressure. Consequently, extra consideration is needed in determination of this parameter.

For the Ballina case, the laboratory test used to derive the pre-consolidation pressure had a considerable impact on the results. The deviation in total vertical settlements of 48% between the two cases can be attributed to the strain rate adopted for the CRS oedometer tests. The tests were conducted at a strain rate of 0.004 mm/ss (compare 0.0024 mm/s recommended by Sällfors (1975) for Swedish clays). Applying the recommended reduction of $0.84 \cdot \sigma_c$ recommended by Pineda et al. (2016) still yielded underwhelming results. Ultimately, the pre-consolidation pressures derived from the IL tests were used for the simulation. However, as they, in contrast to the CRS tests, were conducted at an unusually low strain rate of 5-day loading increments, this likely adds to the differences in the obtained values.

When analysing the behaviour of an embankment improved with vertical drains in general, and especially when utilizing an averaging technique, obtaining an accurate representation of the vertical and horizontal permeability is important for the prediction. Another necessity is obtaining relevant information of parameters representing the physical performance of the PVDs, and the smear effect introduced in the soil through the installation of the drains.

Another parameter with a notable impact on vertical settlements is the modified intrinsic compression index, λ_i^*. The Creep-SCLAY utilizes the intrinsic values of the modified compression index whose properties should be inherent to the soil and should be unaffected by factors like soil structure and strain rate. The obtained values of λ_i^* in Figure 4.3 are consistent with this theory, indicating minimal disparity between the two tests. In principle, both CRS and IL tests could be employed for the boundary value analysis. However, for the Ballina case, it is assumed that both tests were conducted at stress levels too low to fully attain the material's intrinsic state.

Moreover, as touched upon in section 2.1.3, the adopted strain rate in laboratory mainly affects the development of the stress-strain curve after soil yielding has taken place. Citing this reason, the obtained values of the modified swelling index, κ^*, should not be significantly impacted as they are typically derived from stresses lower than the pre-consolidation pressure, or from unloading-reloading curves during the oedometer test. However, the former would typically be affected by sample disturbance. This relationship is evident in Figure 4.3, where the variation in κ^* values derived from CRS, compared to IL tests, is considerably lower. Nevertheless, as the case of an embankment investigated in this thesis is mainly one of compression, not swelling, the modified swelling index has little impact on the simulation results.

The coefficient of lateral earth pressure at rest for the OC and NC region are parameters with a large influence on both vertical and horizontal displacements. Discrepancies in the horizontal deformations along the soil profile could be due to unrealistic K_0-values

obtained for the calibration process. Kelly et al. (2017) presents a K_0-profile in the range 0.65 – 0.85 from SDMT field-tests at the site, while calibrated laboratory tests for layers 3 – 5 indicate K_0-values in the range 0.46 – 0.51. Although, analysing K_0 and K_0^{NC} is difficult to interpret due to their influence over other calculated input parameters for the model. Thus, changing only one parameter exclusively would not give a realistic representation on its influence on the results. As shown in the sensitivity analysis, a more homogenous K_0-profile throughout the clay deposit does not necessarily result in a smoother and more uniform curve for horizontal displacements. Moreover, the tendency of large horizontal displacements in the first two clay layers, where K_0 and K_0^{NC} are larger, should be further investigated as the behaviour is not what is theoretically expected.

The results show some disparities in pore pressures when comparing simulation to measured data in VWP instruments. This can likely be attributed to the homogenisation method used to simulate PVDs increasing the overall permeability of the soil, thus displaying average values of obtained pore pressures. Thus, pore pressures in the model will dissipate faster in all points in improved area. Whereas, in reality, there is little initial change in permeability in the middle between the installed drains where "maximum" excess pore pressures are displayed, resulting in an initial build-up of pore pressures similar to the unimproved case. However, as evident in the results for vertical displacements, this probably has negligible implications on the overall prediction.

7. Conclusions

In conclusion, using numerical analysis to model the time dependent behaviour of embankments constructed on soft soil can be a very useful tool and give very satisfactory results when conducted properly. However, it should be used primarily as an indicator of the expected response as the outcome is highly influenced by the choice of constitutive model, quality of soil sampling and laboratory testing. Above all, the most fundamental factor is the experience and judgement of the geotechnical engineer to achieve reliable predictions.

The results obtained for the PVD-improved embankment demonstrated good predictions of both vertical and horizontal deformations, aligning reasonably well with the measured data over a 3-year period. Moreover, the implemented averaging technique effectively captured the enhanced consolidation settlements introduced by the PVDs. Comparisons with the unimproved embankment indicated limited actual improvements in stability for the improved case in the initial 3-year period. However, spanning over a 40-year period, it was observed that the vertical settlements approached the same order of magnitude for both cases, while the horizontal displacements were significantly larger for the unimproved embankment. Highlighting the time-dependent nature of stability improvement in the soil when using PVDs.

The parameter derivation process and the utilization of high-quality laboratory data were found to be paramount to achieve accurate predictions. The sensitivity analysis revealed significant variations in the results depending on the laboratory test used to derive the pre-consolidation pressure. This discrepancy was attributed to the unusually high strain-rate adopted for the CRS tests, and the unusually low strain-rate employed for the IL-tests. Highlighting the importance, and difficulty, of adjusting for strain rate when using CRS oedometer tests. Furthermore, the vertical hydraulic conductivity of the soil, in situ-lateral earth pressure, and modified creep index proved to be of high influence on the simulation results.

Fundamentally, when modelling boundary value problems using constitutive models that rely on input parameters that represent soil behaviour, it is crucial to adopt a consistent approach to parameter derivation. This becomes particularly important when utilizing advanced models like the Creep-SCLAY1S model, which encompasses various aspects of soil behaviour, such as anisotropy, destructuration and time-dependency.

8. Recommendations for further research

- Class C prediction of the embankment without PVDs should be conducted when measurement data is available.
- A more detailed look into the impact of K_0 and K_0^{NC} on horizontal displacements should be conducted.
- The applicability of the homogenisation technique (employed to model the PVDs in this thesis) in 1D settlement calculation software.

References

Almeida, M. d. S. S. & Marques, M. E. S., 2013. *Design and Performance of Embankments on Very Soft Soils.* 1st Edition ed. London: CRC Press.

Amavasai, A. et al., 2017. *Towards consistens numerical analyses of embankments on soft soils,* Gothenburg: DOI:10.1080/19648189.2017.1354784.

Amavasai, A., Sivavithamparam, N., Dijkstra, J. & Karstunen, M., 2018. Consistens Class A & C predictions of the Ballina test embankment. *computers and Geotechnic,* Volume 93, pp. 75-86.

Amundsen, H., Thakur, V. & Emdal, A., 2016. *Sample disturbance in block samples on low plastic soft clays.* Reykjavik, Proceedings of the 11th Nordic Geotechnical Meeting. Challenges in Nordic Geotechnics.

Barron, R. A., 1948. Consolidation of Fine-Grained Soils by Drain Wells. *Transactions of ASCE,* Volume 113, pp. 718-742.

Basu, P., Basu, D. & Prezzi, M., 2010. Analysis of PVD-enhanced consolidation with soil disturbance. *Proceeding og the Institution of Civil Engineers - Ground Improvement,* 163(G14), pp. 237-249.

Bjerrum, L., 1967. Engineering geology of norwegian normally consolidated marine clays as related to settlements of buildings. Seventh rankine lecture. *Geotechnique,* Volume 17, pp. 83-118.

Brinkgreve, R., 2005. Selection of soil models and parameters for geotechnical engineering application. *Geotechnical special publication,* Volume 128, pp. 69-98.

Buisman, A., 1936. *Results of long duraiton settlement tests.* Harvard University, Cambridge, Massachusetts, USA, ASCE, Proceedings of the 1st international conference of soil mechanical foundation engineering, 1: 103-107.

Burland, J., 1990. On the compressibility and shear strength of natural clays. *Géotechnique,* 40(3), pp. 329-378.

Chai, J.-C. & Miura, N., 1999. Investigation of Factors Affecting Vertical Drain Behaviour. *Journal of Geotechnical and Geoenvironmental Engineering,* 125(3).

Chai, J.-C., Miura, N., Sakajo, S. & Bergado, D., 1995. Behaviour of vertical drain improved subsoil under embankment loading. *Soils and Foundations, Japanese Geotechnical Society,* 35(4), pp. 49-61.

Chai, J.-C., Shen, S.-L., Miura, N. & Bergado, D. T., 2001. Simple Method of Moedling PVD-improved Subsoil. *Journal of Geotechnical and Geoenvironmental Engineering,* 127(11), pp. 965-972.

Claesson, P., 2003. *Long term settlements in soft clays,* Gothenburg: Thesis for degree of cotor of philisophy. Chalmers University of Technology.

Graham, J., 2006. The 2003 R.M. Hardy Lecture: Soil parameters for numerical analysis in clay. *Canadian Geotechnical Journal,* Volume 43, pp. 187-209.

Gras, J.-P., Sivasithamparam, N., Karstunen, M. & Dijkstra, J., 2017. Strategy for consisten model parameter calibration for soft soils using multi-objective optimisation. *Computers and Geotechnics,* Volume 90, pp. 164-175.

Grimstad, G., Degago, S. A., Nordal, S. & Karstunen, M., 2010. Modeling creep and rate effects in structured anisotropic soft clays. *Acta Geotechnica,* Volume 5, pp. 69-81.

Hansbo, S., 1981. *Consolidation of Fine-Grained Soild by Prefabricated Drains.* Balkema, Rotterdam, The Netherlands, Proc., 10th in. Conf. on Soil Mechanics and Foundation Engineering.

Hansbo, S., 1997. Aspect of vertical drain design: Darcian or non-Darcial flow. *Geotechnique,* 47(5), pp. 983-992.

Hansbo, S., 1997. *Practical aspects of vertical drain design,* Göteborg & J&W, Lidingö, Sweden: Chalmers University of Technology.

Hanzawa, H., 1989. Evaluation of design parameters for clays as related to geological stress history. *Soils and Foundations,* 29(2), pp. 99-111.

Hird, C. C., Pyrah, I. C., Russell, D. & Cinicioglu, F., 1995. Modelling the effect of vertical drains in two-dimensional finite element analyses of embankments on soft ground. *Canadian Geotechnical Journal,* Volume 32, pp. 795-807.

Indraratna, B., Baral, P., Rujikiatkamjorn, C. & Perera, D., 2018. Class A and C predictions for Ballina trial embankment with vertical drains standard test data from industry and large diameter test specimens. *Computers and Geotechnics,* Volume 93, pp. 232-246.

Karlsrud, K. & Hernandez-Martinez, F., 2013. Strength and deformation properties of Norwegian clays from laboratory tests on high-quality block samples. *Canadian Geotechnical Journal,* 50(12), pp. 1273-1293.

Karlsson, M., Emdal, A. & Dijstra, J., 2016. Consequences of sample disturbance of rpredicting long-term settlements in soft clay. *Canadian Geotechnical Journal,* 53(12).

Karstunen, M., 2021. *From soft soil modelling to engineering application.* Department of Architecture and Civil Engineering, Chalmers University of Technology, Gothenburg, 18th Nordic Geotechnical Metting.

Karstunen, M. & Amavasai, A., 2017. *BEST SOIL: Soft soil modelling and parameter determination,* Gothenburg: Department of Architecture and Civil Engineering, Chalmers University of Technology.

Karstunen, M. et al., 2005. Effect of anisotropy and destructuration on the Beheaviour of Murra Test Embankment. *International Journal of Geotechnics,* 5(2), pp. https://doi.org/10.1061/(ASCE)1532-3641(2005)5:2(87).

Karstunen, M., Sivasithamparam, N., Brinkgreve, R. B. J. & Bonnier, P., 2013. *Modelling rate-dependent behaviour of structured clays,* s.l.: s.n.

Kelly, R. et al., 2017. Site characterisation for the Ballina field testing facility. *Géotechnique,* 67(4), pp. 279-300.

Larsson, R., 2008. *Jords egenskaper,* Linköping: Statens Geotekniska Institut.

Larsson, R. et al., 2007. *Skjuvhållfasthet - utvärdering i kohesionsjord,* Linköping: Statens Geotekniska Institut.

Leoni, M., Karstunen, M. & Vermeer, P. A., 2008. Anisotropic creep model for soft soils. In: *Géotechnique 58, No. 3.* s.l.:s.n., pp. 215-226.

Leroueil, S., Kabbaj, M., Tavenas, E. & Bouchard, R., 1985. Stress-strain-strain rate relation for the compressibility of sensitive natural clays. In: *Géotechnique 35, No. 2.* s.l.:s.n., pp. 159-180.

Muir Wood, D., 1990. *Soil Behaviour and critical state soil mechanics.* Cambridge: Cambridge University Press. ISBN:0-521-33782-8.

Muir Wood, D., 2016. Analysis of consolidation with constant rate of discplacement. *Canadian Geotechnical Journal,* 53(5), pp. 740-752.

Müller, R., 2010. *Embankments founded on sulphide clay,* Stockholm: Licentiate Thesis, Deparment of Civil and Architectural Engineering, Division of Soil and Rock Mechanics, Royal Institute of Technology.

Olsson, M., 2010. *Calculating long-term settlement in soft clays,* Linköping: Statens Geotekniska Institut.

Olsson, M., 2013. *On rate-dependency of Gothenburg clay,* Gothenburg: Chalmers University of Technology.

Phillips, A. & Sierakowski, R., 1965. One the concept of yield surface. *Acta Mechanica,* pp. 29-35.

Pineda, J. et al., 2019. The Ballina soft soil Field Testing Facility. *AIMS Geosciences,* 5(3), pp. 509-534.

Pineda, J. et al., 2016. Characterisation of Ballina clay. *Géotechnique,* 6(7), pp. 556-557.

Potts, D., 2003. Numerical analysis: Avirtual dream or practical reality?. *Géotechnique,* 53(6), pp. 535-573.

Rowe, R. & Taechakumthorn, C., 2008. Effects of viscous behaviour of geosynthetic reinforcement and foundation soil on the performance of reinforced embankments. *Geotextiles and Geomembranes,* 26(4), pp. 317-334.

Sällfors, G., 1975. *Preconsolidation pressure of soft, high-plastic clays,* Göteborg: PhD Thesis, Geotechnical Department, Chalmers Univeristy of Tehnology.

Schanz, T., Vermeer, P. & Bonnier, P., 1999. The hardening soil model: formulation and verification. *Proceedings of the international symposium "Beyond 2000 in computational Geotechnics",* pp. 281-296.

Sivasithamparam, N., Karstunen, M. & Bonnier, P., 2015. Modelling creep behaviour of anisotropic soft soils. *Computers and Geotechnics ,* I(69), pp. 46-57.

Stolle, D. & Stolle, J., 2011. Weighted residual approach to contant strain rate test. *Canadian Geotechnical Journal,* 48(4), pp. 671-675.

Svanö, G., Christense, S. & Nordahl, S., 1991. *A soil model for consolidation and creep..* Florence, Italy, Proceedings of the 10th European Conference on Soil Mechanics and Foundation Engineering. ISBN 90 5410 002 8.

Terzaghi, K., n.d. Die berechnug der durchlassigkeit des tones aus dem verlauf der hydromechanischen spannungserscheinungen. *Sitzungsber. Akad. Wiss. Math.-Naturwiss. Kl., Abt. Iia,* Volume 132, pp. 125-138.

Ti, K. S., Jafaar, M. S. & Sew, G. S., 2009. A review of Basic Soil Constitutive Models for Geotechnical Application. *J. Bund,* Volume 14, pp. 1-18.

Tornborg, J., Karlsson, M., Kullingsjö , A. & Karstunen, M., 2021. Modelling the construction and long-term response of Göte Tunnel. *Computers and Geotechnics,* Volume 134.

Wheeler, S. J., Näätänen, A., Karstunen, M. & Lojander, M., 2003. An anisotropic elasoplastic model for soft clays. *Canadian Geotechnical Journal,* Volume 40, pp. 403-418.

Yin, Z.-Y. & Karstunen, M., 2011. Modelling strain-rate-dependency of natural soft clays combined with anisotropy and destructuration. *Acta Mecanicha Solida Sinica,* 24(3), pp. 217-229.

Appendix A: Embankment construction sequence

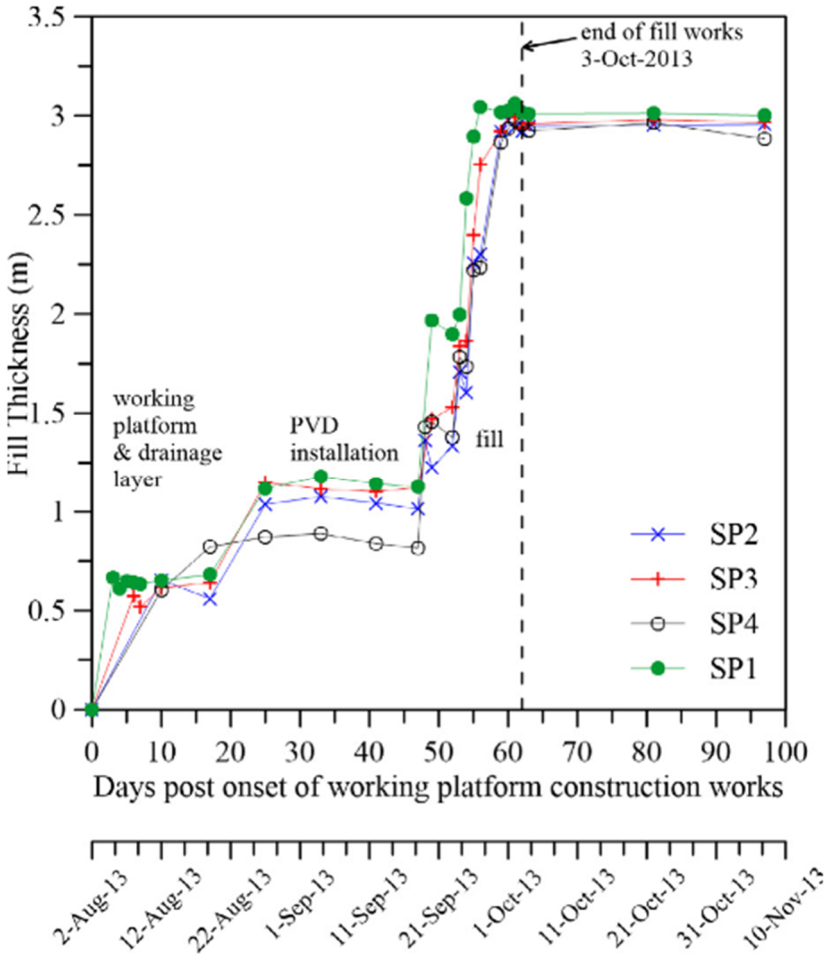

Figure A.1 Embankment construction sequence (Pineda, et al., 2019).

Appendix B: Model input parameters

Table B.1. Initial input parameters derived from laboratory test data.

Parameter type	Parameter	Layers (m)				
		1.5-3.0	3.0-4.0	4.0-6.0	6.0-8.5	8.5-10.5
Conventional parameters	κ^*	0.016	0.023	0.028	0.021	0.022
	v'	0.2	0.2	0.2	0.2	0.2
	λ_i^*	0.110	0.120	0.145	0.121	0.102
	M_c	1.39	1.72	1.58	1.55	1.4
	M_e	0.95	1.15	1.18	0.98	0.99
Anisotropic parameters	ω	30	20	19	22	28
	ω_d	0.94	0.993	1.018	1.014	0.947
	α_0	0.533	0.705	0.624	0.608	0.538
Destructuration parameters	ξ_v	9.8	10.2	8.4	8.9	7.8
	ξ_d	0.27	0.29	0.24	0.25	0.23
	χ_0	2.50	2.00	2.70	2.60	3.00
Viscous parameters	μ_i^*	0.0021	0.0020	0.0025	0.0025	0.0022
	τ	5	5	5	5	5
Initial state parameters	ρ	1.59	1.48	1.44	1.41	1.43
	e_0	2.05	2.42	2.80	3.15	2.90
	POP^*	23	13	6	4	6
	POP^{**}	26.5	15.5	24	18.5	26
	K_0^*	0.65	0.43	0.42	0.41	0.50
	K_0^{**}	0.76	0.50	0.58	0.53	0.64
	K_0^{NC}	0.44	0.33	0.37	0.38	0.43

‘* Values derived using IL tests
‘* Values derived using CRS tests adjusted with factor of 0.84 according to (Pineda, et al., 2016)

Appendix C: Sensitivity analysis

Table C.1. Values used in sensitivity analysis of POP.

	Clay 1	Clay 2	Clay 3	Clay 4	Clay 5
Initial value	17	11	7	5	3
Decreased value	13.5	8	5	3.5	2
From CRS adjusted	21.5	10.5	19	13.5	21
From CRS	31	20	30	26	35

Table C.2. Values used in sensitivity analysis of K_0.

	Clay 1	Clay 2	Clay 3	Clay 4	Clay 5
Initial value	0.86	0.83	0.51	0.52	0.46
Adjusted value	0.86	0.83	0.76	0.78	0.69

Table C.3. Values used in sensitivity analysis of K_0^{NC}.

	Clay 1	Clay 2	Clay 3	Clay 4	Clay 5
Initial K_0^{NC}	0.41	0.33	0.37	0.38	0.44
New K_0^{NC}	0.61	0.49	0.55	0.57	0.66

Table C.4. Values of k_{ev} for different ratios k_h/k_s used in the sensitivity analysis.

	Clay 1	Clay 2	Clay 3	Clay 4	Clay 5
k_h/k_s =3	8,7E-03	6,1E-03	3,3E-03	2,8E-03	2,2E-03
k_h/k_s=12	2,4E-03	1,7E-03	9,3E-04	7,9E-04	6,3E-04
k_h/k_s =20	1,5E-03	1,1E-03	5,8E-04	4,9E-04	3,9E-04

DEPARTMENT OF INFRASTRUCTURE AND
ENVIRONMENTAL ENGINEERING
CHALMERS UNIVERSITY OF TECHNOLOGY
Gothenburg, Sweden 2023
www.chalmers.se

CHALMERS
UNIVERSITY OF TECHNOLOGY